

ACTIVE FLUX BASED V/F WITH STABILIZING LOOPS CONTROL VERSUS VECTOR CONTROL OF IPMSM

Teză destinată obținerii
titlului științific de doctor inginer
la
Universitatea "Politehnica" din Timișoara
în domeniul INGINERIE ELECTRICA
de către

Ing. Ana Adela MOLDOVAN

Conducător științific: prof.univ.dr.ing. Ion Boldea
Referenți științifici: prof.univ.dr.ing. Mircea Radulescu
prof.univ.dr.ing. Iulian Birou
conf.univ.dr.ing. Lucian Tutelea

Ziua susținerii tezei: 16.03.2012

Seriile Teze de doctorat ale UPT sunt:

- | | |
|---|--|
| 1. Automatică | 8. Inginerie Industrială |
| 2. Chimie | 9. Inginerie Mecanică |
| 3. Energetică | 10. Știința Calculatoarelor |
| 4. Ingineria Chimică | 11. Știința și Ingineria Materialelor |
| 5. Inginerie Civilă | 12. Ingineria sistemelor |
| 6. Inginerie Electrică | 13. Inginerie energetică |
| 7. Inginerie Electronică și Telecomunicații | 14. Calculatoare și tehnologia informației |

Universitatea „Politehnica” din Timișoara a inițiat seriile de mai sus în scopul diseminării expertizei, cunoștințelor și rezultatelor cercetărilor întreprinse în cadrul școlii doctorale a universității. Seriile conțin, potrivit H.B.Ex.S Nr. 14 / 14.07.2006, tezele de doctorat susținute în universitate începând cu 1 octombrie 2006.

Copyright © Editura Politehnica – Timișoara, 2012

Această publicație este supusă prevederilor legii dreptului de autor. Multiplicarea acestei publicații, în mod integral sau în parte, traducerea, tipărirea, reutilizarea ilustrațiilor, expunerea, radiodifuzarea, reproducerea pe microfilme sau în orice altă formă este permisă numai cu respectarea prevederilor Legii române a dreptului de autor în vigoare și permisiunea pentru utilizare obținută în scris din partea Universității „Politehnica” din Timișoara. Toate încălcările acestor drepturi vor fi penalizate potrivit Legii române a drepturilor de autor.

România, 300159 Timișoara, Bd. Republicii 9,
tel. 0256 403823, fax. 0256 403221
e-mail: editura@edipol.upt.ro

Preface

The thesis represents an approach and a contribution to the sensorless control methods for General AC Drives. The novel sensorless method, V/f with stabilizing loops control is mostly based on the active flux concept and maximum torque per ampere condition. This control method can be applied for all ac motors. Besides the implementation of both the sensorless and with encoder vector control schemes, the thesis proposes four different correction loops strategies of the interior permanent magnet synchronous motor, in a wide speed range.

Motivation

Though motion-sensorless FOC and DTFC have spread in a spectacular way to all servo-drives, high dynamics response in general AC drives is still a problem we have to deal with.

The motor response and performances under vector control with and without position sensor are first analyzed in Chapter 2 and Chapter 3.

The main target of the thesis is to prove that V/f with stabilizing loops control can provide high dynamic performance, without speed or current regulators (hence their design is not a problem we have to deal with), without coordinate transformations and with less computation effort than sensorless vector control. Under V/f control, the motor starts from any position, thus it does not need an independent starting strategy. Both simulations and experiments have been conducted and comparisons between the proposed control method and sensorless vector control results have been discussed, to prove the above mentioned demands (Chapter 4 and Chapter 5).

In Chapter 6, other three V/f with correction loops control strategies are analytically described and their results are analyzed, in order to find a simpler method to fulfill the imposed requirements. The experimental setups are described during Chapter 7, while the conclusion and the contributions are highlighted in Chapter 8.

The proposed method uses the active flux concept and includes the maximum torque per current condition; it also offers a smooth transition of the motor functioning below base speed region and above the base speed region.

Acknowledgements

"The Ph.D. thesis was partially supported by the strategic grant POSDRU 6/1.5/S/13, ID6998 (2008) of the Ministry of Labour, Family and Social Protection 2007-2013, Romania, co-financed by the European Social Fund—Investing in People".

First of all I wish to express my gratitude to my supervisor Prof. Ion Boldea for his guidance, support and fruitful ideas, which made this work possible. Secondly, I would like to thank Prof. Gh. Daniel Andreescu from Faculty of Automation and Computers for his constructive and priceless discussions.

I also wish to thank Prof. Frede Blaabjerg for his support during the three month research in Aalborg University, Denmark.

Many thanks to Assoc. Prof. Tutelea Lucian and to all my colleagues who contributed to my engineering education.

Most of all, I want to express my love and appreciation for my parents and my husband; their encouragement and understanding were priceless during all this period.

Timișoara, March 2012

Moldovan Ana Adela

Moldovan, Ana Adela

Active Flux Based V/f with Stabilizing Loops Control Versus Vector Control of IPMSM

Teze de doctorat ale UPT, Seria 6, Nr. 26, Editura Politehnica, 2012, 160 pagini, 73 figuri, 9 tabele.

ISSN: 1842-7022

ISBN: 978-606-554-461-1

Keywords: Active flux, stabilizing loops, IPMSM, high dynamics, sensorless control;

Abstract

The present thesis proposes a novel approach of V/f with stabilizing loops control, suitable for all AC General Drives, with Interior Permanent Magnet Motor, used as a case study. The main target is to prove that this control method can provide fast speed and torque control, without the use of PI speed and current controllers, without coordinate transformations and with reduced computation effort, than in sensorless vector control.

This control method is based on active flux concept, it includes the maximum torque per ampere condition and the capability of the drive to work above base speed. Comparisons with existing sensorless control methods have been conducted and results have been interpreted.

To prove once more the stabilizing loops effectiveness, simulation and experimental tests have been performed with open loop V/f control. Increased system stability and fast dynamic performances have been obtained after the two stabilizing loops consideration.

Four different V/f with correction loops control methods have been analytically studied and tested: one of them through both digital simulations and experimental verification, the other three strategies, through digital simulations. Results show significant results for two of them.

Table of Contents

PREFACE	3
MOTIVATION	3
ACKNOWLEDGEMENTS	4
TABLE OF CONTENTS	5
NOMENCLATURE	7
CHAPTER 1 PERMANENT MAGNET SYNCHRONOUS MACHINE DRIVES AND THEIR CONTROL – STATE OF THE ART	9
1.1. GENERAL AC DRIVES	9
1.2. PERMANENT MAGNET ELECTRIC MACHINE DRIVES	10
1.3. PMSM CONTROL TECHNIQUES	11
1.4. OPERATING PRINCIPLE OF IPMSM DRIVES	18
1.5. IPMSM SENSORLESS CONTROL TECHNIQUES	21
1.6. FLUX WEAKENING REGION FOR PMSM	22
1.7. PROPOSED SOLUTION: V/F CONTROL WITH TWO STABILIZING LOOPS	24
1.7.1. Scope and realization	25
1.8. CONCLUSION	26
CHAPTER 2 COMPREHENSIVE CHARACTERIZATION OF IPMSM DRIVE AND VECTOR CONTROL TEST RESULTS, WITH ENCODER	31
2.1. IPMSM STRUCTURE AND EXPERIMENTAL ANALYSIS	32
2.2 STANDSTILL MEASUREMENTS	33
2.3 LOAD PERFORMANCE TESTING	35
2.4 STRUCTURE OF CURRENT CONTROLLERS	37
2.5. IPMSM WITH FRACTIONARY WINDING	38
2.5.1. Experimental results	38
2.5.2. Simulation results	47
2.6. IPMSM WITH DISTRIBUTED WINDINGS	54
2.6.1. Experimental results	54
2.6.2. Simulation results	58
2.7. CONCLUSION	63
CHAPTER 3 ACTIVE FLUX BASED VECTOR CONTROL OF SENSORLESS DISTRIBUTED WINDINGS IPMSM	67
3.1. ACTIVE FLUX CONCEPT	67
3.2. MAXIMUM TORQUE PER AMPERE CONDITION	70
3.3. EXPERIMENTAL RESULTS	72
3.4. SIMULATION RESULTS	76
3.5. CONCLUSION	81

CHAPTER 4 V/F WITH STABILIZING LOOPS CONTROL OF DISTRIBUTED WINDINGS IPMSM: PRINCIPLES AND DIGITAL SIMULATION RESULTS	85
4.1. STANDARD V/F CONTROL.....	85
4.2. V/F WITH STABILIZING LOOPS CONTROL	92
4.2.1. The Proposed Active Flux Error-Based Voltage Amplitude Stabilizing Loop	92
4.2.2. The Proposed Speed Error-Based Voltage Phase Angle Stabilizing Loop	93
4.2.3. The Proposed Control System.....	93
4.3. CONCLUSION	100
CHAPTER 5 V/F WITH STABILIZING LOOPS AND SENSORLESS VECTOR CONTROL OF IPMSM – EXPERIMENTAL CHARACTERIZATION.....	103
5.1. V/F WITH STABILIZING LOOPS CONTROL	103
5.2. SIMULATION RESULTS.....	105
5.3. EXPERIMENTAL RESULTS	108
5.4. CONCLUSION	114
CHAPTER 6 ALTERNATIVE, NEW, STABILIZING LOOPS CONTROL OF TOOTH WOUND IPMSM: PRINCIPLES AND DIGITAL SIMULATIONS.....	117
6.1. V/F WITH MAGNETIC ENERGY & TORQUE BASED CORRECTION LOOPS	118
6.2. V/F WITH REACTIVE POWER AND TORQUE BASED CORRECTION LOOP	123
6.3. V/F CONTROL WITH VOLTAGE PHASE ANGLE CORRECTION AND ACTIVE POWER CALCULATION	127
6.4. CONCLUSION	134
CHAPTER 7 EXPERIMENTAL PLATFORMS	137
7.1. THE FIRST EXPERIMENTAL SETUP	137
7.1.1. Test machine (IPMSM).....	141
7.1.2. Three phase inverter	142
7.2. THE SECOND EXPERIMENTAL SETUP.....	142
7.3. CONCLUSION	144
CHAPTER 8 CONCLUSION AND CONTRIBUTIONS	145
8.1. CONCLUSION	145
8.2. ORIGINAL CONTRIBUTIONS.....	146
8.3. FUTURE WORK	147
SUMMARY IN ROMANIAN	148
Author’s papers related to the Ph. D. thesis	152
AUTHOR’S CV	153
APPENDIX.....	154

Nomenclature

Abbreviations

ac	Alternating current;
dc	Direct current;
DTFC	Direct torque and flux control;
EMF	Electromotive force;
IM	Induction machine;
INFORM	Indirect flux detection by online reactance measurement;
IPMSM	Interior permanent magnet synchronous machine;
HPF	High pass filter;
PI	Proportional integral controller;
PM	Permanent magnet;
PWM	Pulse width modulation;
SVM	Space vector modulation;
VC	Vector control;

Symbols

B	Viscous friction coefficient;
i_a, i_b, i_c	Instantaneous stator a, b, c phase currents;
I_d, I_q	Stator currents in d, q rotor reference frame;
I_α, I_β	Stator currents in α, β stator reference frame;
I_s	Magnitude of the stator current vector;
J	Inertia of the motor shaft and the load system;
L_d, L_q	Rotor d- and q- axis inductances;
L_s	Stator total inductance;
L_{sc}	Short-circuit inductance of the IMs;
p_1	Number of pole pairs of the motor;
R_s	Stator resistance per phase;

T_e	Electromagnetic torque;
V_α, V_β	stator voltage in α, β stator reference frame;
V_{dc}	DC-link voltage;
V_s	Magnitude of the stator voltage vector;
V_{comp}	Compensation voltage;
ω_r	Electrical rotor speed;
θ_{er}	Electrical rotor position;
$\theta_{\Psi_d^a}$	Active flux angle;
Ψ_d^a	Active flux;
Ψ_{PM}	Rotor permanent magnet flux;
Ψ_s	Stator flux linkage;

Subscripts

$a;b;c$	Stator a,b,c phases;
s	Stator quantity;
r	Rotor quantity;

Superscripts

*	Reference quantity;
^	Estimated quantity;

Chapter 1

Permanent Magnet Synchronous Machine Drives and Their Control – State of the Art

This chapter offers a comprehensive overview of the state of the art of the General AC Drives and their control techniques, with the main focus on Interior Permanent Magnet Synchronous Motors (IPMSM). In the beginning, a brief description of the General AC Drives is presented, followed by a classification of the permanent magnet synchronous drives. The permanent magnet synchronous motors characteristics and a review of their control methods, with and without motion sensor will be resumed further on. Finally, the basic principles for the IPMSM, the proposed solution and the conclusion are shown.

1.1. General AC Drives

The electric machine mechanical power was the best source of the mechanical power in the 19th century, which is the period when the electric machinery has been invented. The machine mechanical power represents the main source of mechanical power to support the present industrialized society. More than 60% of today's total electricity produced today is used to run the electric machines. If we talk about the transportation area, we have to say that the combustion engine has dominated during the past century as a source of mechanical power. Nowadays, the electric machines are many times faster than the internal combustion engine, thus, they are applied as main source of traction force in the electric vehicle, the hybrid vehicle and the electrically propelled vessels [1].

An electric machine drive system is an industrial system which converts the electrical energy into mechanical energy – as a motor and mechanical to electrical energy – as a generator [2]. The industrial system is made of several electrical and mechanical parts like: the electric machine, the electric power converter, the control system, the acquisition system and so on.

Through more than one century of their development, the AC Machines have various shapes, each of them suitable for different applications in industry, electric

traction, vehicles, ship propulsion, home appliances, robotics, and so on. An electric machine can be designed as thin disk type, long cylinder type and rotating or linear motion type [1].

Alternating current (AC) Motor Drives are today a mature technology with torque levels from about 0.02 Nm to a few MNm and from high speeds (500 krpm at 100 W) to low speeds (16 rpm, 3 MW, PM Synchronous Wind Generator). The absence of mechanical brushes, the implicit four quadrant operation and motion-sensorless digital control via reasonable cost PWM converters have all contributed to this situation.

The **speed control range** and **torque response quickness** discriminates between **general drives** and so **called servodrives**. A 5(10)/1 speed range with full torque change in stable conditions within hundreds of milliseconds indicates a general AC drive, while a more than 1000/1 speed range with full torque response within milliseconds (1-2 ms) refers to high quality servo-drives [3].

Nowadays, the machine drive system can be easily controlled directly from the information processing system which is based on the rapid power electronics development. Thus, an Induction or a Synchronous machine can be driven through a variable frequency inverter [1].

1.2. Permanent magnet electric machine drives

The shift from DC Motor to the AC Motor occurred as a consequence of not only the power electronics technology improvement, but also because of the control theory for the AC motor and the increased use of permanent magnets. The change from the field flux corresponding to the external winding to the permanent magnet flux increases the machine torque and power density and because of the copper loss elimination, the efficiency is improved. Because of the low torque pulsations, the PM machines are characterized by low vibration and noise [4]. The rugged construction and the simple maintenance of the drive have to be also specified.

The lately increasing cost of the permanent magnets (PMs), their demagnetization at raised temperatures, the need for field weakening control, the machine needs to start from an initial position [6-9], all these are a few of the permanent magnet electric machines disadvantages.

Permanent magnet electric machines are in general AC controlled in the stator and DC excited in the rotor and they are constructed in various design topologies, so their classification follows:

- PM excited DC brush machine;
- Synchronous Motors
 - Brushless AC Motors (sinusoidal back-EMF):
 - Interior permanent magnet synchronous motor;
 - Surface permanent magnet synchronous motor;
 - Brushless DC Motors (trapezoidal back-EMF);
 - Reluctance synchronous motor;
- Stepping motor, Switched Reluctance Motor;

Greater attention has been given to the sinusoidal machines than on trapezoidal ones because they are closer to the other AC Machines both in functioning and in the principles of operation. The difference between the two types of motors is that PM AC Brushless Motors are fed with sinusoidal back-emf waveform, while the DC Brushless Motors need trapezoidal bemb waveform. Even though, both sinusoidal and trapezoidal PM machines are identical in behavior [4]. Anyway, we have to mention that in what concerns the sinusoidal back-emf motors, the rotor position is required continuously, unlike the trapezoidal back-emf motors, for which it is enough if we have the rotor position every sixty degrees to obtain the proper switching sequence.

The absence of brushes and commutation makes the structure of the permanent magnet (PM) synchronous machine very simple, simplicity which makes the AC permanent magnet machines the most attractive from all the PMs machines [5].

1.3. PMSM Control Techniques

Initially, the machine drive system has been controlled using manual operation methods, but their place has been rapidly taken by the automatic control system.

AC drives were equipped with a V/f control, which is easy to implement and low cost control. Field oriented control (FOC) and direct torque and torque control (DTFC) have been the next steps for AC Drives excellent dynamics.

These days, the most important concerns are to eliminate all nonlinear effects and losses, to obtain higher efficiency and to develop intelligent control strategies to allow the system operate at optimal operating conditions [1].

During the last decades research and development of the PMSM control strategies have been made and their implementation has been presented through a lot of scientific papers. In what concerns the power electronics associated with the drive system, the three phase bridge inverter has been widely used, as shown in Fig.1.1. at any instant of time, three power devices (IGBTs) of the three phase bridge inverter are conducting.

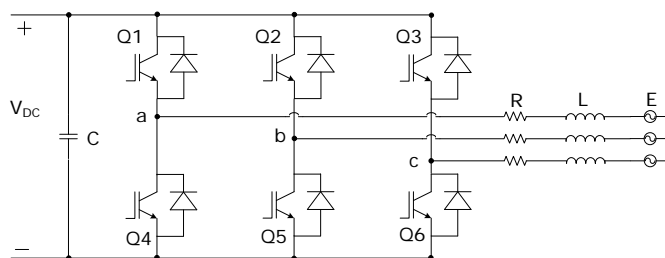


Fig. 1.1. Variable voltage and frequency inverter with pulse width modulation;

Because of the additional performance requirements like maximum torque per current, constant torque angle, maximum efficiency, and so on, various control strategies have been emerged. Almost all of the control methods and their implementation are affected by the machine parameters. Considering the latter, plus the voltage limitations of the inverter, the IPMSM control has to be optimized for each operating condition by an adaptive approach.

As mentioned before, position information is the key factor in the control of PM Synchronous motor drives and this is the reason for the great interest in sensorless control techniques. Among the variety of the position sensors, the most popular one is the resolver which has an acceptable resolution and accuracy, that determine the performance and dynamics of the control. The output of a digital encoder is a train of pulses which is converted to an integer value to determine the gear ratios without loss of information. Hence, the encoder is very important for the complete machine modeling and calculation of all state variables based on the measured values.

There are different techniques through which we can estimate the position information, some of them will be discussed further on.

1. One easy way to obtain the position information is to use **open loop estimatos** using the measured voltages and currents to construct the flux linkage position signal through which the phase angle of the stator current can be controlled [16]. The stationary frame α, β axes flux linkages are:

$$\Psi_{\alpha}(t) = \int (U_{\alpha} - I_{\alpha} \cdot R_s) dt - L_q \cdot I_{\alpha}; \quad (1.1)$$

$$\Psi_{\beta}(t) = \int (U_{\beta} - I_{\beta} \cdot R_s) dt - L_q \cdot I_{\beta}; \quad (1.2)$$

Where R_s is the stator resistance and I_{α}, I_{β} , are the currents expressed in stator coordinates.

The algorithm performance and the precision of the position information depend on the quality of the estimated flux linkages, on the accuracy of the measured voltages and currents and on the parameters variation.

2. We can also determine the rotor position based on a hypothetical rotor position [17-19]. A **hypothetical system of axes (γ, δ)** for the rotor position is considered, not the same with the actual one. The main idea of this control is the system self-synchronization, which means to eliminate the error between the actual and hypothetical axes. The drawback of this method is that it is computationally intensive and requires fast processors for better accuracy.

3. Other sensorless method to determine the real rotor position is based on **Kalman filtering**. A Kalman filter provides optimum filtering for noisy signals and processes with no computationally effort, so it is an efficient candidate for on-line speed and rotor position estimation.

The Kalman filter is an optimum state estimator and consists of a two-step process: prediction and filtering. The filter estimation is constantly corrected by an additional term. The prediction part of the observer estimates the next value, while the filtering part of the observer, corrects the estimation process in a recursive manner, based on the measured values. The most important step in a Kalman filter is to select the proper coefficient for the best position information.

This method is computationally intensive and depends on the model parameters accuracy.

4. Rotor position estimation can be made using **state observers**.

The output of a state observer is defined as a combination of states and it is compared with the equivalent measured output variables of the real motor. The error between the two signals is used to correct the state trajectory of the observer.

For accurate position information and for a nondestructive motor operation, the observer stability is a very important issue.

Difficulties will appear in the implementation process, as the observer optimum gains have to be fixed and initial information of the states is required, to assure the observer proper functioning, during all operating conditions.

5. Another sensorless method for the interior permanent magnet synchronous motors is based on the **back emf** integration.

6. Position information can also be obtained based on the **machine inductance variation**.

For IPM motors the inductance along “q” axis is greater than the one along “d” axis because of low permeability of the magnet material. The inductance can be used to obtain the rotor position, as it is a function of the rotor position. The variation of the self-inductance with rotor position is determined by injecting a frequency sinusoidal signal into one winding and measuring the terminal voltage and current. Using the two motor variables, the phase inductance can be calculated and afterwards, the rotor position can be estimated through a lookup table. The algorithm will search the lookup table for the phase inductance closest to the calculated one. Hence, the position information depends on the accuracy of the inductance calculation.

Position error is higher when there is a large error in the inductance calculation.

A drawback of a great importance for all the above sensorless techniques for rotor position estimation is that none of them are **self-starting schemes**. Most of them are based on arbitrarily energizing two or three windings and expecting the rotor to align in a certain definite position, but this solution leads to low dynamic performance [36].

A specific PWM pattern can be applied to the inverter to align the rotor in the direction of a phase winding, followed by the sensorless control strategy. This strategy is characterized by poor dynamic response and it is not suitable for applications which need a smooth starting into the right direction.

A method that shows high dynamic performance and is the most widespread in industrial drives, is the Indirect Flux Detection by On-line Reactance Measurement (INFORM). The INFORM main idea is to use the effect of the difference between L_d and L_q , so the rotor aligns to a certain position by applying a stationary armature current. Then, I_q is applied to accelerate the rotor. This method creates a noisy rotor angular position, so the Kalman filter is used to improve the rotor position accuracy.

The position detection scheme for PM synchronous motors is mainly based on the parameters variation and measurement of the motor terminal voltages and currents, which are used in different observers or direct calculations. Because of the motor parameter variation with temperature, saturation or measurement inaccuracies, the estimated position can be affected, so errors occur in the position estimation.

The basic PMSM control strategies and their characteristics are presented further on.

Vector control or field oriented control (FOC) was developed during the 1980s, it is based on the steady state relationships and ensures the decoupling between the flux and the torque. The flux is a function of the field current, known as the d-axis current or the flux producing current. Keeping it constant, the torque is controlled by the armature current, which is the q-axis current or the torque producing current.

In standard vector control, the currents in d - q coordinates are required for a precise and independent control of the flux and the torque. Hence, the three phase PMSM input currents will be transformed to the two phase system in rotor reference frame in (6).

The three phase currents for a PMSM are:

$$I_a = I_S \cdot \sin(\omega_r \cdot t); \quad (1.3)$$

$$I_b = I_S \cdot \sin\left(\omega_r \cdot t - \frac{2\pi}{3}\right); \quad (1.4)$$

$$I_c = I_S \cdot \sin\left(\omega_r \cdot t + \frac{2\pi}{3}\right); \quad (1.5)$$

Where ω_r is the rotor speed.

The transformation matrix for the d - q axes currents calculation is:

$$\begin{bmatrix} I_q \\ I_d \end{bmatrix} = \frac{2}{3} \cdot \begin{bmatrix} \cos(\omega_r \cdot t) & \cos\left(\omega_r \cdot t + \frac{2\pi}{3}\right) & \cos\left(\omega_r \cdot t - \frac{2\pi}{3}\right) \\ -\sin(\omega_r \cdot t) & -\sin\left(\omega_r \cdot t + \frac{2\pi}{3}\right) & -\sin\left(\omega_r \cdot t - \frac{2\pi}{3}\right) \end{bmatrix} \cdot \begin{bmatrix} I_a \\ I_b \\ I_c \end{bmatrix} \quad (1.6)$$

The d - q axes currents and the torque angle for a given load are constant values. As shown in the phasor diagram, Fig. 1.2., the permanent magnet flux is along d -axis, hence, I_d current produces only a part of the d-axis flux, the rest of it being provided by the permanent magnets.

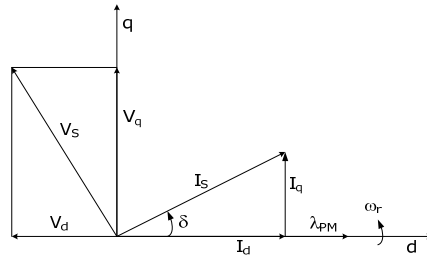


Fig. 1.2. PMSM phasor diagram;

The electromagnetic torque is the sum of the reluctance torque and the field torque and it is given by (7):

$$T_e = \frac{3}{2} \cdot p_1 \cdot [(L_d - L_q) \cdot I_d \cdot I_q + \Psi_{PM} \cdot I_q] \quad (1.7)$$

For $I_d=0$, the electromagnetic torque is:

$$T_e = \frac{3}{2} \cdot p_1 \cdot \Psi_{PM} \cdot I_q; \quad (1.8)$$

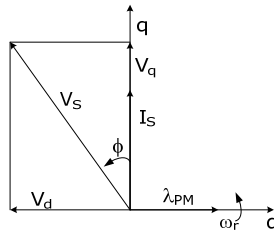


Fig. 1.3. PMSM phasor diagram at constant torque angle control;

The torque expressed in (8) is not constant if we consider that the permanent magnet flux is sensitive to the temperature fluctuations in the rotor [4]. If the iron losses are neglected, we can also minimize the stator current, for the copper losses minimization, so the total losses are minimized at a given torque. Considering this situation, the pair of I_d, I_q is uniquely obtained and therefore we have the maximum torque per ampere operation (MTPA). Through MTPA, the best efficiency is assured while generating the given reference torque [1].

Through **Direct torque and flux control (DTFC)** both the torque and the flux are directly controlled, through a combination of voltage vectors in the PWM inverter which supplies the motor (Fig. 1.4.). The table of optimal switching is based on the measurement results and implies the fact that the stator flux space vector variation follows the applied voltage space vector. If we want to increase the torque,

the flux vector has to be advanced in the direction of the motion. If the estimated stator flux position is calculated, then the voltage vector can be determined and the space vector modulation techniques can be applied. Using the voltage and current observer, and taking into account the voltage and current limits, the flux and then the torque will be calculated [28].

The DTC was initially presented by Takahashi et al. [29]. Some of the DTC [37], [38] main characteristics are the fact that it is well suited for the operation in the constant power region, it does not have an inner current loop, so there is no need for reference currents [30].

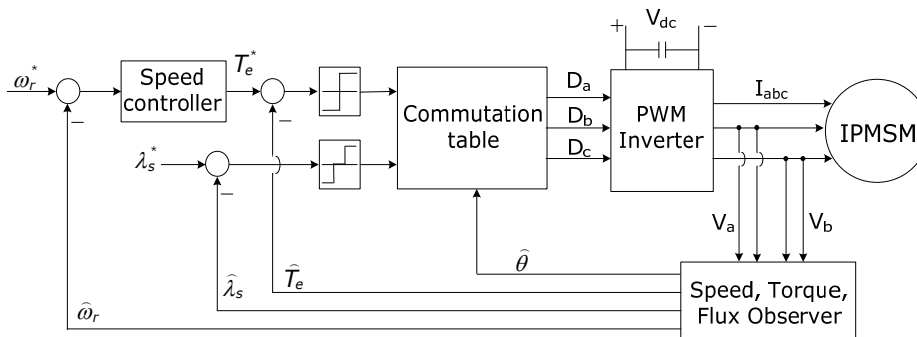


Fig. 1.4. Sensorless DTC (with commutation table) – general scheme;

The key of this control strategy is to find the optimal combination of “d” and “q” currents to get the fastest torque response the best efficiency.

As there are applications like pumps or ventilators that do not require high performance, **scalar control** represents a good solution for the electric drives management. Open loop V/f control, Fig. 1.5., is a scalar control based on the frequency and voltage magnitude proportional relationship. The system becomes instable when fast ramp acceleration is applied, hence the reference frequency is ramped for an increased stability of the drive.

The mathematical relation between the voltage and the machine frequency is given in (1.9):

$$V^* = V_0^* + f^* \cdot k \quad (1.9)$$

Where V_0^* is the voltage boost.

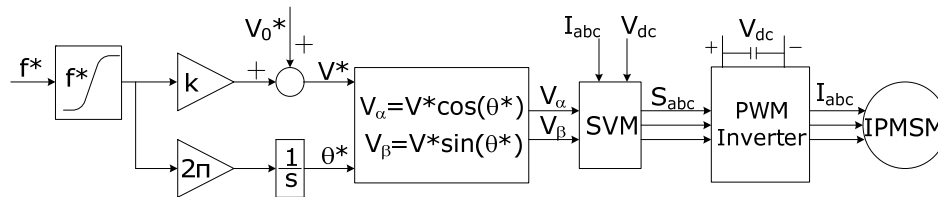


Fig. 1.5. Open loop V/f control scheme, smooth ramp prescribed frequency;

The V/f control strategy is suitable in applications which are characterized by low performance, such as pumps, compressors and fans and results up to full rated speed can be obtained.

Energy saving requirements can be achieved by a proper adjustment of the flux amplitude and trying to minimize the machine losses, for both scalar and vector control methods. In applications like pumps for oil or water movement, where dynamic requirements are not severe, but the efficiency and energy saving are priorities, highly utilized machines are the **interior permanent magnet motors** with the magnets embedded in the rotor structure.

1.4. Operating Principle of IPMSM Drives

The PMSMs have the field generated by the PMs, so the rotor topology depends on how the permanent magnets are placed in the rotor, so we can distinguish two of the most common types, the interior placed permanent magnets (Fig. 1.6a) and the surface mounted permanent magnets (Fig. 1.6b).

There also exists the PMSM with inset magnets, which are placed directly under the rotor surface (salient pole machine).

The IPMSM have the magnets placed in the middle of the rotor laminations in radial or circumferential orientations, this configuration makes them good candidates for high frequency based sensorless control, it is mechanically robust and it is more complex than for the surface mounted magnets. For IPMSM the dq inductances differ so both magnet and reluctance torque are produced.

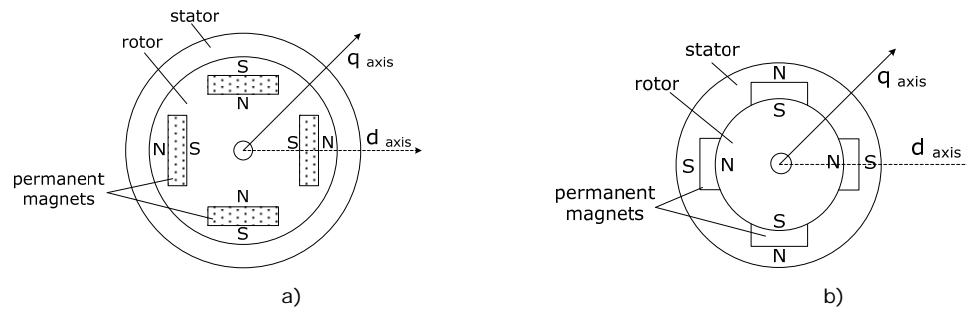


Fig. 1.6. a) IPMSM structure; b) SPMSM structure;

The „d” axis saturation occurs due to the magnet, but it does not significantly change when the fundamental current is injected, in contrast with the „q” inductance which can vary as the operating conditions change.

The market of industrial motor drives for low and medium power applications more and more adopts the Interior Permanent Magnet Synchronous Motors (IPMSMs), especially because of the recent progress of the rare earth magnet such as NeFeB.

Interior Permanent Magnet Synchronous Motors (IPMSMs) are known to have several advantages:

- increased efficiency (the copper loss associated with field windings does not exist);
- rugged construction (the lack of brushes and the use of PMs to generate the field allow to design these machines with less weight and compact size);
- high torque density (as the d, q-inductances are not equal, the reluctance torque contribution has also to be considered);
- moreover, the capability of operating above base speed (in case of high saliency, the speed domain at constant power goes above 3/1);
- high power factor;
- easy maintenance;

The permeability of the PMs which is almost equal to that of air and the fact that the PMs are inserted inside of the rotor (as shown in Fig. 1.7.), contribute to the asymmetry of the rotor reluctance. This PMSM configuration is desirable because of the higher efficiency point of view and of the smaller stator excitation for the same power output.

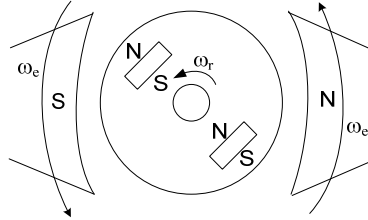


Fig. 1.7. IPMSM operating principle [1];

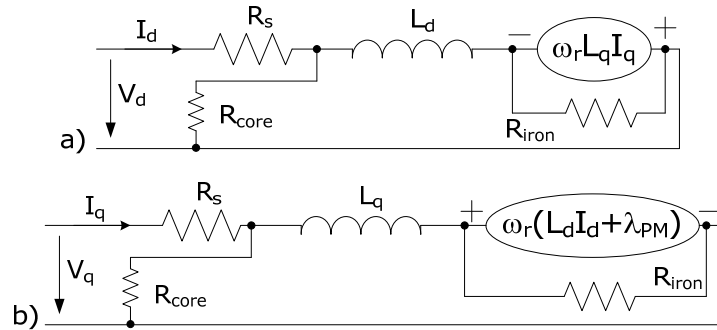


Fig. 1.8. IPMSM a) d-axis equivalent circuit; b) q-axis equivalent circuit;

Based on the motor equivalent schemes along d, q axes, shown in Fig. 1.8.

a), b) the „d” and „q” voltage equivalent equations can be written:

$$V_d = R_s \cdot I_d + L_d \cdot \frac{d}{dt} \cdot I_d - \omega \cdot L_q \cdot I_q ; \quad (1.10)$$

$$V_q = R_s \cdot I_q + L_q \cdot \frac{d}{dt} \cdot I_q + \omega \cdot (L_d \cdot I_d + \Psi_{PM}) ; \quad (1.11)$$

The use of an IPMSM for electric drive applications requires the initial rotor position information [7-9] and continuous rotor position feedback to power the motor with sinusoidal voltages and currents from the inverter system. The rotor position information is generally provided by an encoder, a resolver or a Hall sensor. Position sensors limit the operation of the motor because they are temperature sensitive, they are speed limited, they introduce mechanical oscillations and they need special external circuits to assure the position information accuracy. Some other drawbacks of the position sensors are the higher cost of the drive, the machine size is increased (in case of small power drives), while the system reliability and robustness are also decreased. Due to all these limitations, the trend is to eliminate position sensors; consequently, motion-sensorless field oriented

control (FOC) and direct torque and flux control (DTFC) drives are used more and more [10-15].

1.5. IPMSM Sensorless Control Techniques

Intensive research of advanced sensorless control schemes for AC drives has been realized during the last few years.

Sensorless control schemes main advantages are the absence of the position sensor which makes the drive more compact, assures less maintenance, lower cost of the drive, reduced electrical noise and so on. Moreover, sensorless control schemes can be used for emergency operations in case of the position sensor failure, which will keep the drive running until a repair allows an emergency stop and avoids damages.

The first class of sensorless methods uses the classical dynamic equations of the AC machine, with a sinusoidal flux density distribution, neglecting the space harmonics and other secondary effects. The second category exploits the asymmetries of the machine resulting from either the geometry of the design or from the saturation of the iron path.

Servo-drives and general drives (speed control range between 10/1 and 1000/1), but with fast full torque response (2-4 milliseconds), motion-sensorless FOC and DTFC drives have spread in a spectacular way [20-25].

Most flux, position, speed estimators for motion sensorless drives are based on fundamental methods and a simple solution is the integration of the induced voltages [10-12]. These strategies are limited to 3-5 rpm minimum speed safe operation (with some torque perturbation rejection), though occasionally down to zero speed operation is shown in peculiar conditions [21]. Therefore, at low speeds we have to correct the integrator for a practical range of operations down to zero speed.

For non-hesitant starting under load and prolonged 1-5rpm operation, frequency injection (or special PWM voltage) state estimators are used [22-26]. We have to take into consideration that using FOC or DTFC control method, some problems usually arise at startup because of the unknown initial rotor position.

A question arises: is it possible to obtain high dynamic response control in General AC Drives (speed control range 10/1-30/1) with implicit self-starting capability by adequately and quickly stabilizing V/f control systems?

We have to see where we stand with V/f control. Assessing carefully the progress so far, we notice that, with two exceptions [31], [32], all stabilizing loops are slow in action.

They provide: slip frequency compensation in IMs for stability and small steady state error without speed close loop [33]; voltage on stator leakage reactance boost and slip frequency compensation and a novel nonlinear torque – speed estimation based slip frequency compensation for IMs [33] and frequency dynamic correction based on the DC-link power pulsation with stability analysis [34] for speeds up to 2500 rpm for PMSMs. None of the above V/f control schemes with stabilizing loop is characterized by quick response in torque or speed.

In contrast, in [32], for a SPMSM, a V/f control strategy with two stabilizing loops: ΔV for reference voltage amplitude and $\Delta \gamma$ for voltage reference angle are applied: the first one slow, the second one faster, but both based on zeroing the interior steady state reactive power ($i_d=0$ control): $Q_i = 0$.

Starting from this situation, we want to introduce here a general fast dynamics, V/f control with two stabilizing loops for all AC drives, again one for voltage amplitude and one for voltage angle. This method represents our proposed solution and will be better described further on, as it is supposed to provide fast dynamics speed and torque response, even when full load torque is applied.

1.6. Flux weakening region for PMSM

The speed and torque of variable speed drive systems which are controlled by PWM inverters are limited by the inverter current and DC-link voltage rated values and by the electric machine. These limits have a great impact on the PMSM speed range, with maximum torque capability, so to extend the IPMSM operation range, the flux weakening has to be considered.

Improving the control methods, we can extend the synchronous motor flux-weakening region [1]. Therefore, by a proper flux weakening method, the current reference can be set to achieve the maximum available torque taking into account the voltage and current constraints. The speed up to which the motor is controlled under MTPA mode is called base speed and it is called the constant torque region, while after the base speed is overcome, we have the described flux weakening region.

To better understand the flux weakening scope in a drive we have to know the maximum operating speed.

R. Krishnan considers in [4] that the flux weakening control schemes can be classified in two main categories, one based on the machine model and its parameters, which can be indirect or direct control scheme and the second one which do not consider the machine parameters and is classified in two categories: adaptive control scheme and six-step control scheme.

Some of the most used flux weakening methods and both advantages and drawbacks will be presented further on.

Flux Weakening Control with **Feed-Forward compensation** is based on the steady-state voltage equations of the motor. The torque command is limited to the available maximum value at the operating speed, while the optimal current is calculated considering the current and voltage constraints (12), (13) from the steady-state equations (14) and (15).

$$V_d^2 + V_q^2 \leq V_{s\max}^2 \quad (1.12)$$

$$I_d^2 + I_q^2 \leq I_{s\max}^2 \quad (1.13)$$

Where, $V_{s\max}$ is imposed by the DC-link voltage of a PWM inverter and $I_{s\max}$ can also be imposed by the inverter, as well as by the AC machine. The two values are considered to be constant on the assumption that the DC voltage is a constant value [4].

$$V_d = R_s \cdot I_d + L_d \cdot \frac{d}{dt} \cdot I_d - \omega_r \cdot L_q \cdot I_q \quad (1.14)$$

$$V_q = R_s \cdot I_q + L_q \cdot \frac{d}{dt} \cdot I_q + \omega_r \cdot (L_d \cdot I_d + \Psi_{PM}) \quad (1.15)$$

Therefore, the voltage phasor can be written:

$$V_s = \sqrt{V_d^2 + V_q^2} \quad (1.16)$$

The main drawback of this open loop compensation method is the parameters variation, which degrades the system performance.

Flux Weakening Control with **Feedback Compensation** keeps the current regulator output voltage within the constraint value, by using the difference between the voltage limit and the current regulator output voltage as feedback to the flux weakening regulator.

The output of the flux weakening regulator represents the “d” axis current, used further on to adapt the machine flux, Fig. 1.9.

This method is characterized by the robustness to the parameters variation during different operating conditions.

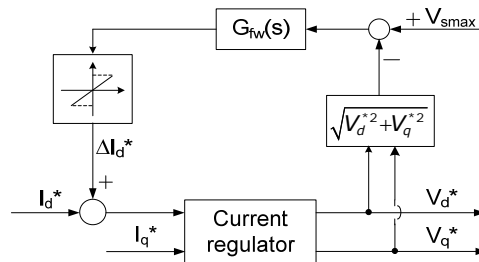


Fig. 1.9. Flux weakening scheme, with I_d^* correction.

1.7. Proposed solution: V/f control with two stabilizing loops

Field oriented control (FOC) and Direct Torque and Flux Control (DTFC) of AC Drives are credited with fast torque response, but in General purpose sensorless AC Drives, the online software and hardware effort and their reliability may seem prohibitive for general applications [10-15] or, at least for synchronous motors, case in which a starting strategy is necessary [20-25].

Starting from this situation, we introduce here a general fast dynamics, V/f control with two stabilizing loops for all AC drives, one for voltage amplitude and one for voltage angle. The stabilizing loops are based on the “active flux” concept, MTPA operation and flux weakening are also considered.

The “active flux” concept introduced in [35] is used to develop the two novel stabilizing loops for V/f control.

The use of the proposed control strategy avoids the usual switching from signal injection based to model based position estimation in FOC or DTFC during starting.

By implementing the control described above, we want to prove that V/f with stabilizing loops control can provide high dynamic performance, without the usual speed or current regulators, without coordinate

transformations and with less computation effort than sensorless vector control, for general AC Drives.

All on-line calculations are based on the active flux concept in order to simplify mathematical expressions with securing both flux weakening and close to maximum efficiency operation in the process.

Both experiments and simulations have been conducted and the results have been compared to validate the effectiveness of the proposed V/f control.

1.7.1. Scope and realization

Open loop V/f control is rather simple to implement and use, but it is prone to instability areas, the drive is vulnerable to fast ramp accelerations or large torque perturbations [28]. This V/f control strategy can only give results for moderate performance. Therefore, it needs stabilizing loops to reduce oscillations and improve drive stability of the drive. For this reason, V/f control can be implemented only with one current stabilizing loop or a frequency correction loop, though there can also be a second loop to control the voltage vector amplitude or phase.

IPMSM can be controlled with standard V/f scheme, which represents a good compromise in applications like fans, pumps, heaters, where the reduced energy consumption is a demand, but fast speed or torque response is not a requirement.

Hence, to remove the drawbacks of this control method and to gain stability and fast speed and torque response, we proposed two correction loops, one for the voltage vector amplitude correction, the other one for the voltage vector phase. More than that, using the corrected V/f control, firstly, we solve the initial rotor position problem and secondly, we gain lower computation time, as no PI regulators for current or speed are used. To prove the above mentioned claims, four different V/f control strategies with stabilizing loops have been proposed and analyzed. Comprehensive digital simulations and experimental results have been developed for each method. Results for the above described control strategies are illustrated in the following chapters.

Besides V/f with stabilizing loops, the sensorless field oriented control active flux based has also been discussed in the thesis and comparisons between the two control methods were displayed.

1.8. Conclusion

In this chapter, a state of the art of the permanent magnet synchronous drives and a review of their control with and without motion sensor have been presented.

Both advantages and disadvantages of the two main control strategies with and without position sensors have been highlighted.

The use of the encoder is important for a complete modeling of a machine, for the calculation of all state variables and not the least, for safety reasons: emergency stop, controlled stop in case of blackout.

If we consider the industrial motor drives point of view, we can surely say that the use of synchronous motors has become more and more interesting.

Yet, there is still a hesitant acceptance for the sensorless control schemes on the manufacturer's side taking into account the practical requirements which have to be fulfilled [27].

For the implementation of the sensorless control schemes in commercial drives the following aspects have to be considered: parameters automatic tuning and compensation of their variation, a suitable starting procedure, a smooth switching between the mode with and without sensors.

References

- [1] Seung-Ki Sul, "Control of Electric Machine Drive Systems", pp. 424, John Wiley and Sons, INC., Publication, ISBN: 978-0-470-59079-9;
- [2] C. Lascu, "Direct Torque Control of Sensorless Induction Machine Drives", Ph. D. Thesis, Timisoara, 2002;
- [3] I. Boldea, A. Moldovan, V. Coroban-Schramel, G.D. Andreescu, L. Tutelea, „A class of fast dynamics Vf sensorless AC General Drives with PM-RSM as a case study”, Optimization of Electrical and Electronic Equipment (OPTIM), 2010 12th Int. Conf. on, 20-22 May 2010, ISBN 978-1-4244-7019-8, pp. 453-459;
- [4] R. Krishnan, "Permanent Magnet Synchronous and Brushless DC Motor Drives", CRC Press, Taylor & Francis Group, 2010, ISBN 978-0-8247-5384-9;
- [5] R. Ancuti, „Fast Dynamics Response of Sensorless Control of High Speed Surface Permanent Magnet Synchronous Motor Drives”, Ph. D. Thesis, „Politehnica” Publishing House, 2008;
- [6] K. Hyunbae, Kum-Kang Huh, R.D. Lorenz, T.M. Jahns, "A novel method for initial rotor position estimation for IPM synchronous machine drives", Industry Applications, IEEE Trans. on, Sept.-Oct. 2004, vol. 40, no. 5, pp. 1369-1378 ISSN: 0093-9994;
- [7] Q. Jilong, T. Yantao, G. Yimin, Zhucheng, "A Sensorless Initial Position Estimation Scheme and Extended Kalman Filter Observer for the Discret Torque Controlled PMSM Drive", Proc. of Electrical Machines and Systems, ICEMS 2008, International Conference on, pp. 3945-3950, 17-20 October, 2008, ISBN: 978-1-4244-3826-6;
- [8] G. Wang; R. Yang; Y. Wang; Y. Yu; D. Xu; "Initial rotor position estimation for sensorless interior PMSM with signal injection", Proc. of Power Electronics Conference (IPEC), 2010 Internat, pp. 2748-2752;
- [9] C. Xiang, G. Shan Mao, Y. Sheng Wen, W. Lei, "Study on initial rotor position identification of permanent magnet synchronous motor based on high frequency signal injection", Proc. of Informatics in Control, Automation and Robotics (CAR), 2010 2nd International Asia Conference on, Vol.2, ISSN 1948-3414;

- [10] C. Lascu, I. Boldea, F. Blaabjerg, "Direct torque control of sensorless induction motor drives: A sliding-mode approach", *IEEE Trans. on Ind. Applicat.*, Vol. 40, No. 2, pp. 582–590, 2004;
- [11] P. Guglielmi, M. Pastorelli, G. Pellegrino, A. Vagati, "Position sensorless control of permanent-magnet-assisted synchronous reluctance motor", *IEEE Trans. on Ind. Applicat.*, Vol. 40, No. 2, pp. 615–622, 2004;
- [12] S. Morimoto, M. Sanada, Y. Takeda, "Mechanical sensorless drives of IPMSM with online parameter identification", *IEEE Trans. on Ind. Applicat.*, Vol. 42, No. 5, pp. 1241–1248, 2006;
- [13] S. K. Sul, Y. Yoon, S. Morimoto, K. Ide, "High Bandwidth Sensorless Algorithm for AC Machines Based on Square-wave Type Voltage Injection", *Proc. of IEEE ECCE 2009*, pp. 2123-2130, 2009;
- [14] P. Guglielmi, M. Pastorelli, A. Vagati, "Cross-Saturation Effects in IPM Motors and Related Impact on Sensorless Control", *IEEE Transactions on Industry Applicat*, 2006, Vol. 42, No.6, pp. 1516-1522;
- [15] N. Bianchi, S. Bolognani, "Sensorless-Oriented-Design of PM Motors", *Proc. of Ind Applicat Conference, 42nd IAS Annual Meeting. Conference Record of the 2007 IEEEPP*, pp. 668-675;
- [16] N. Ertugrul, Acarnley, P. "A new algorithm for sensorless operation of PM motors"; *Industry Applications*, *IEEE Trans. on*, Vol. 30, No.1, pp. 126–133;
- [17] N. Matsui, M. Shgyo, "Brushless DC Motor Without Position and Speed Sensors, " *IEEE Transactions on Industry Applications*, Vol. 28, No.1, pp.120-127, January/February 1992;
- [18] N. Matsui, T. Takeshita, K. Yasuda, "A New Sensorless Drive of Brushless DC Motor", *IEEE IECON*, pp.430-435, 1992;
- [19] N. Matsui, "Sensorless-Operation of Brushless DC Motor Drives", *IEEE IECON 93 Proceedings*, PP. 739-744, 1993;
- [20] Z. Chen, M. Tomita, S. Ichikawa, S. Doki, and S. Okuma, "Sensorless control of interior permanent magnet synchronous motor by estimation of an extended electromotive force", in *Conf. Rec. IEEE IAS 2000 Annual Meeting, Rome, Italy, 2000*, vol. 3, pp. 1814–1819;

-
- [21] L. Harnefors, J. Luomi, M. Hinkkanen, „Reduced-Order Flux Observers with Stator-Resistance Adaptation for Speed-Sensorless Induction Motor Drives“, IEEE ECCE 2009;
- [22] M. Linke, R. Kennel, and J. Holtz, “Sensorless speed and position control of synchronous machines using alternating carrier injection”, in Proc. IEEE Int. Electric Mach. Drives Conf. (IEMDC’03), Madison, 2003, vol. 2, pp.1211–1217;
- [23] S. Shinnaka, “New mirror-phase vector control” for sensorless drive of permanent – magnet synchronous motor with pole saliency”, IEEE Trans on. Ind. Applicat., vol. 40, no. 2, pp. 599–606, Mar.–Apr. 2004;
- [24] M. W. Degner and R. D. Lorenz, “Using multiple saliencies for the estimation of flux, position, and velocity in AC machines”, IEEE Trans.on Ind. Applicat., vol. 34, no. 5, pp. 1097–1104, Sep./Oct. 1998;
- [25] H. Kim, K. K. Huh, M. Harke, J. Wai, R. D. Lorenz, and T. A. Jahns, “Initial rotor position estimation for an integrated starter alternator IPM synchronous machine”, in Proc. 10th Eur. Conf. Power Electron. Applicat. (EPE-2003), Toulouse, France, 2003, pp. 1875–1881;
- [26] Ide, K. Iura, Inazumi, M., Hybrid sensorless control of IPMSM Combining high frequency injection method and back EMF method, IECON 2010 - 36th Annual Conference on IEEE Industrial Electronics Society, 7-10 Nov. 2010, pp. 2236, ISBN: 978-1-4244-5225-5;
- [27] M. Pacas, „Sensorless Drives in Industrial Applications“, IEEE Industrial Electronics Magazine, vol. 5, Issue. 2, 17 June 2011;
- [28] I. Boldea and S.A. Nasar, Electric Drives, 2nd edition, New York: CRC Press Taylor and Francis, ISBN 0-8493-4220-1, 2005;
- [29] I. Takahashi, T. Noguchi, “A New Quick-Response and High-Efficiency Control Strategy of an Induction Motor”, IEEE Trans. Ind. Appl., Vol. IA-22 (1986), pp. 820-827;
- [30] M. Meyer, T. Grote, J. Böcker, “Direct Torque Control for Interior Permanent Magnet Synchronous Motors with Respect to Optimal Efficiency”, Power Electronics and Applications, 2007 European Conference on, ISBN: 978-92-75815-10-8, pp.1–9, 2-5 Sept. 2007;

- [31] R. Ancuti, I. Boldea, G.D. Andreescu, D. Iles, "Novel motion sensorless control of high-speed small-power surface mount PMSM drives with experiments", Record of OPTIM -2008, vol.3, pp.11-18 (IEEEExplore);
- [32] R. Ancuti, G.D. Andreescu and I. Boldea, "Four rotor position and speed simplified estimators for vector control of high-speed SPMSM with test comparisons", Journal of electrical engineering, JEE, vol.7, no.4, Politehnica Publishing House, Timisoara, 2007.
- [33] K. Koga, R. Ueda, T. Sonada "Constitution of V/f control for reducing steady state error to zero in induction machine drive to zero in IM drive system"; IEEE Trans. on, vol. IA-28, no. 2, 1992, pp. 463-471;
- [34] P.D.C. Perera, F. Blaabjerg, J.K. Pedersen, P.T. Thogersen, "A sensorless stable V/f control method for PMSM drives", Industry Application IEEE Trans. on Vol.39, no.3, 2003, pp.783-791;
- [35] I. Boldea, M.C. Paicu, G.D. Andreescu, "Active flux concept for motion-sensorless unified ac. drives", IEEE Transactions on Power Electronics, vol. 23, no.5, 2008;
- [36] P. Vas, "Sensorless vector and Direct Torque Control", Oxford University Press, 1998, ISBN 0-19-856465-1;
- [37] Das, S.P. Gupta, R.K., Direct torque control (DTC) of interior permanent magnet synchronous motor (IPMSM) with and without speed/position sensors, Power Electronics (IICPE), India International Conference on, 28-30 Jan. 2011, ISBN: 978-1-4244-7883-5;
- [38] Y. Inoue, S. Morimoto, M. Sanada, "Examination and Linearization of Torque Control System for Direct Torque Controlled IPMSM", Industry Applications, IEEE Trans on, Jan.-feb. 2010, Vol. 46, No. 1, pp. 159, ISSN: 0093-9994.

Chapter 2

Comprehensive characterization of IPMSM Drive and Vector Control Test Results, with Encoder

Because of its numerous advantages, the Interior Permanent Magnet Synchronous Machines are increasingly used during high performance industrial drives, especially related to automotive domain [1], [2], [16], [19], [20]. Thus, precise estimation of the motor parameters [17] is needed, especially if we admit that motor sensorless functioning [21] is our main concern.

The aim of this chapter is to present a comprehensive experimental and theoretical characterization and parameter determination of IPMSM, through experimental analysis. Both standstill and running tests have been performed, using a lab IPMSM prototype, as case study.

After the motor characterization, the following interest in this chapter is to digitally and experimentally implement a vector control scheme and to achieve results for two different IPM synchronous machines. The first motor is an IPMSM prototype, with fractionary windings which has been built up by "Electromotor" Enterprise, Timisoara and its capabilities will be determined further on, by experimental tests, while the second one is a Siemens Machine, with distributed windings, with given and well established parameters. The specifications for both IPM motors are given in Chapter 7, Table 7.1 and Table 7.2, respectively.

As there is no standard motor configuration, we have to admit that diligent work like: analytical optimization, FEM analysis, direct geometrical optimization, prototype construction and experimental validation is needed in order to obtain better motor topologies that can achieve the application requirements [2]. We also have to specify that the rotor saliency [18] was not taken into consideration.

Further on, field oriented control tests at different speeds, for both no-load and also at load operation have been conducted and results are afterwards shown and discussed.

2.1. IPMSM Structure and Experimental analysis

Experimental analysis has the scope to provide the machine parameters which are necessary for further system simulations and experimental tests. Accurate estimation and validation of machine parameters is of a great importance for the development of high performance drive systems [3].

In order to efficiently analyze performance and design fast and efficient controllers, accurate knowledge of the machine parameters is needed [4]. There are three essential parameters that have to be well known and they are: permanent magnet linkage and d and q axis inductances [22], [23]. Therefore, a comprehensive measurement procedure will be described during this chapter.

Firstly, the IPM synchronous machine structure and vector diagram are shown (Fig. 2.1.) and its mathematical model is written afterwards (2.1) – (2.3).

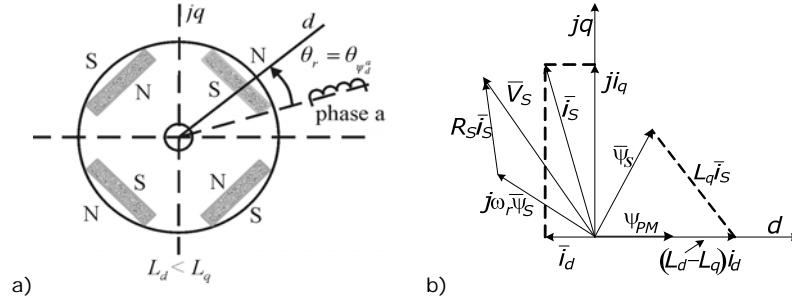


Fig. 2.1. Vector diagrams for IPMSM, $L_d < L_q$: a) IPMSM structure; b) IPMSM vector diagram, I_d

$$\bar{V}_s = R_s \cdot \bar{i}_s + \frac{d\bar{\lambda}_s}{dt} + j \cdot \omega_r \cdot \bar{\lambda}_s; \quad (2.1)$$

$$\bar{V}_s = V_d + j \cdot V_q; \quad \bar{i}_s = i_d + j \cdot i_q; \quad \bar{\Psi}_s = (L_d \cdot I_d + \lambda_{PM}) + j \cdot L_q \cdot I_q; \quad (2.2)$$

$$T_e = \frac{3}{2} \cdot p \cdot (\lambda_{PM} + (L_d - L_q) \cdot I_d) \cdot I_q; \quad (2.3)$$

Where \bar{V}_s , \bar{i}_s and $\bar{\Psi}_s$ are the stator voltage, current and flux vector; L_d , L_q are the dq axes inductances; λ_{PM} is the permanent magnet flux linkage; R_s is the stator resistance; ω_r is the electrical rotor speed and p is the number of pole pairs.

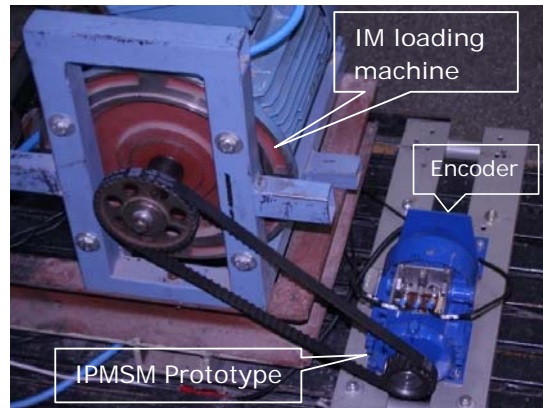


Fig. 2.2. IPMSM-laboratory prototype, with fractionary windings

The experimental motor (Fig. 2.2.), the complete laboratory setup, including the power electronic and the measurement devices are fully described during Chapter 7.

There are several methods presented in the literature for the estimation of electromagnetic excited SM [3], [5]-[10], but most of them cannot be applied to PMSM, if we take into account that the PM excitation cannot be disabled or require rather expensive and complicated equipment.

The mathematical machine model embedded in system simulations and experiments need precise parameters, if accurate results are expected [5]. Further on, several tests for model parameters estimation will be embedded in a quick, inexpensive and practical guide for IPMSM drive experimental characterization.

The torque is not directly measured; it is estimated from the measured currents. The measurement procedure consists of several tests which were chosen in order to allow the machine parameters estimation in a wide area of variation. It has to be mentioned that the thermal and acoustic behavior were not considered.

2.2 Standstill measurements

First, we have to measure the phase resistance (Fig.2.3), as it is used further on for other parameter determination.

There are a few easy ways to estimate the resistance, like: a precision Ohmmeter a RLC bridge or a multimeter.

Supposing that the motor is symmetrical, we can consider that each phase has the same impedance. The measurements have been done directly on the motor terminals. The resistance measurement has been done by supplying the machine from a dc voltage source (4).

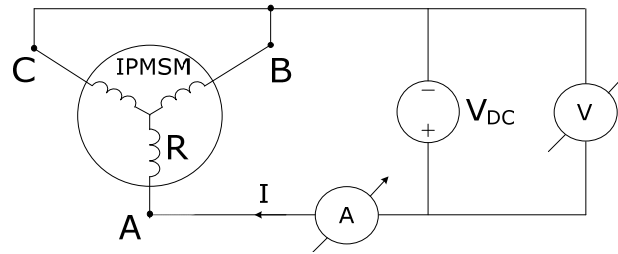


Fig. 2.3. The phase resistance measurement scheme

The equivalent motor resistance (R_{ech}) has the formula:

$$R_{ech} = \frac{V_{DC}}{I} \quad (2.4)$$

With the above described method, we obtained $R=0.138 \Omega$, but when supplied by an inverter, the voltage drops within the latter and along the cables should be considered, increasing the equivalent resistance to $R=0.2 \Omega$.

A static test with locked rotor, in order to prevent any induced voltage caused by the magnetic field movement was performed to estimate the inductances along d, q axes (Fig. 2.4).

While supplying the machine from an autotransformer as in Fig. 2.4 the rotor d axis aligns itself along phase a axis. This way, L_d can be obtained from the equivalent impedance. The same experiment can be repeated for q axis, but this time the rotor should be locked.

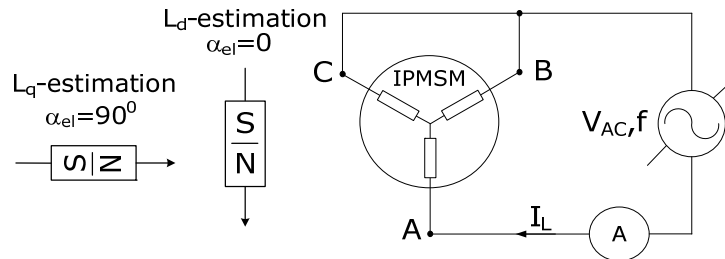


Fig. 2.4. "d, q" inductance estimation scheme

To simplify the modeling and all the calculations, an average value for both inductances $L_d=1.14e-3H$ and $L_q=1.286e-3H$ was considered, while the permanent magnet flux linkage was considered constant, $\lambda_{PM}=0.02\text{ Wb}$, even if in reality, it depends with the temperature.

2.3 Load performance testing

The IPMSM prototype was verified on a laboratory test-rig. It was controlled using vector control and both speed and current regulators were implemented through „Matlab/Simulink Package“. Experiments were carried out on the test-bench using DSpace 1103 and Control Desk interface.

TABLE 0.1

Experimental values for IPMSM, at different speeds and loads.

IPMSM						
n [rpm]	Te [Nm]	Vs [V]	P1 [W]	P2 [W]	Efficiency	I _s ^{peak} [A]
600	0.5	6	48.4	31.5	0.65	5.4
	1	7.5	111.6	63	0.56	10.8
	1.5	8.6	188.6	95	0.5	16.2
	2	9.6	278	127	0.47	21.6
	2.5	10.5	380	160	0.421	27
	3	12	496	192.5	0.388	32.4
1200	0.5	10.6	82	63	0.76	5.4
	1	13	175.2	126	0.72	10.8
	1.5	15	279.5	190	0.68	16.2
	2	16.5	392	255	0.65	21.5
	2.5	17.5	515	317	0.6155	27
	3	18.6	645	382	0.5922	32.5
1800	0.5	16.2	113	94	0.832	5.4
	1	19	232	188	0.81	10.8
	1.5	21	356.5	285	0.799	16.2
	2	23	482	380	0.788	21.5

To verify that the machine can produce the required torque at a specified speed, it was run as a generator. An induction motor drive held the speed constant at an imposed value, while the IPMSM prototype was in torque control.

Using the existing experimental bench (described during Chapter 7), experiments have been conducted to determine the motor efficiency, the losses and the peak value for the stator current at different speeds and loads, to show the motor capabilities. The measurement results are shown below, in Table 2.1.

As results show (Fig. 2.5), the IPMSM has a better efficiency at high speeds, where $\eta=83,2\%$, for 1800 rpm and 0.5 Nm load, than at lower speeds, where $\eta=38,8\%$ for 600 rpm and 3 Nm.

The rather small specific volume of the machine (as required in automotive applications) explains the moderate efficiency.

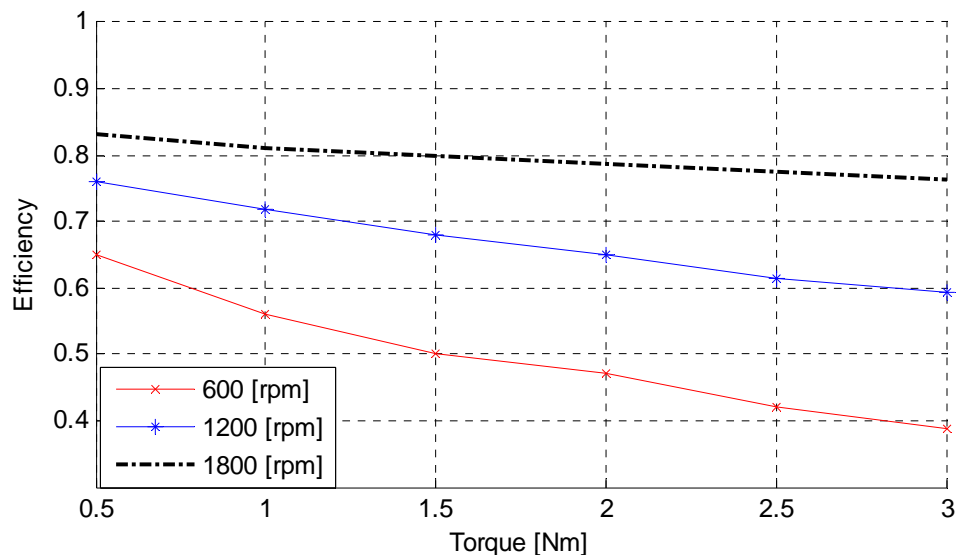


Fig. 2.5. Efficiency versus torque for different speed values

Further on, vector control general scheme is presented in Fig. 2.6. and experimental results are displayed next. The encoder is used to give the position information, information which is then used for both coordinate transformation and speed measurement.

2.4 Structure of current controllers

Both speed and current controllers were implemented, as shown in Fig. 2.7. and their parameters were adjusted in order to obtain fast dynamic responses.

The anti-wind-up speed controller regulates the speed to obtain the reference I_q^* current. Other two identical PI controllers are used to regulate the currents in d, q coordinates, to obtain the voltage reference values, V_d^* and V_q^* . During steady-state, the rotor fixed reference frame currents become constant (dc.) values [11]. This means that the PI regulators have to control the currents with no steady-state error.

Due to the cross-coupling in rotor coordinates, changes in V_d^* are reflected in V_q^* and afterwards in I_q^* . This is not a desirable situation, if we think about the system performance, because the currents should be independently controlled. Therefore, to avoid sluggish response of the drive and the current regulators saturation, voltage decoupling [12] was considered.

The torque was estimated, taking into account only its reluctance component, as i_d was prescribed 0 from the beginning.

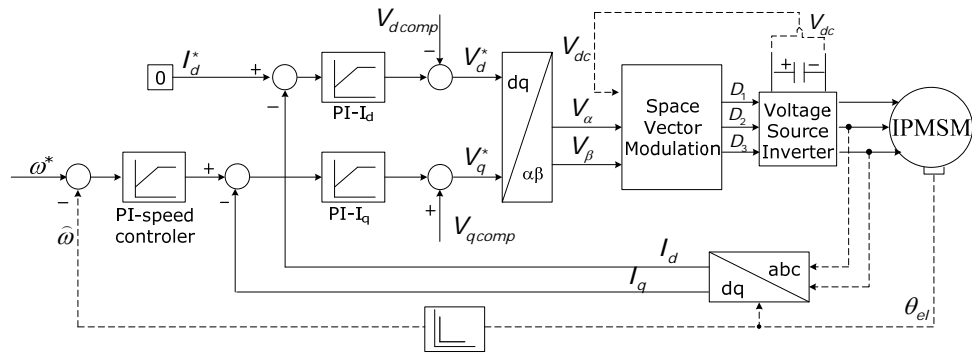
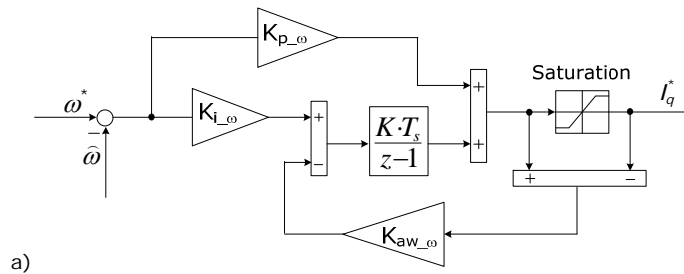


Fig. 2.6. Current Vector control – general scheme (I_d^*)



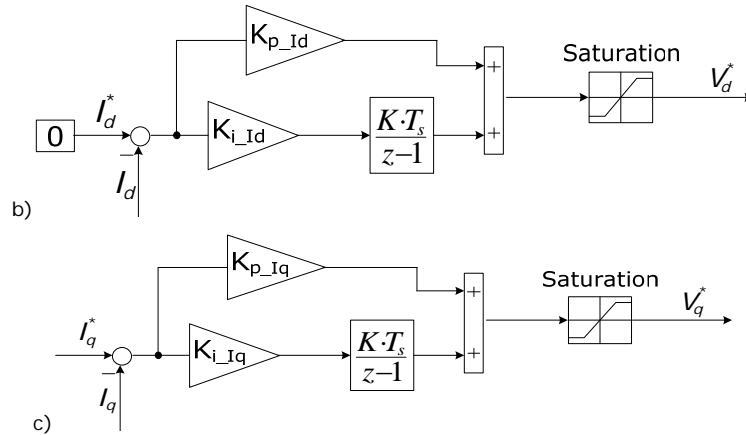


Fig. 2.7. PI controller structure: a) speed anti-wind-up PI; b) I_d current PI; c) I_q current PI

2.5. IPMSM With Fractionary Winding

2.5.1. Experimental results

First, experimental vector control results for different speeds and loads are shown, for the IPM synchronous motor prototype, with fractionary winding. Experiments were carried out for 600 rpm, 1200 rpm and 1800 rpm.

The machine general control scheme was developed in Matlab/Simulink environment and built automatically using the dSpace system, as in Fig. 2.8.

I_d^* current was prescribed zero, while the speed and current controllers have been implemented using the above shown schemes (Fig. 2.7.a,b,c), taking into account the below determined coefficients.

PI speed controller	$K_p=0.1$	$K_i=2$
PI i_d controller	$K_p=1$	$K_i=300$
PI i_q controller	$K_p=1.3$	$K_i=330$

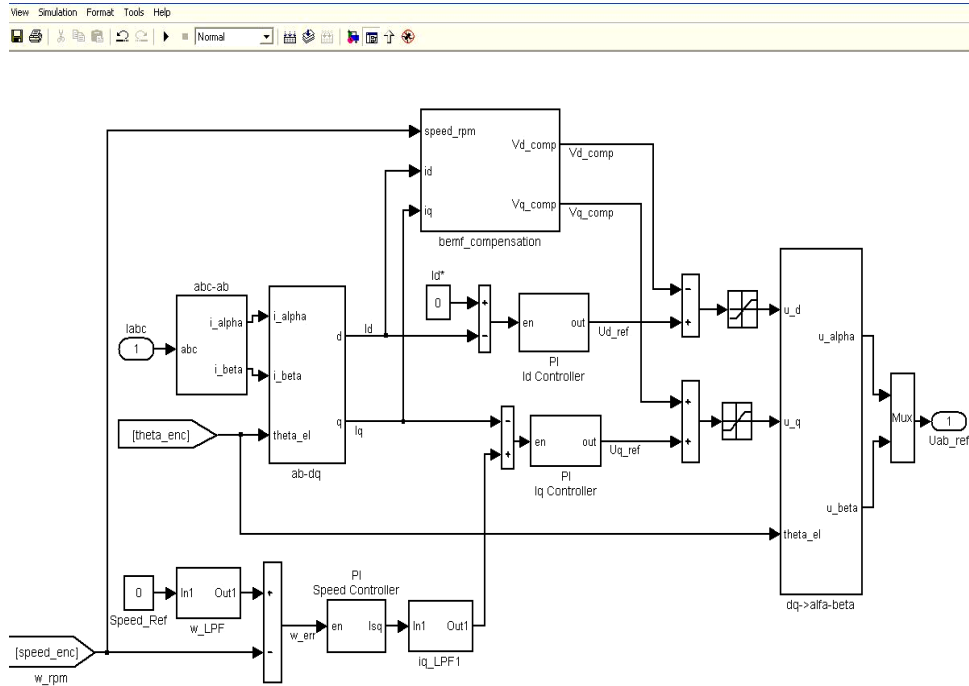


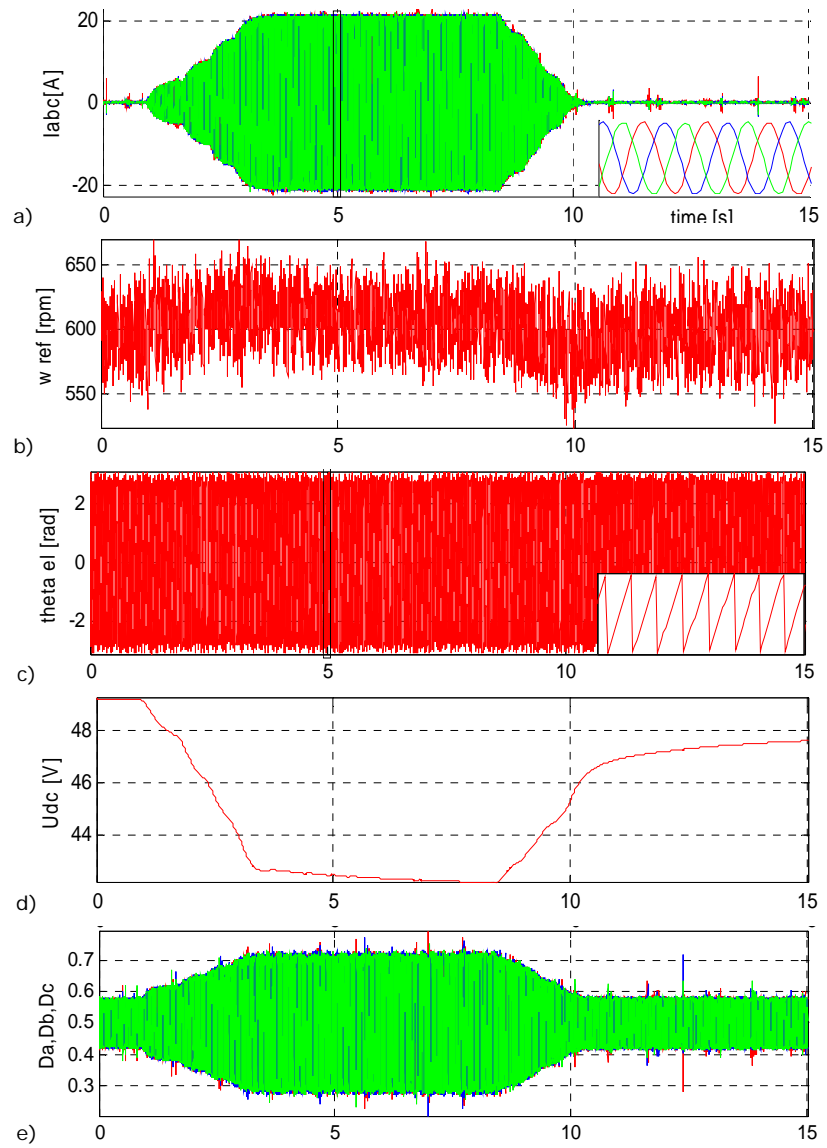
Fig.2.8. Vector control with encoder feedback in Matlab/Simulink, real-time implementation

Vector control results for 600 rpm (Fig. 2.9b) and a two seconds ramp up to 2 Nm load are shown during figure 2.9.

The shown results were taken when the machine was functioning in steady state regime, state when the load was also applied.

It can be noticed that the currents are fast increasing to more than 20 A (Fig. 2.9a) when a ramp load of 2 Nm (Fig. 2.9g) is applied at 1s, which results in dc voltage decrease in Fig. 2.9d. When the machine unloading two seconds slope occurs, the currents decrease, while the dc voltage rise back to its initial value. It can be easily observed that during both loading and unloading of the motor, the speed, which is a bit noisy from the beginning, varies with about ± 25 rpm around the target.

The noise during the measurements is a consequence of the timing belt [15] presence, which connects the IPM synchronous motor to the IPM synchronous generator. It introduces noise,



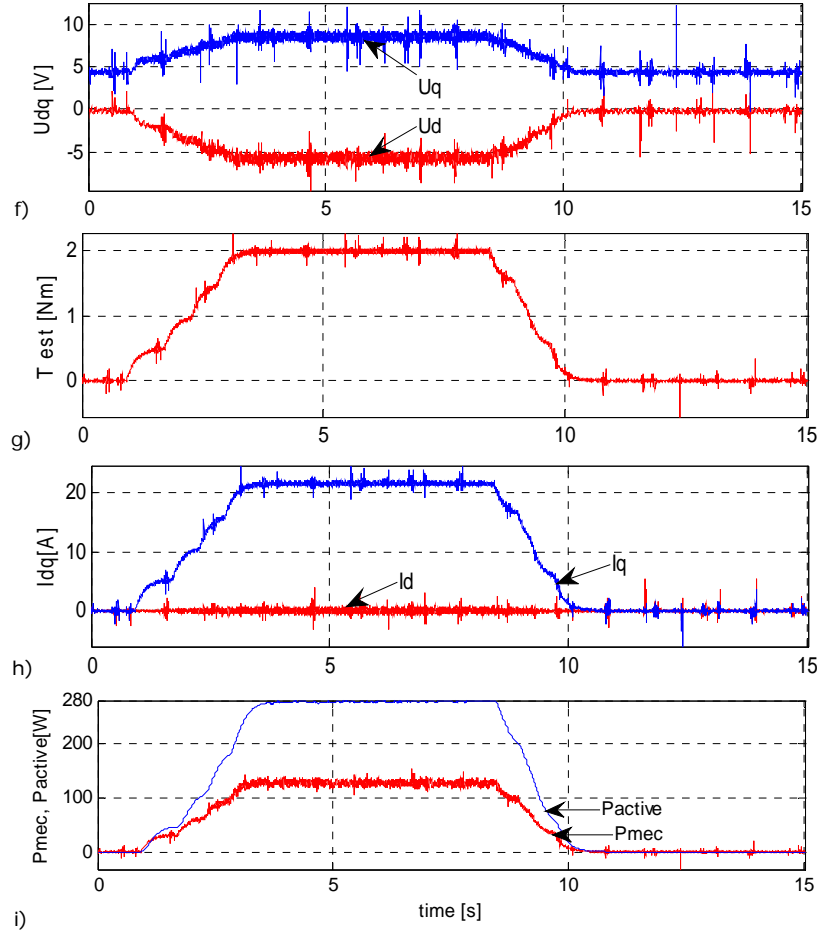


Fig. 2.9. Vector control experimental results for $n=600\text{rpm}$; $T_L=2\text{Nm}$: a) phase currents, b) speed, c) rotor position, d) estimated torque, e) dc voltage, f) inverter duty cycles, g) d,q voltage, h) d,q current; i) mechanical and active power;

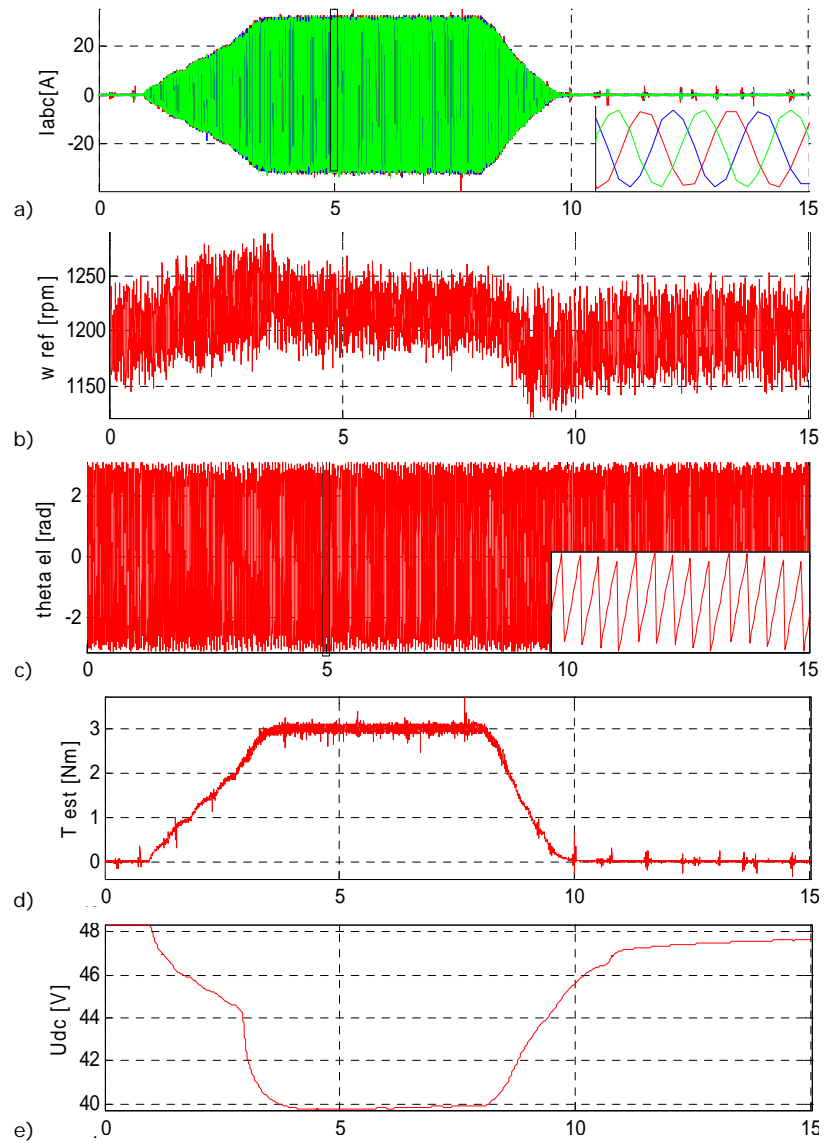
As we have previously mentioned, these experiments were conducted considering $I_d=0$, as it can be seen from Fig. 2.9h). The active and mechanical power (equations 2.6 and 2.7) have been illustrated in Fig. 2.9i, while the efficiency (2.8) was analytically calculated for each case and it was given in Table 2.1.

$$P_{active} = \frac{3}{2} \cdot (I_\alpha \cdot U_\alpha + I_\beta \cdot U_\beta) \quad (2.6)$$

$$P_{mec} = P_{active} - \frac{3}{2} \cdot I^2 \cdot R_s \quad (2.7)$$

$$\eta = \frac{P_{mec}}{P_{active}} \quad (2.8)$$

Further on, vector control results for 1200 rpm (Fig. 2.10 b) and a two seconds ramp up to 3 Nm load (Fig. 2.10d) are shown in figure 2.10.



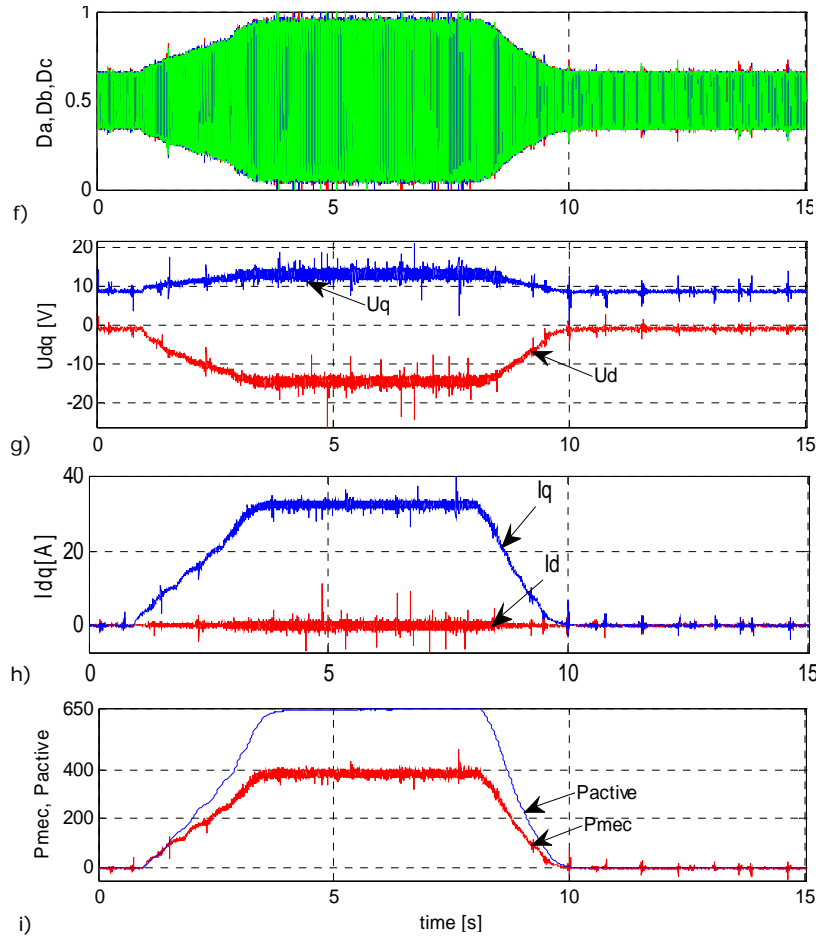
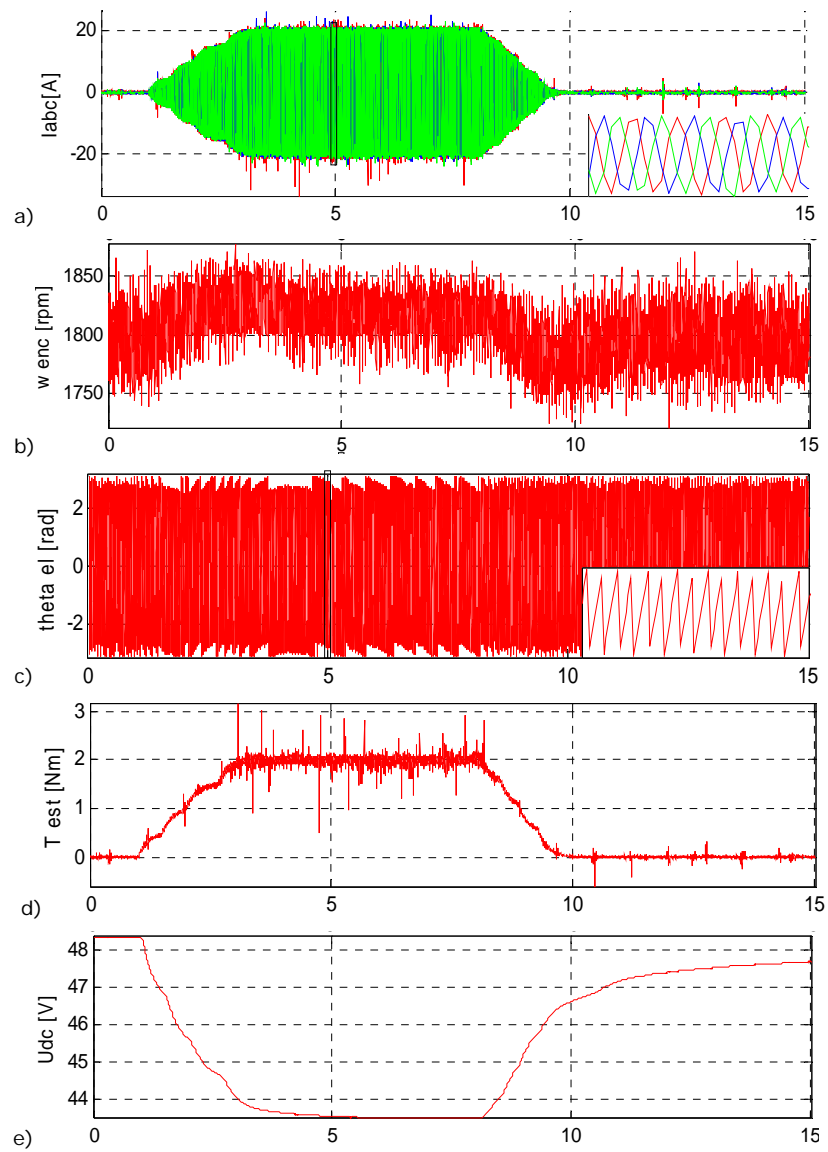


Fig. 2.10. Vector control experimental results for $n=1200$ rpm; $T_L=3$ Nm: a) phase currents, b) speed, c) rotor position, d) estimated torque, e) dc voltage, f) inverter duty cycles, g) d,q voltage, h) d,q current; i) mechanical and active power;

In this case, the currents are growing up to 33 A (Fig. 2.10 a), while the dc voltage is decreasing to 40 V (Fig. 2.10 e). After machine stabilization and after 5 s of steady-state operating mode, a 2s unloading slope is applied, the currents decrease, while the dc voltage rises back to their initial values.

During Fig. 2.11., the machine is functioning in steady-state at 1800 rpm (Fig. 2.11.b), a two seconds ramp up to 2 Nm load (Fig. 2.11.d) was applied, followed by a two seconds slope machine unloading. The speed varies again with ± 25 rpm around the target corresponding to the motor loading and the unloading.



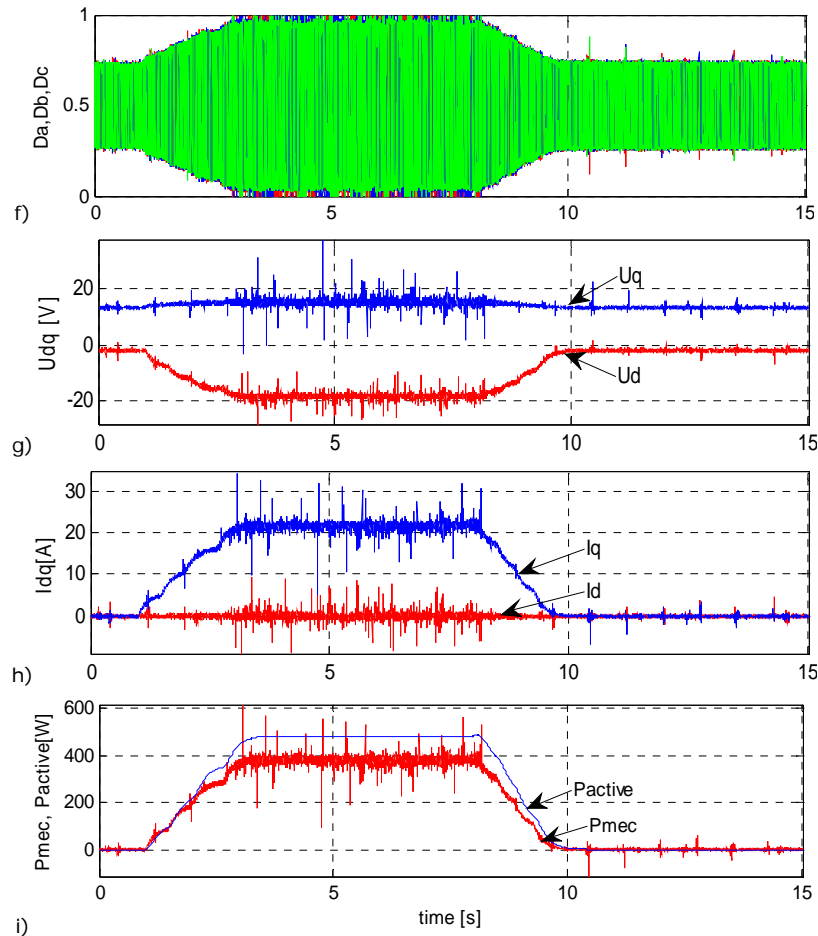


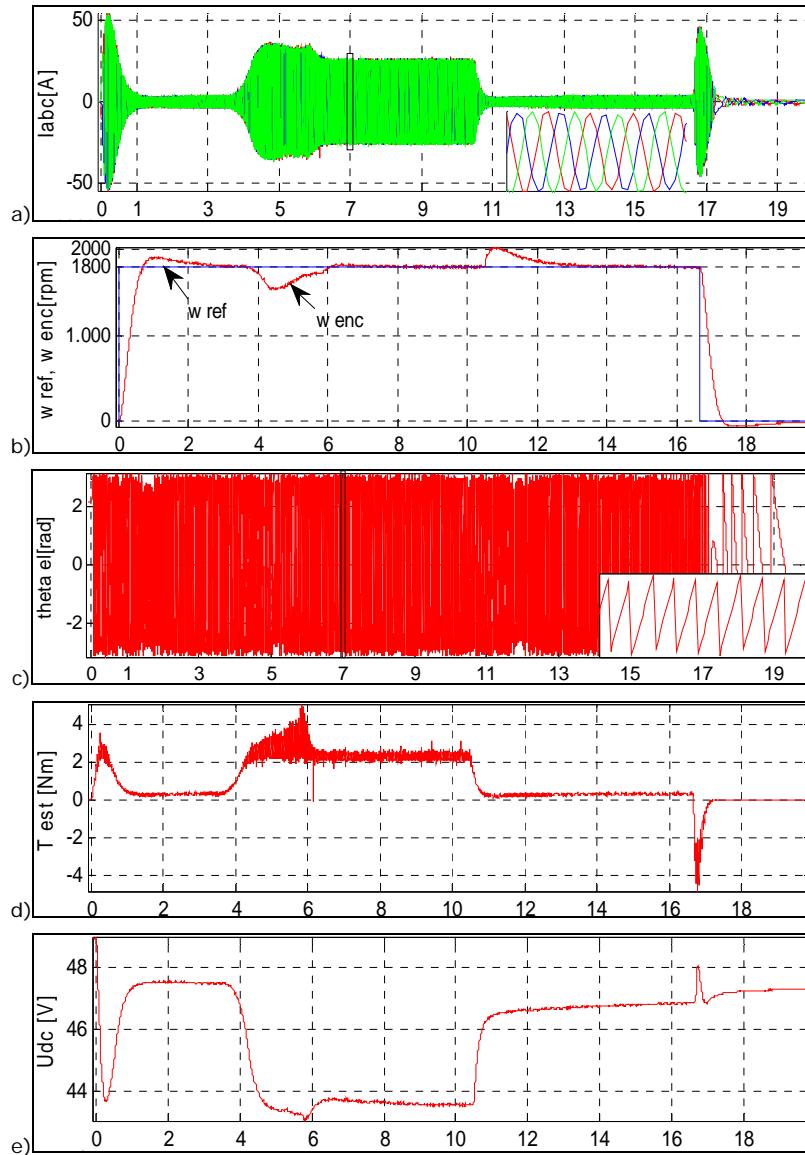
Fig. 2.11. Vector control experimental results for $n=1800\text{rpm}$; $T_L=2\text{Nm}$: a) phase currents, b) speed, c) rotor position, d) estimated torque, e) dc voltage, f) inverter duty cycles, g) d,q voltage, h) d,q current; i) mechanical and active power;

Further on, motor acceleration from zero speed up to 1800 rpm, followed by a rather fast 2 Nm step loading and afterwards the unloading, is shown in Fig. 2.12.

The machine accelerates in less than one second, but the speed overshoot is about 5,5% from the operating speed and the motor stabilizes after 2s (Fig. 2.12b). After the motor stabilization, a step load of 2Nm is applied at 3.5s, and the unloading occurs at 10,5s (Fig. 2.12b).

The speed varies in both moments with a 10% overshoot. The dc voltage varies with the loading and it is fast decreasing when the load is applied (Fig.

2.12d), but rises up to its initial value when the motor unloading occurs (Fig. 2.12e). Some noise can be observed in torque and current waveforms as the currents are fast growing (Fig. 2.12a) when the load is applied.



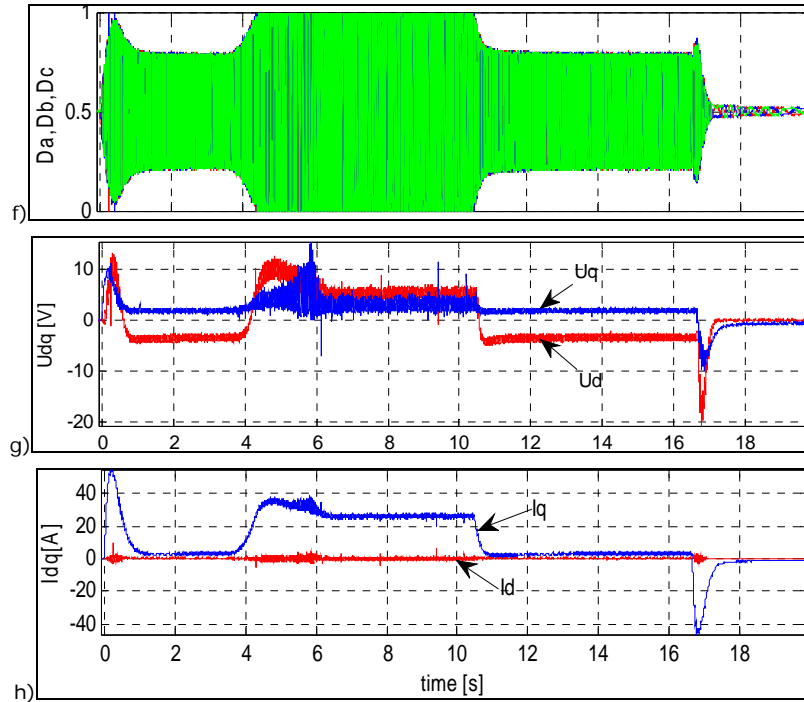


Fig. 2.12. Vector control – experimental results: 1800 rpm, 2Nm load : a) phase currents, b) speed, c) rotor position, d) estimated torque, e) dc voltage, f) inverter duty cycles, g) d,q voltage, h) d,q current

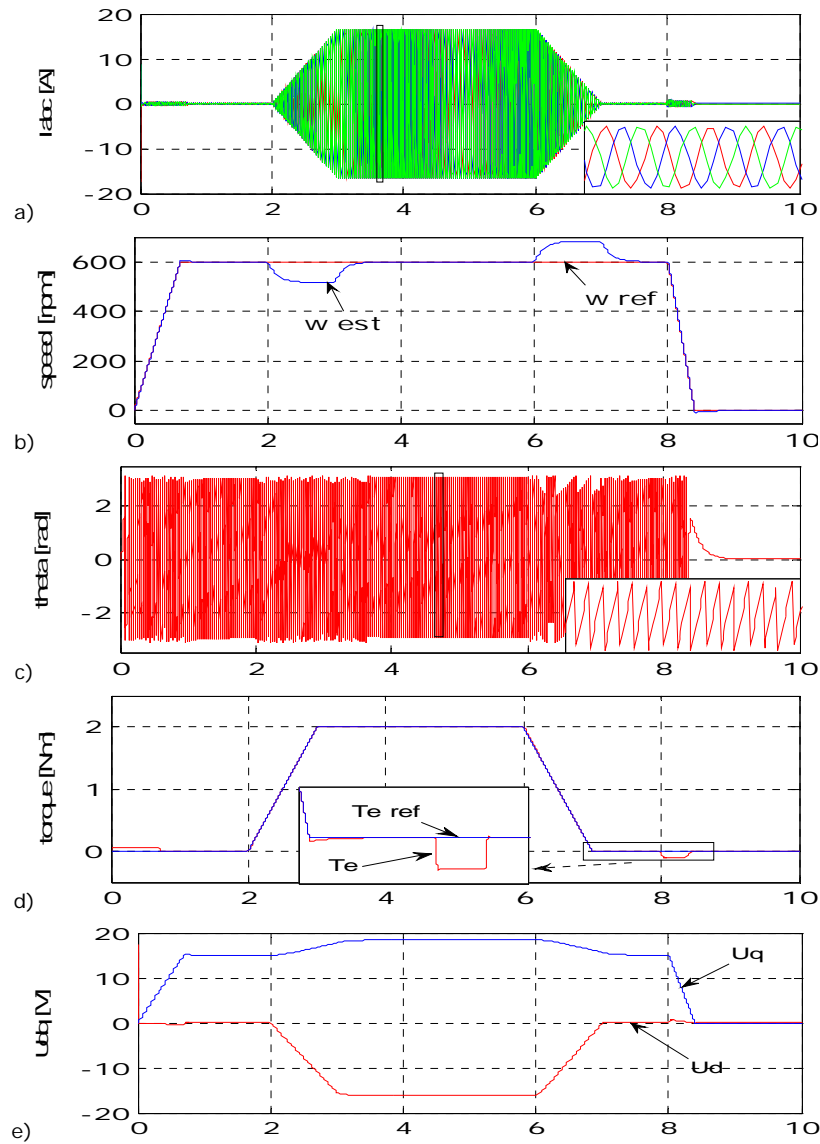
As laboratory experiments have shown the motor performances for different running conditions, the motor response in digital simulations will be investigated in what follows.

2.5.2. Simulation results

For a better comparison and validation of the experimental results previously obtained, digital simulations have been conducted for the above described running conditions.

First, the machine acceleration up to 600 rpm (Fig. 2.13b) and a proportional with speed 2 Nm torque (Fig. 2.13d) is prescribed for the motor loading. Afterwards, a 1.5 s slope was applied for the motor unloading, followed by a 400 ms slope for the motor braking.

When the machine loading and unloading occurs, its speed varies with $\pm 100\text{rpm}$ around the target.



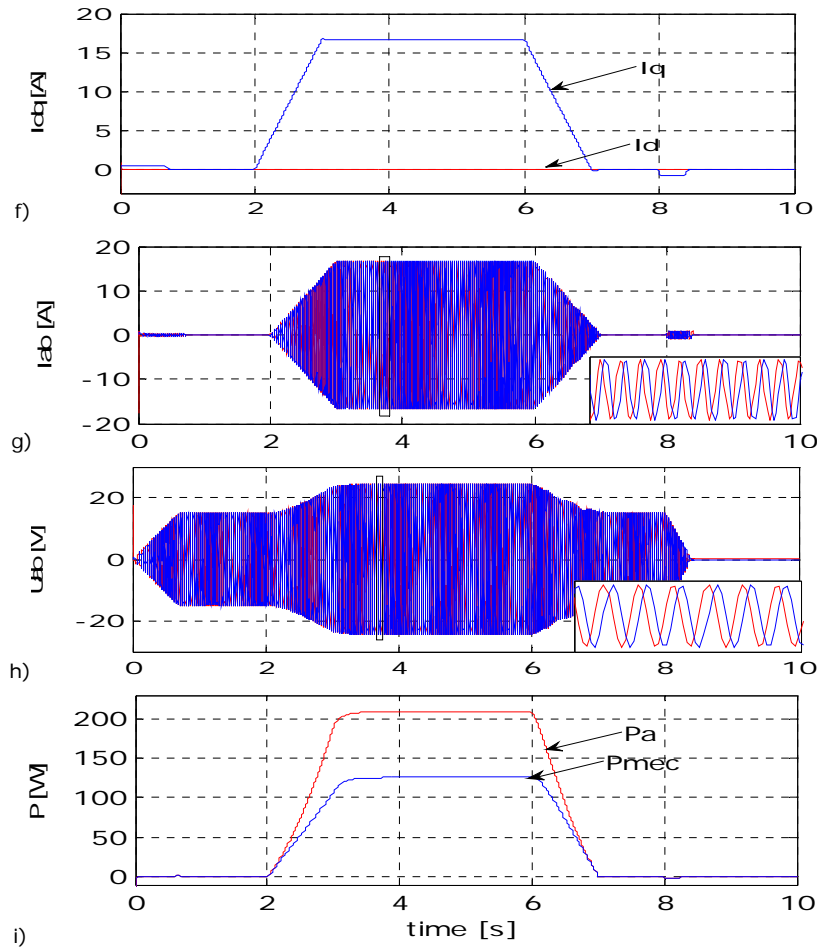
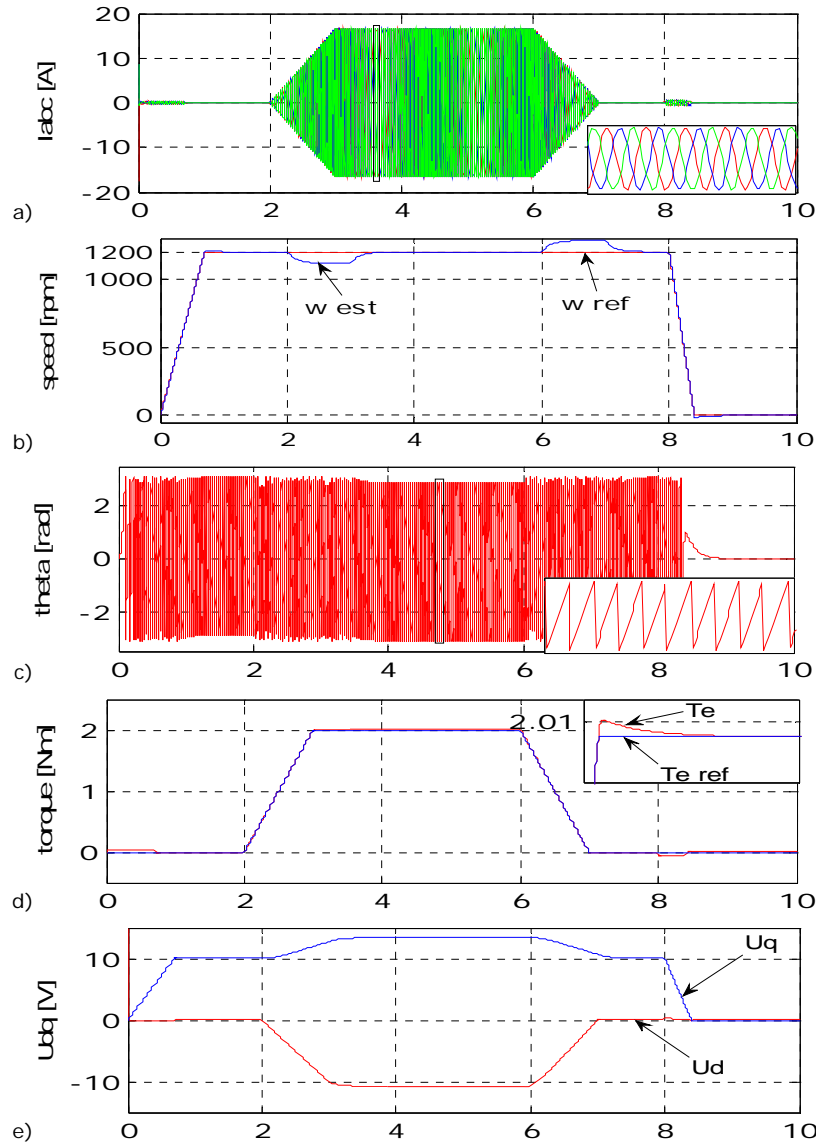


Fig. 2.13. Vector control simulation results for $n=600\text{rpm}$, $T_L=2\text{Nm}$: a) three phase currents, b) speed, c) rotor position, d) estimated torque, e) d,q voltage, f) d,q current; g) α , β current; h) α , β voltage; i) mechanical and active power;

The actual torque follows the target very closely, as no important oscillations are visible. If we compare these results with the experimental ones, we can easily admit that the machine torque response is a bit faster during simulations than in experiments.

During experiments, the current, the calculated active and mechanical power values, are higher than the ones from simulations. Even so, during simulations, the efficiency is 60%, which is with 13 percent higher than in experiments.

Further on, simulation results for machine acceleration up to 1200 rpm (Fig. 2.14b) and a proportional with speed, 2 Nm load torque (Fig. 2.14d), are shown below.



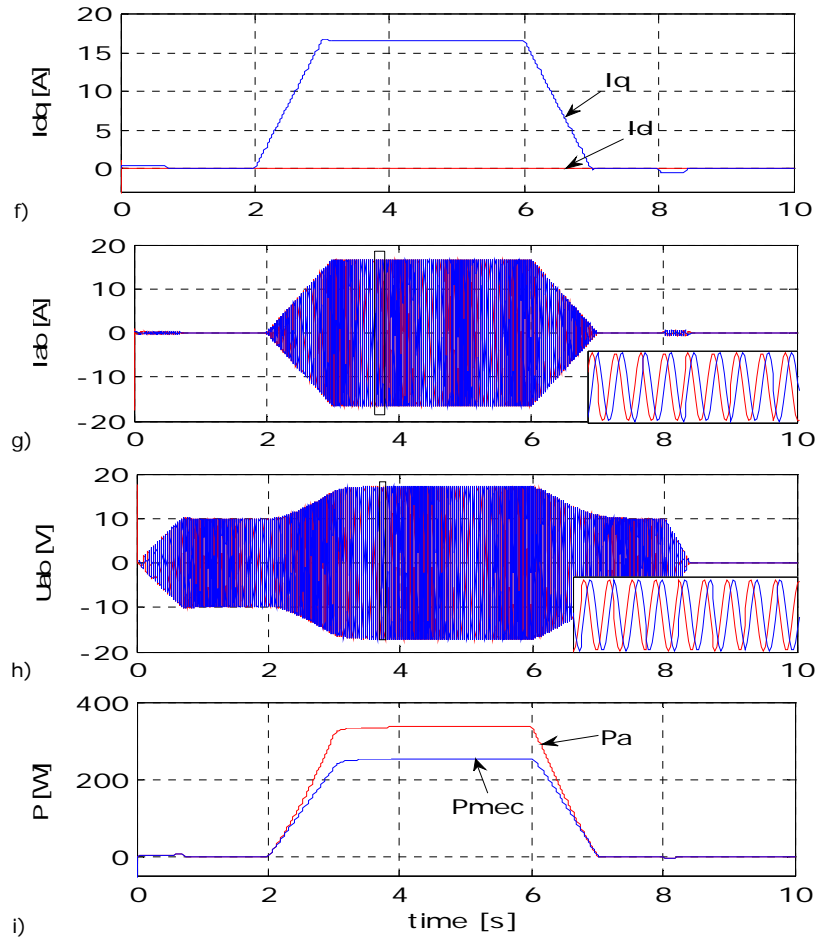


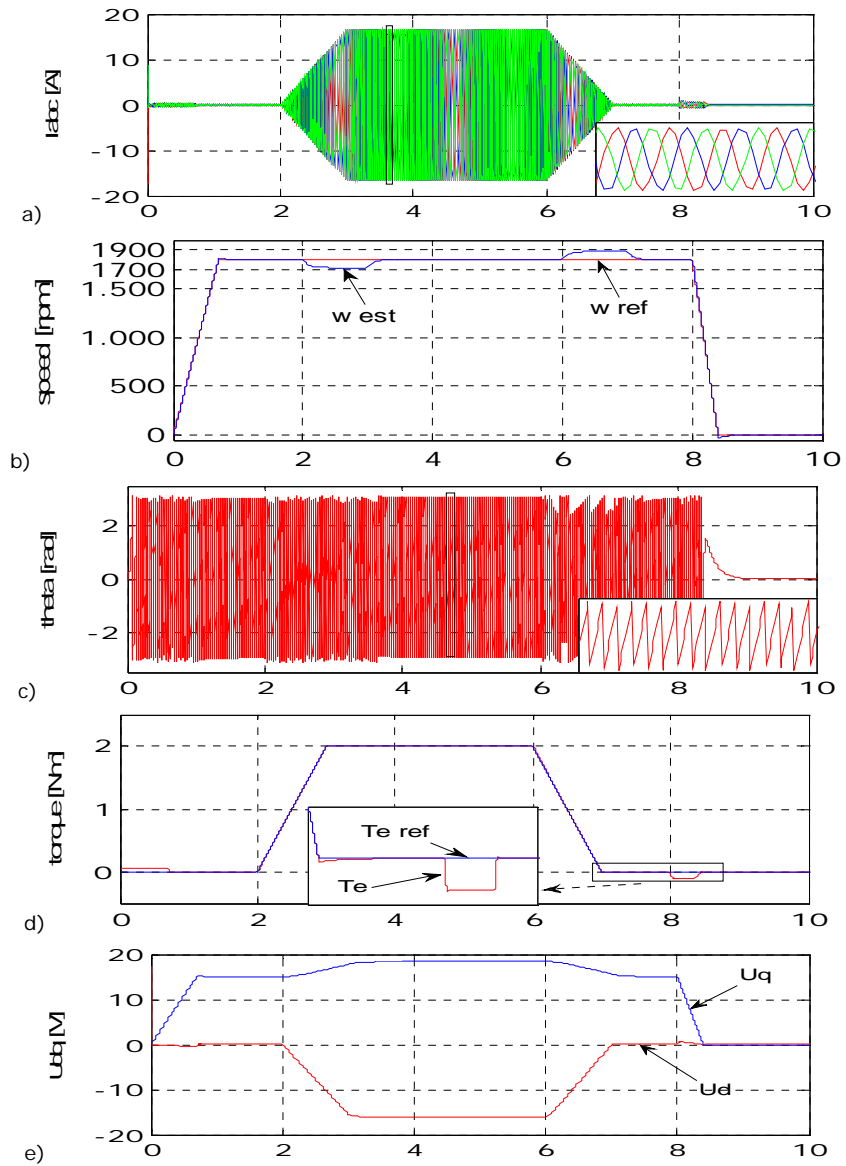
Fig.2.14. Vector control simulation results for $n=1200\text{rpm}$; $T_L=2\text{Nm}$: a) phase currents, b) speed, c) rotor position, d) estimated torque, e) d,q voltage, f) d,q current; g) α , β current; h) α , β voltage; i) mechanical and active power;

A 1s slope was applied for the motor unloading, followed by a 400 ms slope for the motor braking. As previously mentioned, the machine speed varies with ± 100 rpm around the target when the load is applied and when the unloading occurs.

The actual torque follows the target closely; very small oscillations around the target are visible.

In this case, the efficiency is 75 % for the simulation obtained results, which means a value with 10 percent higher than the one obtained from experiments.

Next, simulation results for machine acceleration up to 1800 rpm (Fig. 2.15b) are shown. A proportional with speed full load torque (2 Nm) was applied after the motor stabilization and it is represented in Fig. 2.15d.



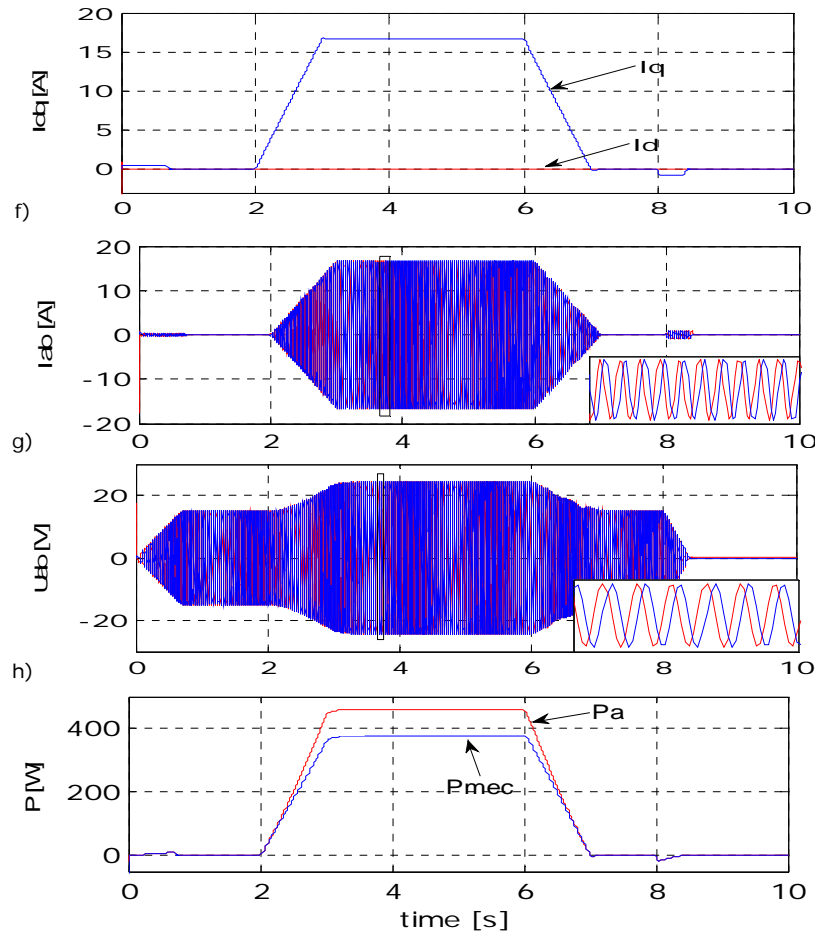


Fig.2.15. Vector control simulation results for $n=1800\text{rpm}$; $T_L=2\text{Nm}$: a) phase currents, b) speed, c) rotor position, d) estimated torque, e) d,q voltage, f) d,q current; g) α , β current; h) α , β voltage; i) mechanical and active power;

A 1s slope was also applied for the motor unloading, followed by a 400 ms slope for the motor braking.

The difference between the active and mechanical power is very small, but in this case, the obtained efficiency is 81,9%, with 3,1% higher than during experiments.

All these results show that experimental results are affected by noise, by the voltage drop on the cables, by the raising temperature which modifies the motor parameters. We also have to specify that the IPM synchronous motor was

synchronized with an induction machine load through a timing belt, which is flexible, but introduces noise and vibration directly related to the speed, width and pitch of the timing belt used [13]. We also have to specify that the IM inertia is a few times higher than of the IPM synchronous motor.

During simulations assumptions have been made, the inverter was considered ideal, which explains the drive response in the simulation results.

2.6. IPMSM with Distributed Windings

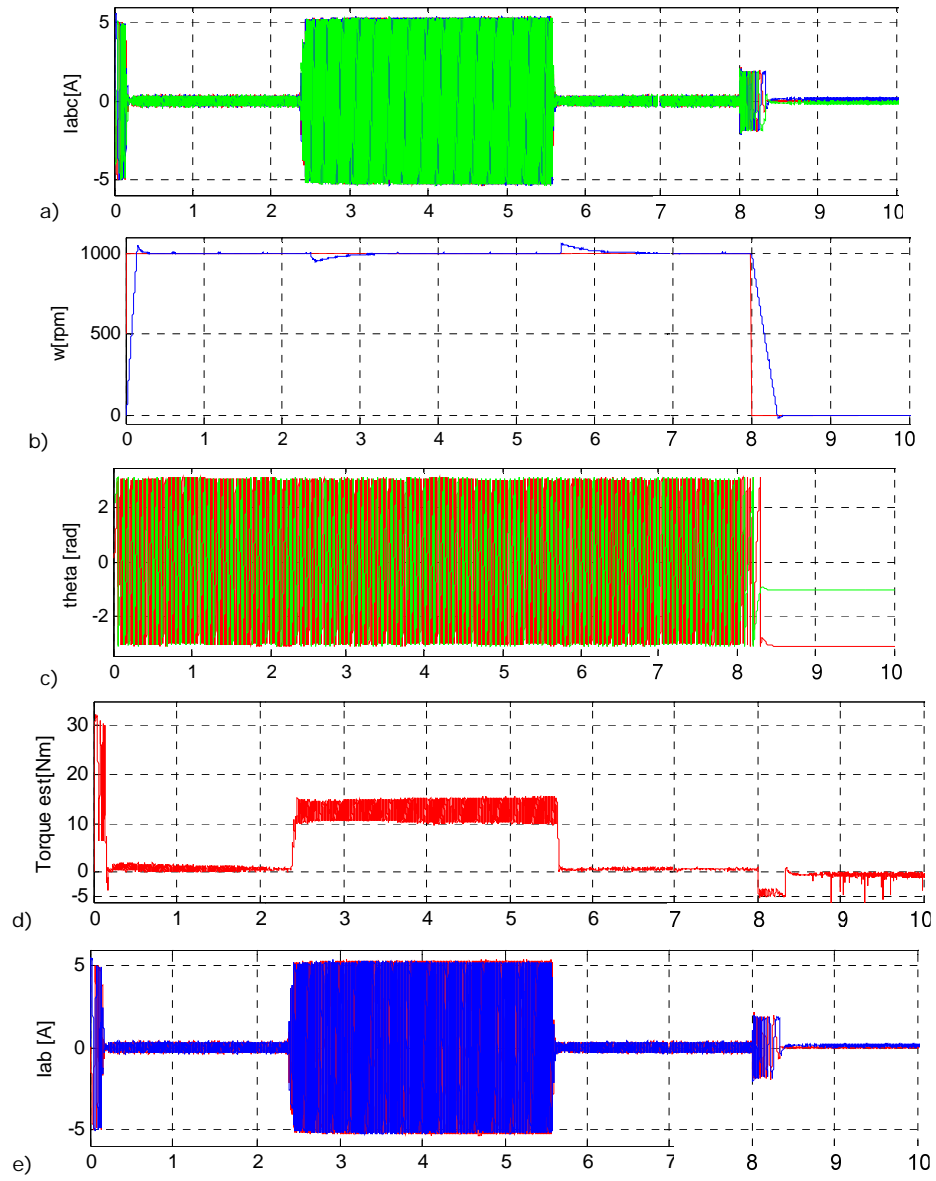
Considering as second prototype a Siemens IPM synchronous machine (shown in Fig. 2.16.), with well known parameters, as given in Table 7.1, vector control strategy has been tested and results follow.



Fig. 2.16. IPMSM with distributed windings

2.6.1. Experimental results

The laboratory setup (Fig.2.16) contained two IPM synchronous motors, one of them was functioning as a motor, the other one was working as a generator. First, motor acceleration from zero speed up to 1000rpm, in 200ms is shown in Fig. 2.17b.



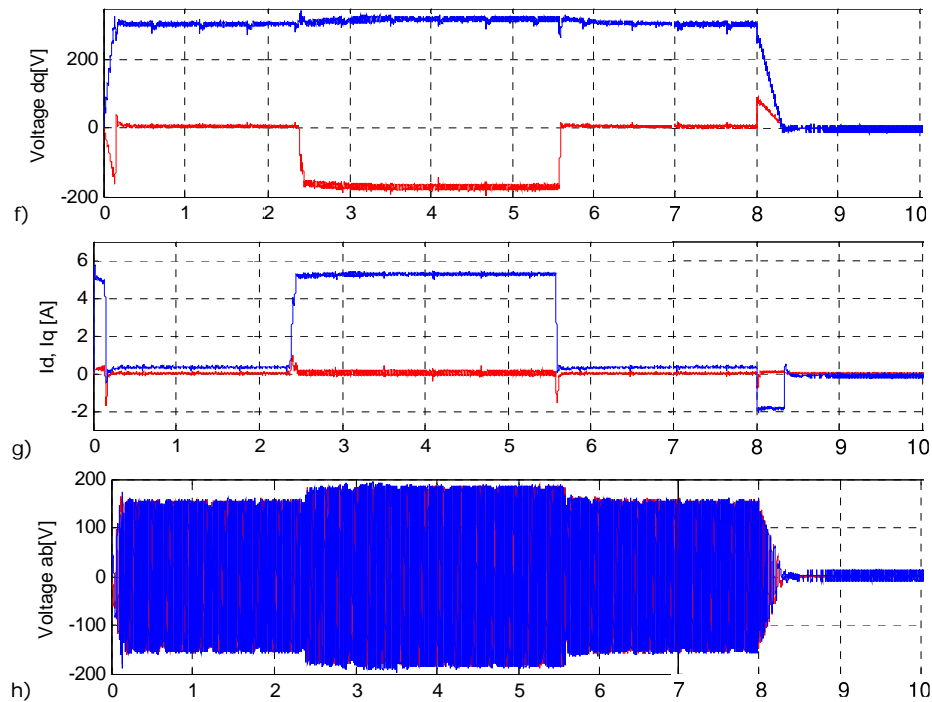


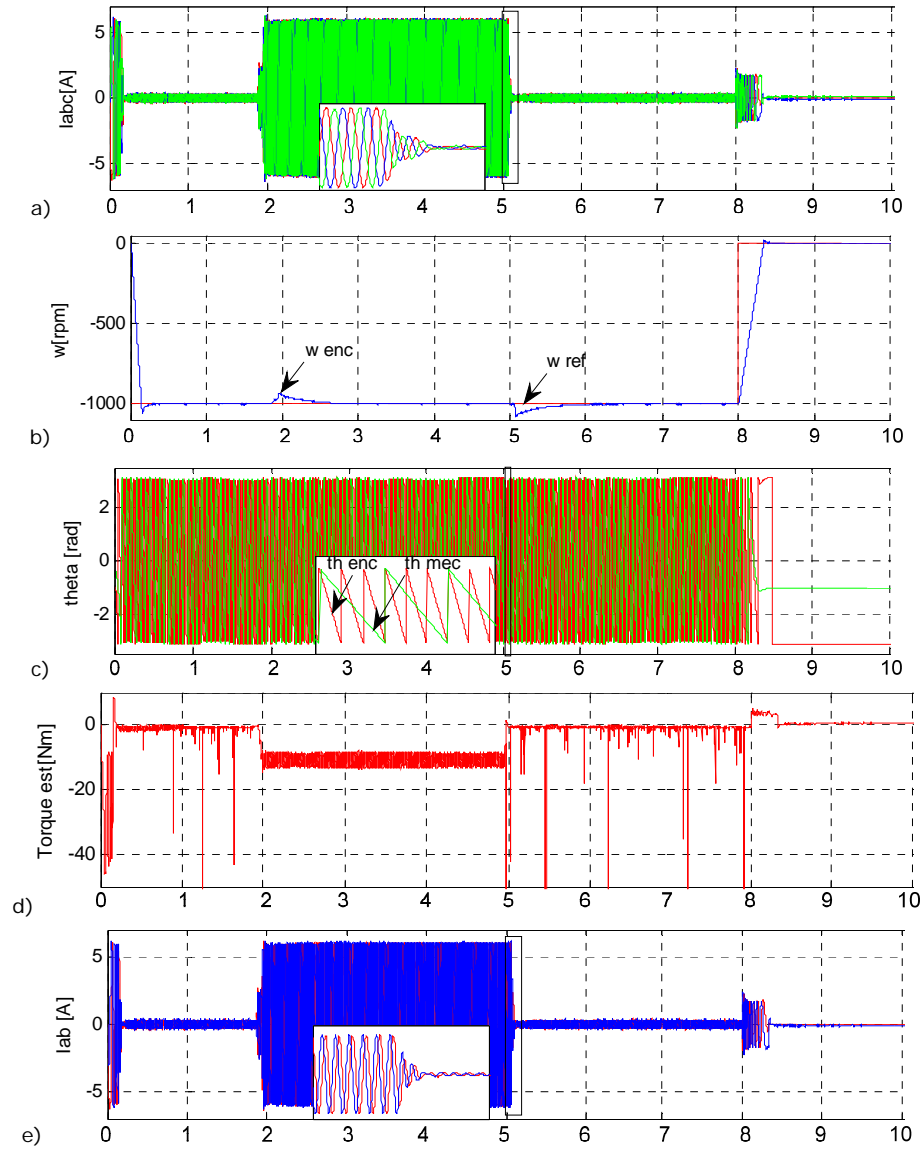
Fig. 2.17. Vector control experimental results for $n=1000\text{rpm}$; $T_L=12\text{Nm}$: a) phase currents, b) speed, c) rotor position, d) estimated torque, e) α , β current, f) d, q voltage, g) d, q current; h) α , β voltage;

A PM generator using a resistive load was needed for the step loading (at 2,4 s) and unloading (at 5,6 s) of the motor at full torque (Fig. 2.17d). A 5% speed overshoot can be observed in Fig. 2.17b, followed by the position representation in Fig. 2.17c.

After the 12 Nm step loading and unloading, the motor speed needs 500 ms to reach again the target and to stabilize. After the unloading, the machine decelerates back to zero speed and it needs about 400 ms to stabilize, as it can be noticed in Fig. 2.17 b. Thus, we have to admit that the motor speed response is a little sluggish.

Motor start-up response from zero speed to -1000 rpm, in about 200 ms is shown in Fig. 2.18 b). After the step loading (at 1,9 s) and unloading (at 5,1 s) at full torque (Fig. 2.18 d), the motor speed needs almost 700 ms to recover. A 5% speed overshoot can be observed in Fig. 2.18 b) and some ripples are present in torque response (Fig. 2.18 d). Rotor position is represented in Fig. 2.18 c).

The motor speed response is a little sluggish, considering that it needs about 400 ms to go back to zero speed and to stabilize, as it can be noticed in Fig. 2.18 b.



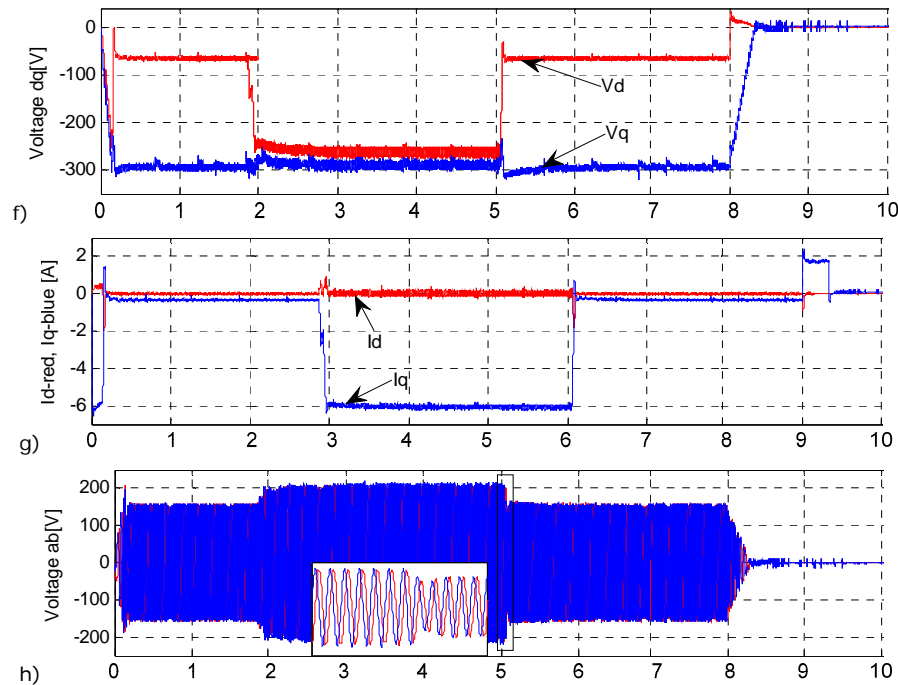


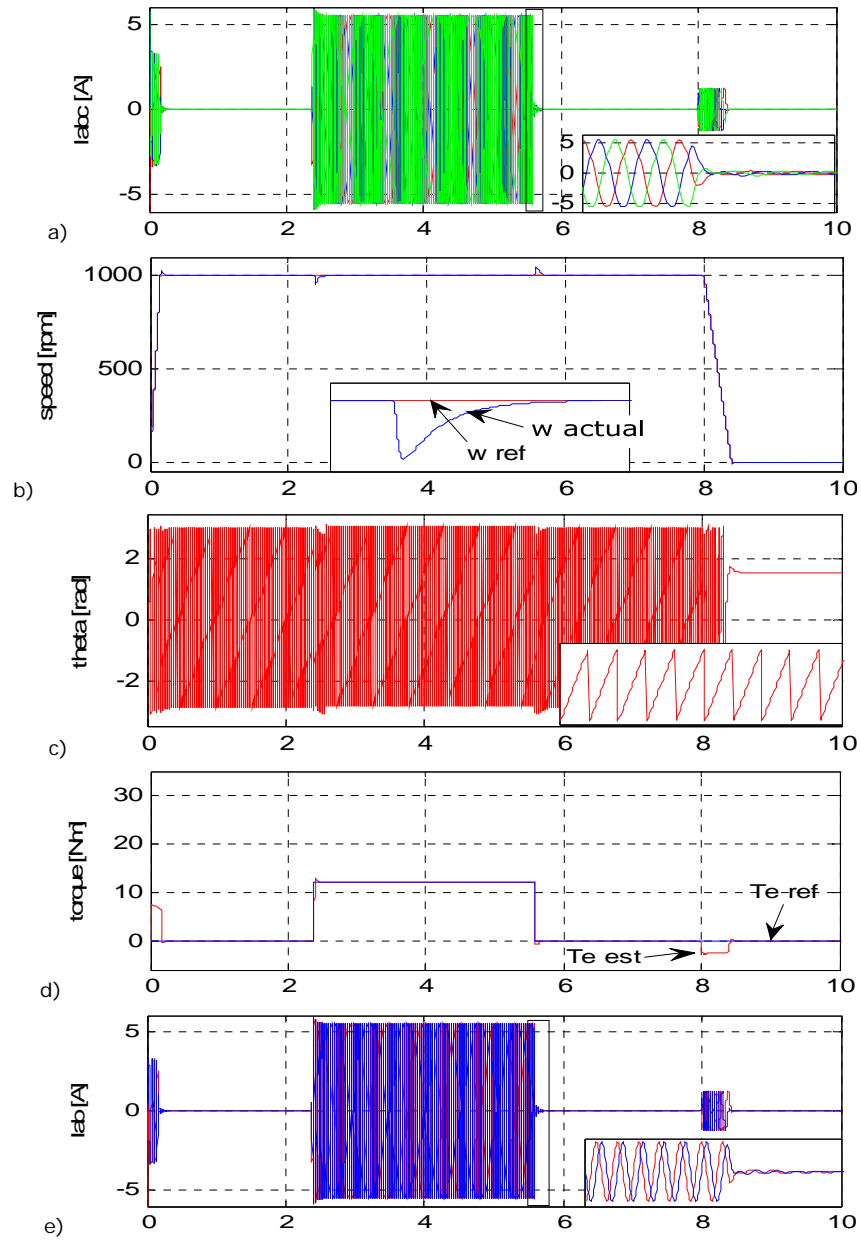
Fig. 2.18. Vector control experimental results for $n=-1000\text{rpm}$; $T_L=12\text{Nm}$: a) phase currents, b) speed, c) rotor position, d) estimated torque, e) α , β current, f) d, q voltage, g) d, q current; h) α , β voltage;

2.6.2. Simulation results

Comprehensive simulations have been conducted during the same operating conditions as the experiments and their results are presented further on.

First, fast acceleration up to 1000 rpm (150 ms), full torque step loading at 2.38 s, and unloading at 5.58 s is presented in Fig. 2.19 b). It can be noticed the machine rather fast (less than 150 ms) speed response, though it needs about 400 ms to decelerate from 1000 rpm to zero speed. The realized torque follows the reference one rather closely, but some visible oscillations are present when the motor starts, when the loading and the unloading occurs and when the braking process ends (Fig. 2.19 d).

When the machine is loaded at its nominal torque value, the currents are close to their maximum values.



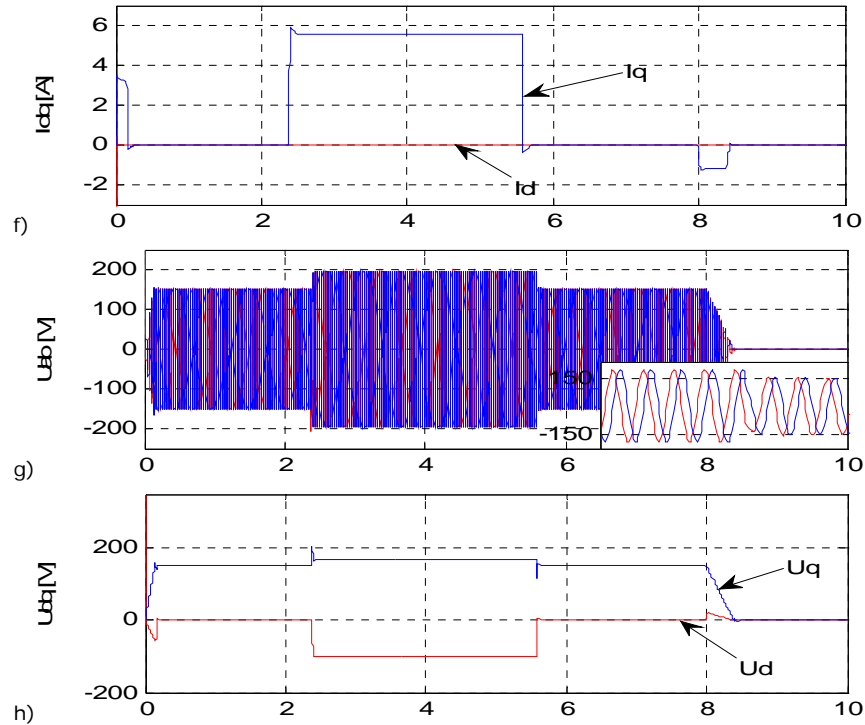
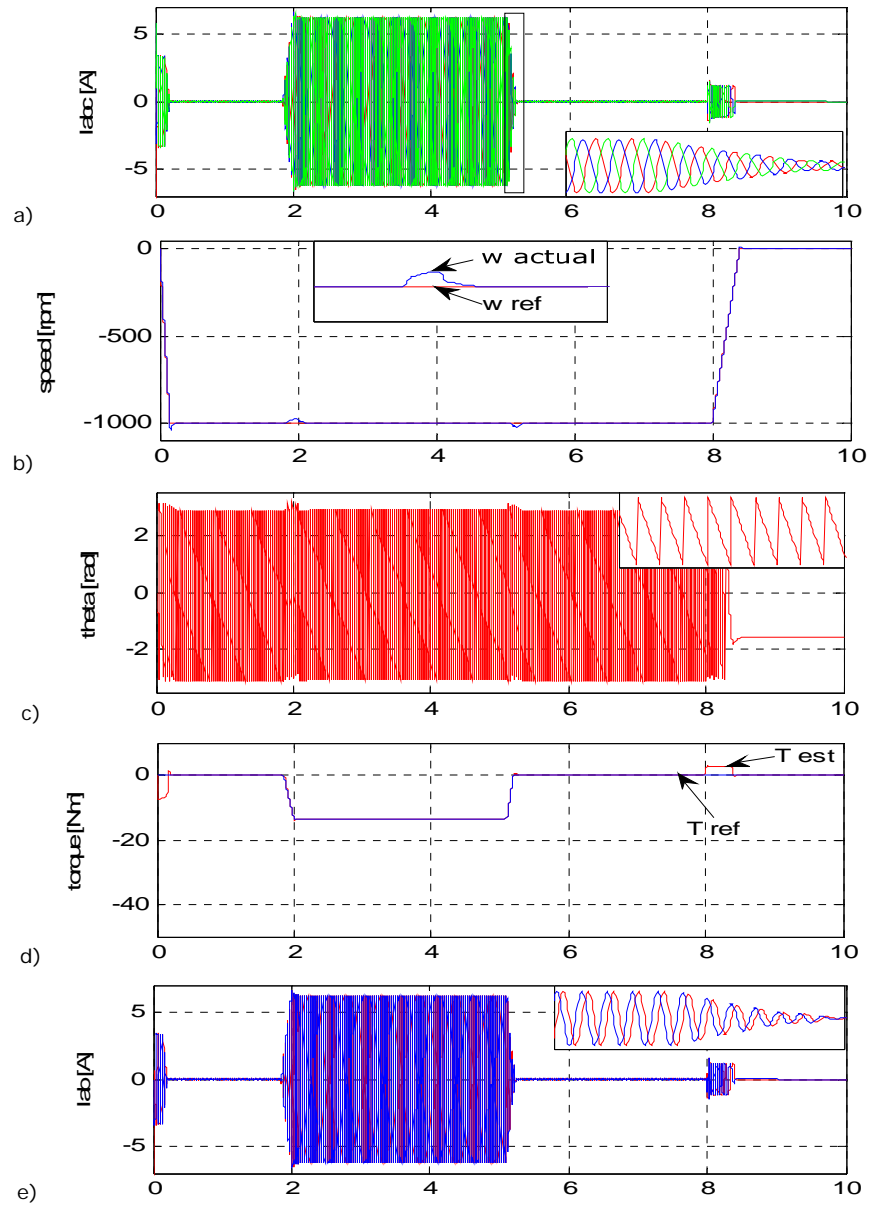


Fig.2.19. Vector control simulation results for $n=1000\text{rpm}$; $T_L=12\text{Nm}$: a) phase currents, b) speed, c) rotor position, d) estimated torque, e) α , β current, f) d, q current, g) α , β voltage; , h) d,q voltage;

The results for machine startup from zero speed to -1000 rpm (Fig. 2.20 a), followed by a full torque fast ramp loading (at 1.85 s) and unloading (at 5.1 s), are shown below, in Fig. 2.20d.

Machine fast acceleration (150 ms) can be seen in Fig. 2.20a. A slight speed variation, displayed in the zoomed region can be noticed when the load is applied and when the unloading occurs. The machine is loaded at the nominal torque value and it is shown that the machine manages to follow the target with small variations at start – up and when the deceleration is applied.



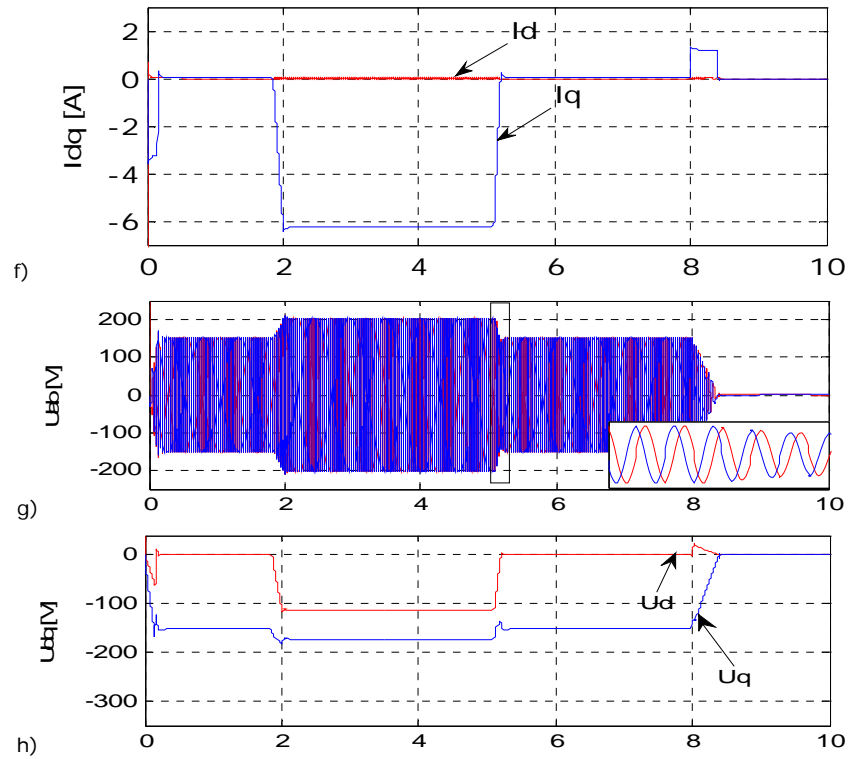


Fig. 2.20. Vector control simulation results for $n=-1000\text{rpm}$; $T_L=12\text{Nm}$: a) phase currents, b) speed, c) rotor position, d) estimated torque, e) α , β current, f) d, q current, g) α , β voltage; , h) d, q voltage;

If we compare the simulation with the experimental results, we can easily observe that the motor has pretty much the same behaviour in both inquiries. Even though, some ripples can be noticed during experimental tests, ripples that are not visible in simulations, where some approximations have been made: the inverter was considered ideal, the voltage drop on cables has been neglected.

2.7. Conclusion

A comprehensive procedure for PMSM characterization has been presented and a set of measurements was defined for PMSM parameter estimation.

Two different IPM synchronous motors, one with fractionary, the other with distributed windings have been studied and their capabilities were tested through experiments and simulations.

Vector control with speed and current regulators has been implemented, with voltage decoupling consideration for both motor prototypes. Comprehensive experiments have been conducted to validate the digital simulation results.

First, the IPMSM with fractionary windings has been tested under vector control and motor acceleration response at different speeds: 600rpm, 1200rpm, 1800rpm have been compared with the simulation results.

Secondly, the IPMSM with distributed windings has been tested at both acceleration and deceleration from zero speed to 1000 rpm and from zero speed to -1000 rpm respectively. Afterwards, the experimental results have been compared with simulation results; both of them have proved similar performances.

Considering the drawbacks related to the presence of a position sensor, a sensorless control method will be discussed further on.

References

- [1] Iles-Klumpner, D., Serban, I, Risticevic, M. "Automotive Electrical Actuation Technologies", Proceedings of Proceedings of Vehicle Power and Propulsion Conference, pp. 1-6, ISBN 1-4244-0158-5, Windsor, 6-8 Sept 2006, Canada;
- [2] Iles-Klumpner, Risticevic, M., Boldea, I. "Advanced Optimization Design Techniques for Automotive Interior Permanent Magnet Synchronous Machines", Electric Machines and Drives, May 2005 IEEE Int. Conf. on, pp. 227 – 234, ISBN: 0-7803-8987-5
- [3] Munteanu A., Boldea I., Agarlita S.C., "Experimental Characterization of Surface Permanent Magnet Synchronous Motor Drive", Days of ASTR – 2011, 22-23 Sept., 2011, pp. 87 - 92, ISSN 2066 – 6586, Timisoara, Romania;
- [4] Iles-Klumpner, D., Serban, I, Risticevic, M., Boldea, I. "Comprehensive Experimental Analysis of the IPMSM for Automotive Applications" Proceedings of 12th International Power Electronics and Motion Control Conference, pp. 1776-1783, ISBN 1-4244-0121-6, Portoroz, 30 Aug-1Sept 2006, Slovenia;
- [5] Rukmi Dutta, Rahman M. F., "A comparative Analysis of Two Test Methods of Measuring d- and q- Axes Inductances of Interior Permanent Magnet Machine"; IEEE Transactions on Magnetics, vol. 42, No. 11, pp. 3712-3718, November 2006;
- [6] Miller, T. J. E., "Methods for testing permanent magnet polyphase AC motors", Record of IEEE-IAS Annual Meeting, pp. 494-499, 1981;
- [7] Groza, V., Biriescu, M., Liuba, G., Cretu, V. "Experimental determination of synchronous machines reactances from DC decay standstill", Proceedings of IEEE 18th International Instrumentation and Measurement Technology Conference, pp. 1954-1959, ISBN 0-7803-6646-8, Budapest, 2001;
- [8] Gorman, S. F., Chen, C., Cathey, J.J., "Determination of permanent magnet synchronous motor parameters for use in brushless DC motor drive analysis", IEEE Transactions on Energy Conversion, Vol. 3, No. 3, pp. 674-679, ISSN 0885-8969, September, 1988;
- [9] Heins, G.H.G., De Boer, F.G., Vafi, S. "Characterization of the mechanical motor parameters for a permanent magnet synchronous motor using induced torque harmonics", Proceedings of Power Engineering Conference, pp. 1-6, ISBN 978-0-646-49488-3, 9-12 Dec. 2007;

-
- [10] Ji-Young, L., Sang-Ho, L., Geun-Ho, L., Jung-Pyo, H., Jin, H. "Determination of parameters considering magnetic nonlinearity in an interior permanent magnet synchronous motor", IEEE Transaction on Magnetics, Vol 42, pp. 1303-1308, ISSN 0018-9464, Apr. 2006;
- [11] Quntao, A., Li, S. "On-line parameter identification for vector controlled PMSM drives using adaptive algorithm", Proceedings of Vehicle Power and Propulsion Conference, p. 1-6, ISBN 978-1-4244-1848-0, 3-5 Sept 2008;
- [12] Petkovska, L., Cvetkovski, G. "Hybrid analytical-FEM analysis of single phase Permanent Magnet Synchronous Motor", Proceedings of IEEE EUROCON Conference, p 709-716, ISBN 978-1-4244-3860-0, 18-23 May 2009;
- [13] C. Perera, "Sensorless Control of Permanent – Magnet Synchronous Motor Drives", Ph. D. Dissertation, December 2002, Institute of Energy Technology, Aalborg University, Denmark;
- [14] I. Boldea and S. A. Nasar, „Electric Drives, 2nd Edition“, New York: CRC Press, Taylor and Francis, 2005;
- [15] M. Callegari, F. Cannella, "Lumped parameter model of timing belt transmissions", In 15th IMETA Congress of Theoretical and Applied Mechanics, Ancona, 2002;
- [16] D. Ahmadi, A. Nasiri, "A Novel Digital Control Method of PMSM for Automotive Applications", Vehicle Power and Propulsion Conference, 2007. VPPC 2007 IEEE, pp. 180 – 184, ISBN: 978-0-7803-9760-6;
- [17] N. Henwood, J. Malaize, L. Praly, "PMSM identification for automotive applications: Cancellation of position sensor errors", IECON 2011 - 37th Annual Conference on IEEE Industrial Electronics Society, pp. 687 – 692, 7-10 Nov. 2011, ISBN: 978-1-61284-969-0;
- [18] O. Wallmark, S. Lundberg, M. Bongiorno, "Input Admittance Expressions for Field-Oriented Controlled Salient PMSM Drives", Power Electronics, IEEE Trans on, March 2012, No. 3, pp. 1514–1520, ISSN: 0885-8993;
- [19] J. Malaize, W. Dib, S. Toru, "Adaptive torque control of Permanent Magnet Synchronous Motors in automotive applications", Vehicle Power and Propulsion Conference (VPPC), 2010 IEEE, pp. 1–6, 1-3 Sept. 2010, ISBN: 978-1-4244-8220-7;

- [20] D. Iles-Klumpner, I. Serban, M. Risticvic, "PMSM Drive Systems for Electric Active Steering (EAFS) Application: a Comparative Characterization", Vehicle Power and Propulsion Conference, 2006. VPPC '06. IEEE, 6-8 Sept. 2006, pp. 1 – 6, ISBN: 1-4244-0158-5;
- [21] S. Tairov, L. C. Stevanatto, "Adjustment of PMSM Drive Parameters for Sensorless Vector Control", Electronics, Robotics and Automotive Mechanics Conference, CERMA, 25-28 Sept. 2007, pp. 95–99, ISBN: 978-0-7695-2974-5;
- [22] A. Gebregergis, M. Islam, T. Sebastian, R. Ramakrishnan, "Evaluation of inductance in a permanent magnet synchronous motor", Electric Machines & Drives Conference, IEEE International, 15-18 May 2011, pp. 1171–1176, ISBN: 978-1-4577-0060-6;
- [23] H. Peter, I. Hahn, "Determination of differential inductances of permanent magnet synchronous machines for sensorless control", Electric Machines & Drives Conference (IEMDC), IEEE International, 15-18 May 2011, pp. 1579–1584, ISBN: 978-1-4577-0060-6.

Chapter 3

Active Flux Based Vector Control of Sensorless Distributed Windings IPMSM

During this chapter a rather novel concept “Active Flux” or torque-producing flux and its application for all AC Drives, with the main focus on Interior Permanent Magnet Synchronous Motors (IPMSM), is introduced. Only IPMSMs without cage windings in the rotor were used for control investigations. Therefore, the maximum torque per ampere (MTPA) condition must be considered.

First experimental, secondly simulation results, are shown and compared to prove the effectiveness of the proposed sensorless control strategy.

3.1. Active Flux Concept

“Active Flux” or “torque producing flux” is a generalized concept introduced by Prof. Boldea et al. in [1]. **The active flux vector turns all salient pole machines into non-salient pole ones, thus the rotor position and speed estimation becomes simpler.**

The active flux $\bar{\Psi}_d^a$ of any AC machine is defined as:

$$\bar{\Psi}_d^a = \bar{\Psi}_s - L_q \cdot \bar{i}_s \quad (3.1)$$

Where $\bar{\Psi}_s$ is the stator flux vector, \bar{i}_s the stator current vector and L_q is q axis machine inductance. By this concept all ac machine models “lose” their magnetic saliency [1].

The active flux, Ψ_d^a , multiplies the “ I_q ” current to produce the torque (3.2), for all AC machines:

$$T_e = \frac{3}{2} \cdot p_1 \cdot \Psi_d^a \cdot I_q \quad (3.2)$$

The active flux vector is aligned along the rotor flux vector axis for induction motors and along the rotor “d” axis for all synchronous machines: it is drawn along PM axis for PMSM, along excitation axis for dc-excited SM, excitation axis for RelSyn.

The active flux definition formulae for different AC machines [1] are written below (eqs. 3.3 – 3.6):

$$\Psi_d^a = \Psi_{PM} + (L_d - L_q) \cdot I_d \text{ for Interior PM Synchronous Motor } (L_d < L_q); \quad (3.3)$$

$$\Psi_d^a = (L_d - L_q) \cdot I_d \text{ for PM-RSM } (L_d \gg L_q); \quad (3.4)$$

$$\Psi_d^a = \Psi_{PM} \text{ for Surface Permanent Magnet Synchronous Motor } (L_d = L_q); \quad (3.5)$$

$$\Psi_d^a = (L_s - L_{sc}) \cdot I_d \text{ for Induction Machine (IM) } (L_s \gg L_{sc}); \quad (3.6)$$

Where L_d , L_q are the d-q inductances, Ψ_{PM} is the PM flux linkage and L_s , L_{sc} are the no-load and the short-circuit inductances of the IMs.

The active flux $\hat{\Psi}_d^a$ observer (Fig. 3.1) is based on the „active flux concept“ and its implementation scheme consists of the voltage model of stator flux $\hat{\Psi}_s$, which is used to estimate the stator flux components $\hat{\Psi}_\alpha$ and $\hat{\Psi}_\beta$ (eq. 3.7 and 3.8). The active flux components $\hat{\Psi}_{d\alpha}^a$ and $\hat{\Psi}_{d\beta}^a$ are obtained after subtracting the term $L_q \cdot \bar{I}_s$ (eq. 3.9 and 3.10), where \bar{I}_s is measured.

The compensation voltage is also taken into account and it is based on the error between the voltage model and current model (Fig. 3.2) for active flux calculation, through a PI controller. The compensation voltage takes care of the inverter nonlinearities [2], like: deadtime, integrator offset, stator resistance variation, which shows a notable influence at low speeds.

$$\hat{\Psi}_\alpha = \frac{T}{1 + sT} \cdot (V_\alpha^* + V_{comp} - R_s \cdot I_\alpha); \quad (3.7)$$

$$\hat{\Psi}_\beta = \frac{T}{1 + sT} \cdot (V_\beta^* + V_{comp} - R_s \cdot I_\beta); \quad (3.8)$$

$$\hat{\Psi}_{d\alpha}^a = \hat{\Psi}_\alpha - L_q \cdot I_\alpha; \quad (3.9)$$

$$\hat{\Psi}_{d\beta}^a = \hat{\Psi}_\beta - L_q \cdot I_\beta; \quad (3.10)$$

Using the active flux components along „ α , β “ axes, we can also estimate its position and speed (3.11–3.13), which is exactly the rotor speed.

$$\hat{\theta}_r = \text{atan} \frac{\hat{\Psi}_{d\beta}^a}{\hat{\Psi}_{d\alpha}^a} \quad (3.11)$$

$$\hat{\omega}_r = \frac{d\hat{\theta}_r}{dt} = \frac{d}{dt} \left(\text{atan} \frac{\hat{\Psi}_{d\beta}^a}{\hat{\Psi}_{d\alpha}^a} \right) \quad (3.12)$$

$$\hat{\omega}_r = \omega(\hat{\Psi}_d^a) = \frac{\hat{\Psi}_{d\alpha}^a[k-1] \cdot \hat{\Psi}_{d\beta}^a[k] - \hat{\Psi}_{d\beta}^a[k-1] \cdot \hat{\Psi}_{d\alpha}^a[k]}{T_s \cdot |\hat{\Psi}_d^a[k]|^2} \quad (3.13)$$

Where “ T_s ” is the sampling period and index (-1) denotes variables delayed with one sampling period.

Using the active flux components we can also determine the estimated rotor position (eq. 3.11), which is then used as feedback in the current observer model (Fig. 3.2).

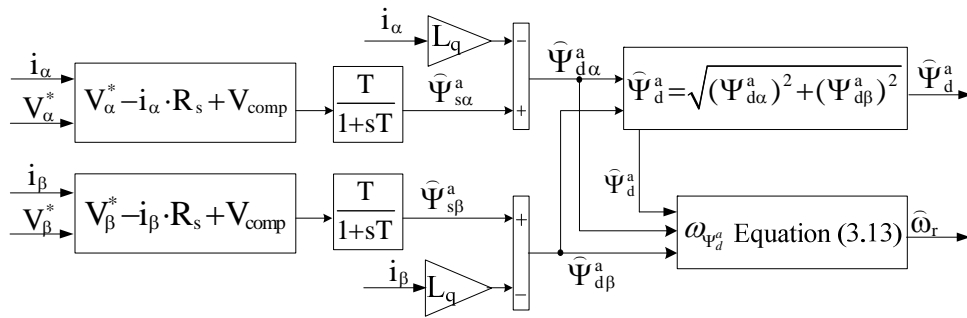


Fig. 3.1 Active flux amplitude and its speed (rotor speed) observer.

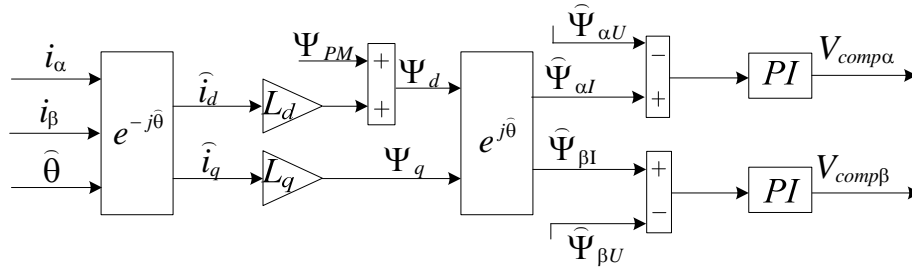


Fig. 3.2 Voltage compensation scheme along “ α , β ” axes, based on active flux – current model

The active flux observer has almost the same structure for all AC Drives and it can be applied for motion sensorless control in a wide speed range. The performance of the sensorless control is ensured by the accuracy of the rotor speed and position estimation.

3.2. Maximum Torque per Ampere Condition

Interior Permanent Magnet Synchronous Motors are often used in applications where wide constant – power speed range is required. With maximum torque per ampere (MTPA) condition, optimized machine control is obtained within the base speed range [3]-[5].

The difference between the q-axis and d-axis inductance ($L_d < L_q$) contribute to the additional torque production, so called the reluctance torque. Even if the magnitude of the stator current is fixed, the produced torque varies according to the input current vector.

The MTPA control strategy [20] is a commonly used alternative to deal with the efficiency optimization below the base speed. By proper selection of amplitude and phase of the stator current vector, it allows exploiting both the magnet and the reluctance torque to maximize the torque per ampere ratio [6].

In the IPMSM d-q current plane, there are many current reference pairs (i_d^* , i_q^*) which are able to generate the specific torque, therefore, the current reference whose magnitude is the minimum at the specific torque should be found in order to control the drive using the MTPA condition.

During last decades, many researchers have paid attention to the MTPA condition and thus, different control strategies have been developed and studied [7]. Some MTPA control methods are based on seeking the minimum stator current magnitude for a required electromagnetic torque value, current which will be further on impressed to the machine [8], [9], [19], [21].

Research has been reported to decrease the copper loss in order to obtain machine maximum efficiency [10]. Most of them have found the MTPA operating point using the machine parameters [11], [12]. However, these methods depend of parameter variations regardless of the huge efforts to compensate them by using on-line estimation techniques [13]-[15] or pre-made look-up tables [16], [17] which consider parameters variation and are used to correct the MTPA trajectory [18].

All analytical approaches toward MTPA condition use rated motor parameters, which are considered to be constant in every operating point. This means that the variation of the motor inductances L_d and L_q with the d - q axes currents and also the effects of the dependence of the permanent magnet flux linkage on the temperature are not taken into account. As these values can suffer important variations, efficient control system must be considered to adapt to them.

The most followed approach to this problem is to obtain the MTPA trajectory by differentiating the motor torque equation with respect to the stator current and equalizing it with zero to obtain the prescribed “d” current, formulae which are frequently used in simple control systems [21].

Thus, we will use this MTPA control method, so, to avoid rotor position estimation we need to “fix” the desired longitudinal current i_d^* versus stator current i_s to consider both maximum torque/current below base speed for up to full torque and at low torque during flux weakening. Maximum torque per flux for limited voltage (during full available torque requirement with flux weakening) at high speeds is obtained by adding a correction $-\Delta i_d^*$ to i_d^* when reference voltage $V_s^* > V_{smax}$ (V_{smax} - maximum PWM inverter voltage vector).

For the IM and RSM this operation is synthesized in (3.14) and (3.15):

$$i_d^* = i_{di}^*, \quad i_{di}^* = \frac{i_s}{\sqrt{2}} \quad \text{if } \Delta V = V_s^* - V_{smax} < 0 \quad (3.14)$$

$$i_d^* = i_{di}^* - \Delta i_d^* \quad \text{for } \Delta V > 0; \quad \Delta i_d^* = k_p \cdot \left(1 + \frac{1}{T_i} \cdot s\right) \cdot \Delta V; \quad (3.15)$$

k_p, T_i – PI regulator proportional and integration time constants;

For the SPMSM, maximum torque/current corresponds to:

$$i_{di}^* = 0; \quad i_d^* = 0, \quad \text{if } \Delta V < 0 \quad (3.16)$$

$$i_d^* = -\Delta i_{di}^*; \quad \Delta i_{di}^* = k_p \cdot \left(1 + \frac{1}{T_i} \cdot s\right) \cdot \Delta V, \quad \text{if } \Delta V > 0 \quad (3.17)$$

For PM-RSM and IPMSM, the maximum torque/current conditions are reflected by equations (3.18 – 3.20) [22]:

$$T_e = \frac{3}{2} \cdot p_1 \cdot \left(\Psi_{PM} \cdot i_q + (L_d - L_q) \cdot i_d \cdot i_q\right) \quad (3.18)$$

$$\frac{dT_e}{di_q} = 0 \quad (3.19)$$

$$2 \cdot i_{di}^{*2} + \frac{i_{di}^* \cdot \Psi_{PM}}{L_d - L_q} = i_s^2; \quad (3.20)$$

$$\text{As } L_d - L_q < 0 \text{ and } i_d^* < 0, \quad i_{di}^* > -\frac{i_s}{\sqrt{2}}, \quad \text{for } \Delta V < 0 \quad (3.21)$$

The maximum torque/current formula may also be considered:

$$\hat{i}_d^* = -\frac{1}{4} \cdot \frac{\Psi_{PM}}{L_d - L_q} - \frac{1}{2} \cdot \sqrt{\frac{1}{4} \cdot \left(\frac{\Psi_{PM}}{L_d - L_q} \right)^2 + 2 \cdot I_s^2}; \quad (3.22)$$

Ψ_{PM} , I_{sn} , L_d , L_q - in p.u. values, for $\Delta V < 0$

$$\hat{i}_d^* = i_d^* - \Delta i_{di}^*; \quad \Delta i_{di}^* = k_p \cdot \left(1 + \frac{1}{T_i} \cdot s \right) \cdot \Delta V; \quad \text{for } \Delta V > 0, \quad \hat{i}_d^* \leq -\frac{\Psi_{PM}}{L_d} \quad (3.23)$$

With \hat{i}_d^* given in Ψ_d^{a*} formulae (3.3–3.6), the corresponding \hat{i}_q^* current is straightforward $\hat{i}_q^* = \sqrt{I_s^2 - \hat{i}_d^{*2}}$, with I_s (stator phase current amplitude), as measured.

Considering the above mentioned MTPA condition, the active flux concept, and keeping the „d” axis current at zero, a sensorless control strategy was developed for IPMSM. Both experimental and simulation results are shown and discussed further on.

3.3. Experimental results

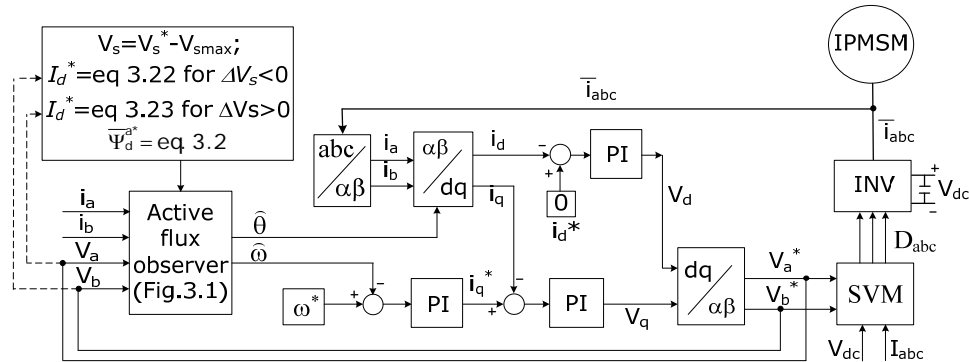
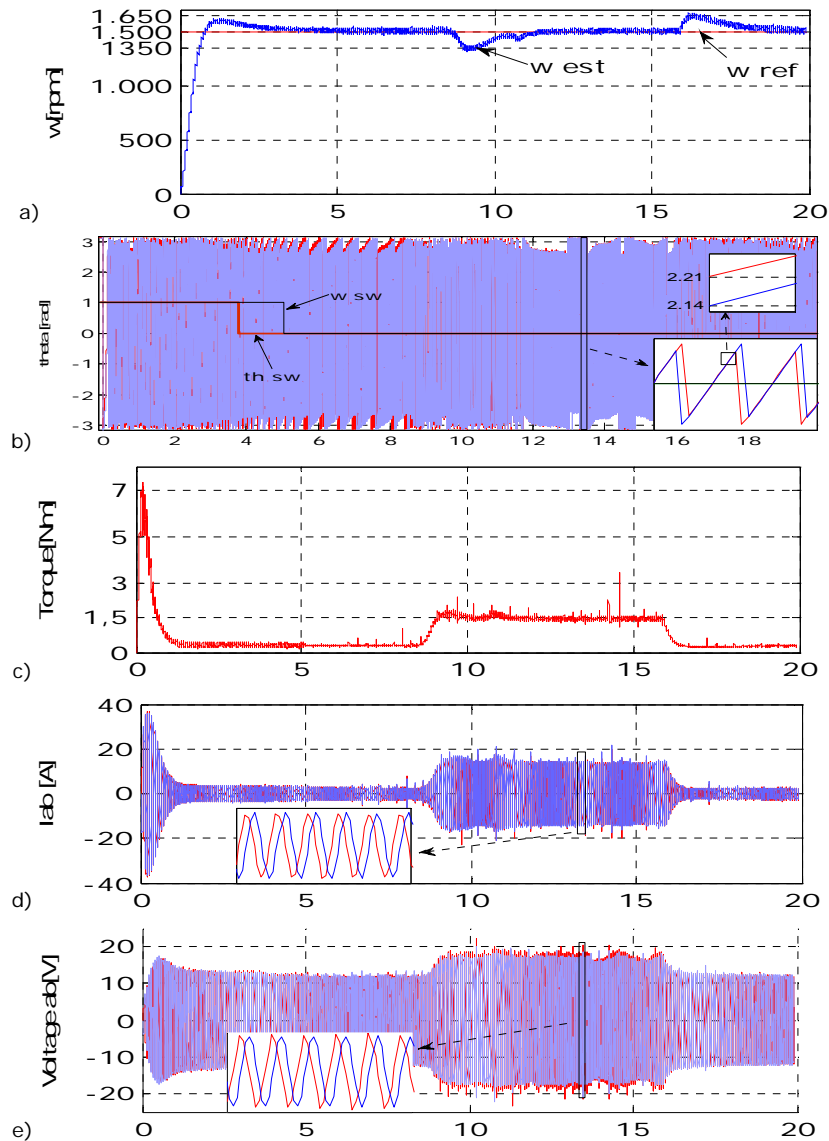


Fig. 3.3 Sensorless control scheme

Results were obtained for the machine acceleration from zero speed up to 1500 rpm. The machine started using the encoder feedback position (Fig. 3.4a). It can be noticed that the machine needs almost one second to accelerate and about two seconds to stabilize. After its stabilization toward the prescribed speed, the switch from the actual to the estimated position was imposed (at 3,8s), followed by the switch from the real to the estimated speed (at 5 s), Fig. 3.4b.

Next, when the sensorless machine operation became stable, an 1,5 Nm load (Fig. 3.4c) was applied at 8,5s, followed by the machine unloading at 16s. The machine speed recovers after two seconds.

As it is shown in Fig. 3.4b, there is a slight difference of 0.07 rad, which means four electrical degrees, between the estimated and actual rotor position.



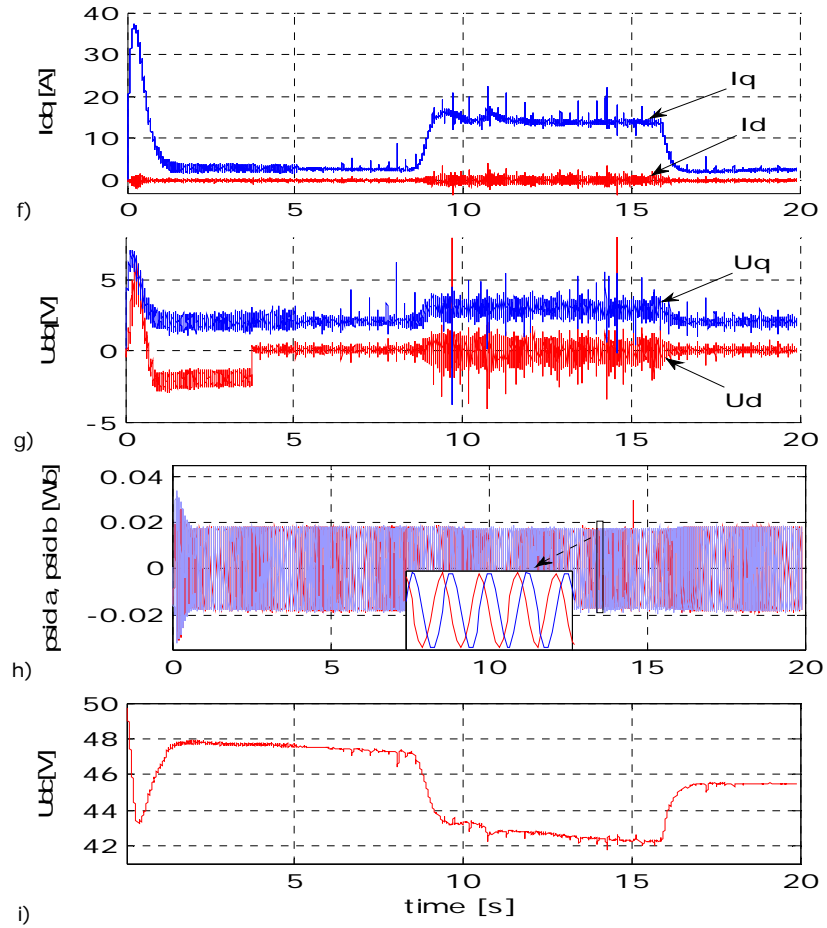


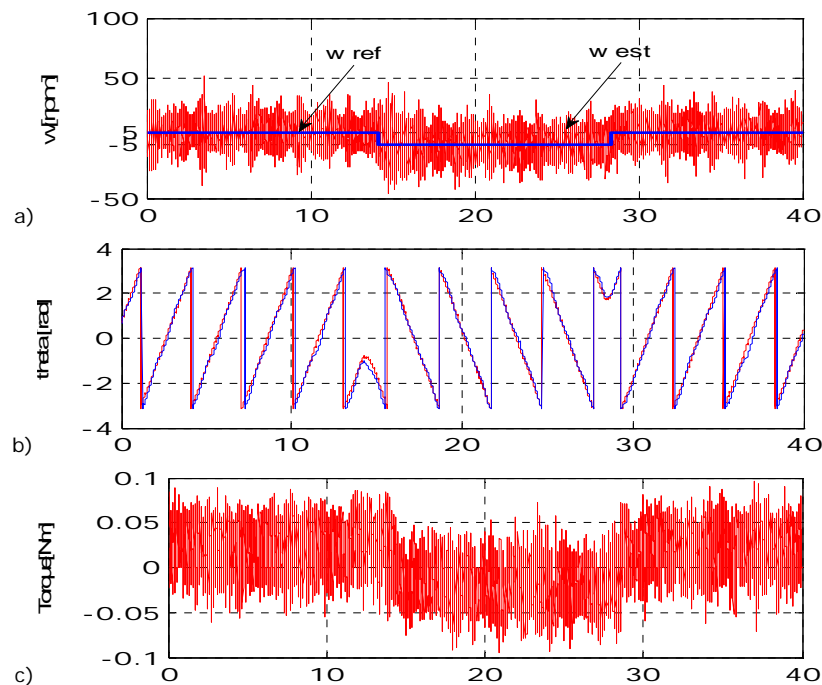
Fig. 3.4. Experimental sensorless vector control results for 1500 rpm at 1,5 Nm load: a) speed; b) rotor position; c) torque; d) α , β currents; e) α , β voltages; f) d , q currents; g) d , q voltages; h) α , β fluxes; i) battery voltage;

In Fig. 3.4f, we can easily notice that the d axis current is maintained at zero, as initially required, while I_q current is proportional with the IPMSM torque. The α , β currents and voltages are represented in Fig. 3.4d and 3.4e, respectively. Fig. 3.4g shows the d , q voltages, while the active flux components along α , β axes are displayed in Fig. 3.4h.

The inverter dc-link voltage is influenced by the applied load, so, as shown in Fig. 3.4i, it falls from 47V to 42 V and when the unloading occurs, it rises back up to almost 46V.

The same operating conditions, as described above were used to drive the motor into the low speed region, so, a ± 5 rpm speed profile was prescribed for the IPM synchronous motor. Experimental results and their discussion are presented below. The experimental steady-state results at 5 rpm, followed by the speed reversal at -5 rpm and then back to 5 rpm (after self – acceleration (not shown)), at no load is presented in Fig. 3.5a. The motor estimated speed follows the reference one with increased noise. In Fig. 3.5b, the estimated angle follows very close the actual one, with a difference of about 0,2 rad, which means approximately 11,5 electrical degrees, during the most critical instants of time.

The torque, shown in Fig. 3.5c is close to zero, as there is no load applied. Both the current waveforms, in Fig. 3.5d and Fig. 3.5f and the voltages, in Fig. 3.5b are pretty noisy. Even if it is almost constant, some ripples can also be noticed in the inverter dc - link voltage, Fig. 3.5g.



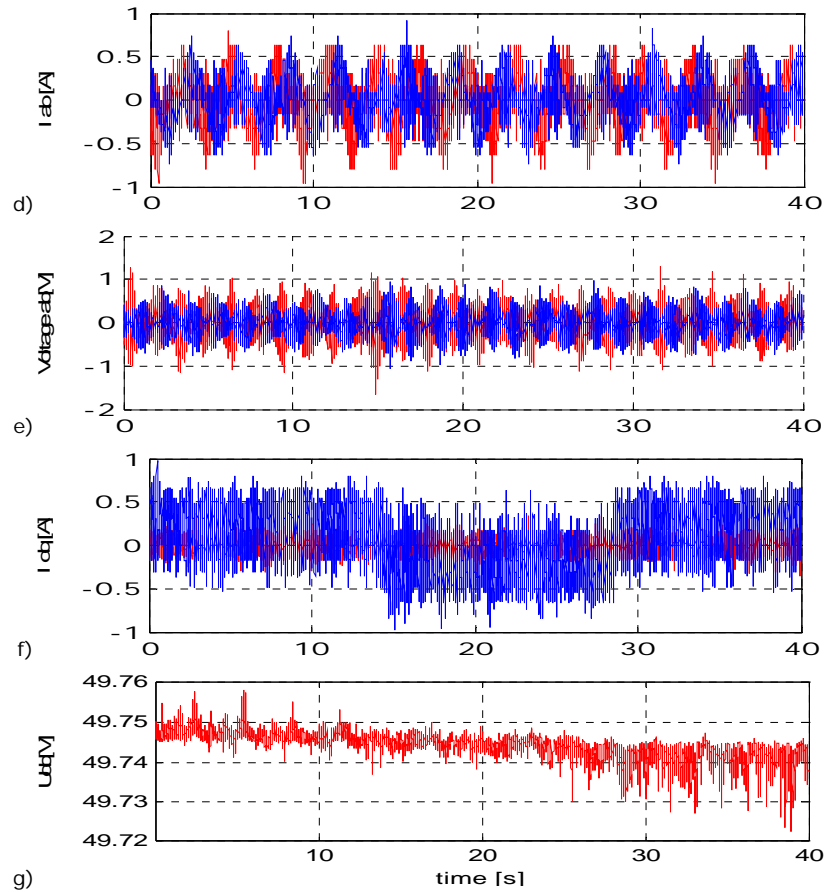


Fig. 3.5. Experimental sensorless vector control results for ± 5 rpm steady – state speed, at no load: a) speed; b) rotor position; c) torque; d) α , β currents; e) α , β voltages; f) d , q currents; g) battery voltage;

3.4. Simulation results

For better comparisons, the above presented sensorless control scheme (Fig. 3.3), was also modeled in Matlab/Simulink package and results have been obtained under the same operating conditions, as previously considered, during experiments. The IPM synchronous motor simulation scheme is presented in Fig. 3.6. We have to specify that during simulations, some assumptions have been made: the inverter was

considered ideal, the viscous friction coefficient has been neglected and the IPMSM parameters have been considered as being constant.

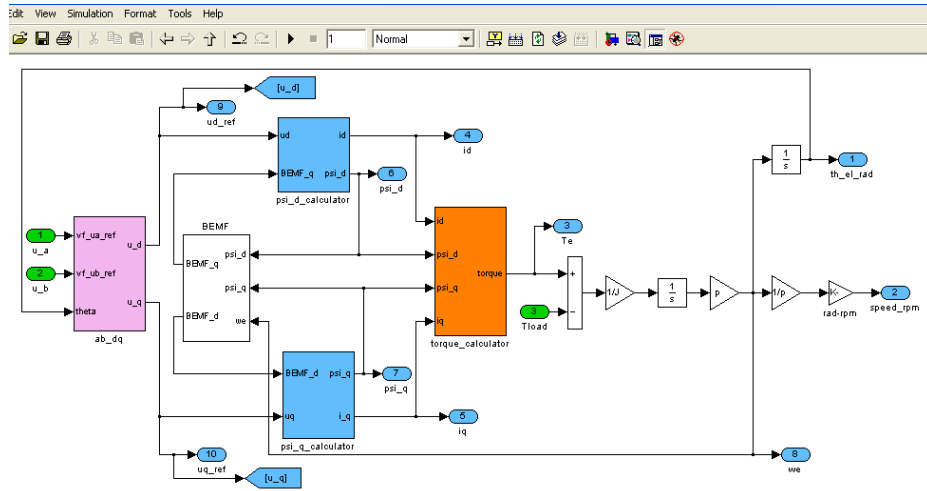
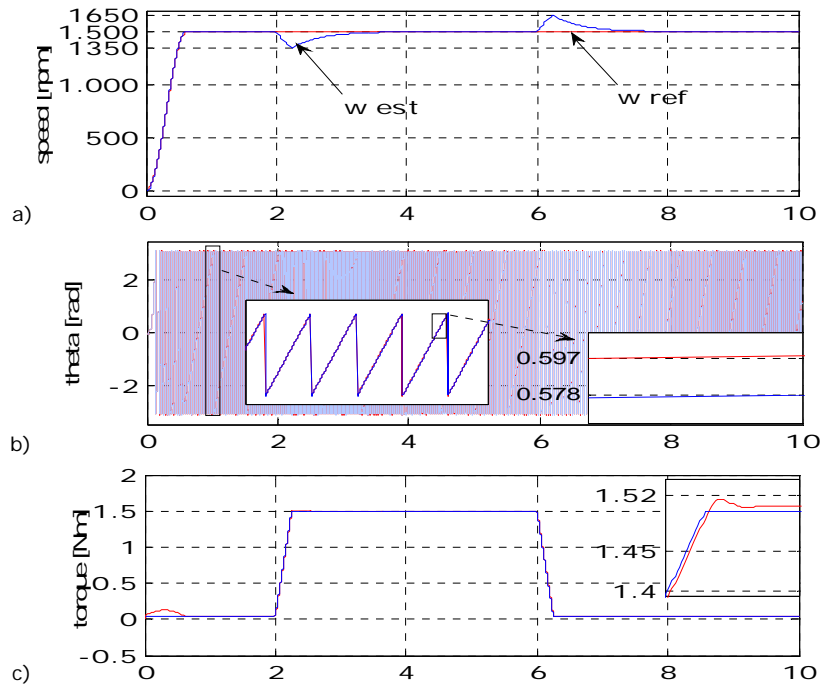


Fig. 3.6 IPMSM simulation model



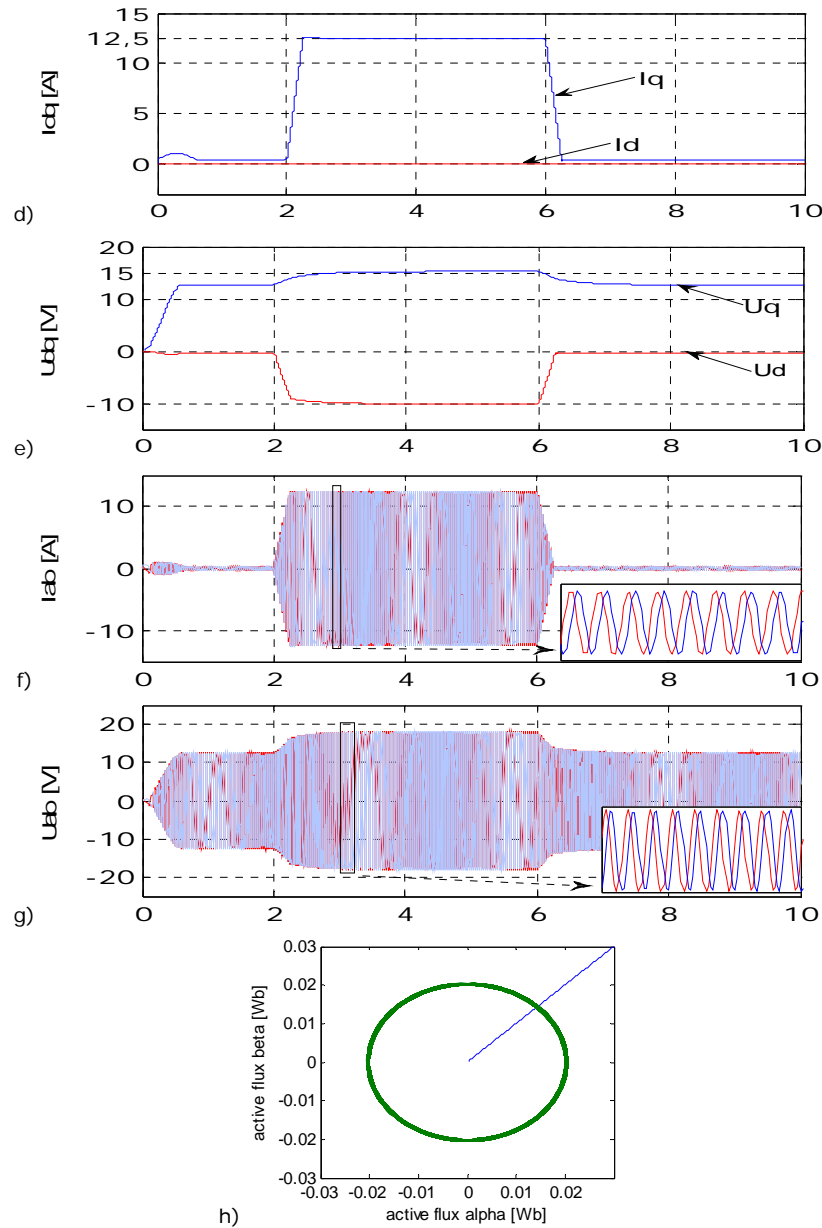


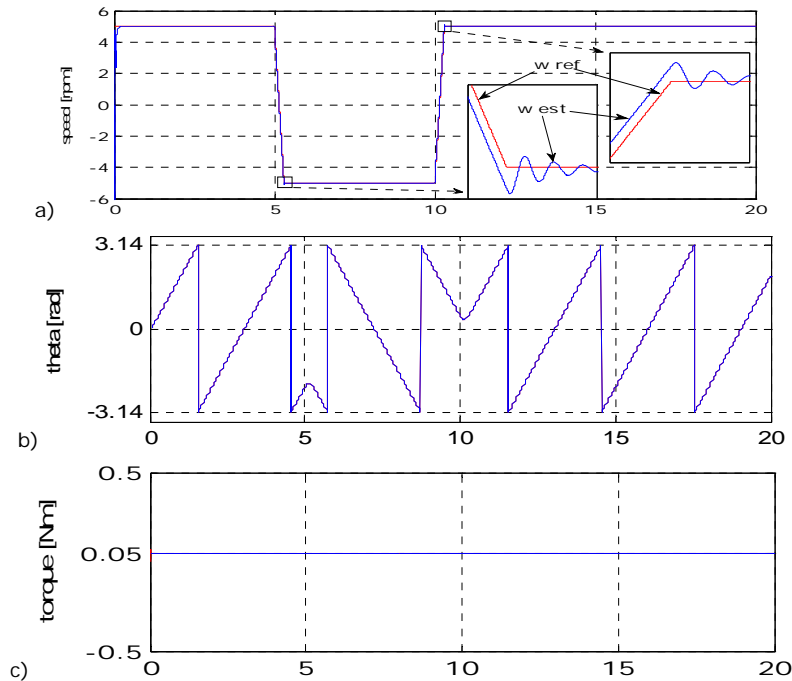
Fig. 3.7. Simulation results for sensorless vector control for 1500 rpm and 1,5 Nm load: a) speed; b) rotor position; c) torque; d) d, q currents; e) d, q voltages; f) α, β currents; g) α, β voltages; h) active flux – alpha versus beta hodograf;

Firstly, the machine acceleration from zero speed up to 1500 rpm (Fig. 3.7a), followed by a 1,5 Nm loading and afterwards the motor unloading (Fig. 3.7c), is illustrated in Fig. 3.7. The estimated speed follows the reference one, though some oscillations of ± 150 rpm are also present due to the machine loading and unloading.

During Fig. 3.7b, a 0.02 rad (1,15 electrical degree) difference between the encoder and the estimated rotor position can be seen.

The d axis current is kept to zero, while the q axis current is proportional with the machine torque, as seen in Fig. 3.7d. The d, q voltages are represented in Fig. 3.7e., while the α, β currents and voltages are shown in Fig. 3.7f. and Fig. 3.7g., respectively. Figure 3.7h shows the active flux (α versus β active flux components) hodograph.

The sensorless vector control scheme was also applied for the machine functioning into the low speed region. Further on, simulation results for a ± 5 rpm steady state speed profile are presented.



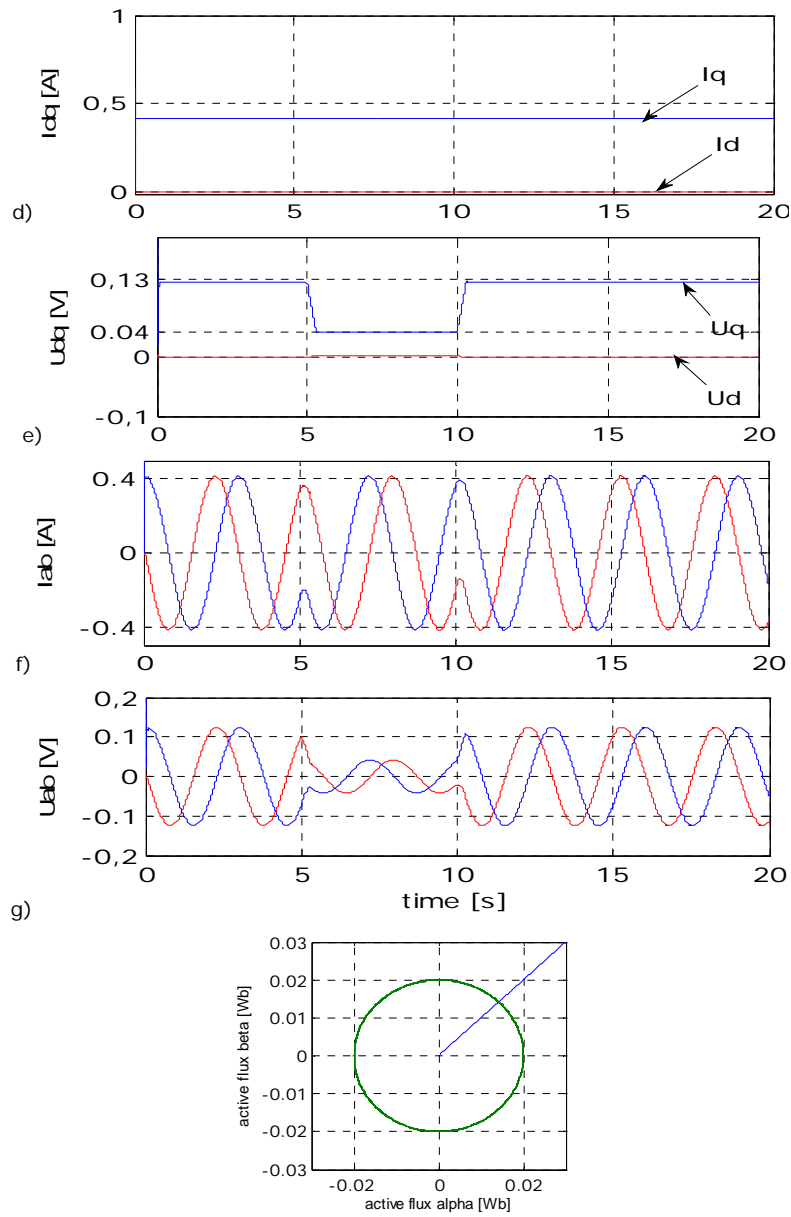


Fig. 3.8 Simulation results for sensorless vector control for ± 5 rpm at no load: a) speed; b) rotor position; c) torque; d) d, q currents; e) d, q voltages; f) α, β currents; g) α, β voltages;

First, the machine works at 5 rpm speed, at 5s the speed reversal at -5 rpm is applied and at 10s the reversal back to 5 rpm at no load is presented in Fig. 3.8a. The motor estimated speed follows the reference one with small noise.

As it can be seen from Fig. 3.8b, the estimated rotor position is overlapped on the encoder one. The d, q currents and voltages are represented in Fig. 3.8d. and 3.8e., whereas the α, β currents and voltages are shown in Fig. 3.8f. and Fig. 3.8g.

During Fig. 3.8h the active flux (α versus β active flux components) hodograph is represented. Now, if we consider both the experimental and the simulation results, an extensive comparison can be achieved.

Simulation results prove that the machine can reach the target ten times faster than in real experiments. During experiments, the machine speed stabilizes within approximately 4s, while in simulations it stabilizes in about fifty milliseconds.

If we discuss the case when the machine accelerates up to 1500 rpm, for both the motor loading and the unloading, the speed varies with ± 150 rpm and it stabilizes in about two seconds, in experimental tests. For the same operating conditions, simulation results show that the speed varies only with ± 20 rpm and it stabilizes in about 200 ms, which is ten times faster than during experiments. More than this, the difference between the encoder and the estimated rotor position is more than two times lower in simulations than in experiments. Moreover, as the simulations use a simplified drive model and most of the losses are neglected, both the currents and the voltages are lower than in real experiments.

On the other hand, if we take into account the results obtained for motor functioning at 5 rpm, we will previously notice the increased noise of the experimental results. Besides this, in what concerns the simulations, there is no difference between the encoder and the estimated rotor position, while a higher than 11 degrees difference between the two signals is registered in experiments.

3.5. Conclusion

This chapter focuses on both experimental and simulation performance of the sensorless control of IPMSM, through active flux concept and maximum torque per ampere condition. The proposed control scheme is shown and both the active flux observer and the compensation methods were afterwards discussed.

The proposed sensorless control strategy was applied for an IPMSM prototype in a speed range down to 5 rpm and up to 1500 rpm.

We claim that the proposed observer for speed and position estimation can be implemented in sensorless control schemes for all ac drives.

During simulations a couple of assumptions have been made, the inverter was considered ideal, what determines the implicit simulations better response if compared to the experimental ones.

Moreover, during experiments, the achieved signals are affected by increased noise and vibrations, which is not the case for simulations, where the parameters were considered constants.

References

- [1] I. Boldea, M.C. Paicu, G.D. Andreescu, "Active flux concept for motion-sensorless unified ac. drives", *IEEE Trans on Power Electronics*, Vol. 23, No.5, 2008, pp. 2612-2618;
- [2] F. Blaabjerg, J.K. Pedersen, P. Thogersen, "Improved modulation techniques for PWM-VSI drives", *IEEE Trans on Ind. Electronics*, Vol. 44, No. 1, pp. 87–95, 1997, ISSN 0278-0046;
- [3] Y.A.-R.I. Mohamed, T.K. Lee, "Adaptive self-tuning MTPA vector controller for IPMSM drive system", *IEEE Trans on Energy Conversion*, vol. 21, pp. 529-551, September 2006;
- [4] H. Hajime, T. Yoshio, K. Keiji, "Novel sensorless control for pm synchronous motors based on maximum torque control frame", *European Conference*;
- [5] S. Bolognani, S. Calligaro, R. Petrella, "Adaptive Flux-Weakening Controller for IPMSM Drives";
- [6] A. Consoli, G. Scarcella, G. Scelba, A. Testa, "Steady-State and Transient Operation of IPMSMs Under Maximum-Torque-per-Ampere Control", *IEEE Trans on Ind. Appl.*, vol. 46, no. 1, Jan./feb. 2010;
- [7] T.M. Jahns, G.B. Kliman, T.W. Neumann, "Interior Permanent-Magnet Synchronous Motors for Adjustable-Speed drives", *IEEE Trans. On Ind. Appl.*, Vol IA-22, pp. 738-747, July/Aug. 1986;
- [8] Y.A.-R.I. Mohamed, T.K. Lee, "Adaptive self-tuning MTPA vector controller for IPMSM drive system", *IEEE Transactions on Energy Conversion*, vol. 21, pp. 529-551, September 2006;

-
- [9] S. Bolognani, L. Sgarbossa, M. Zordan, "Self-tuning of MTPA current vector generation scheme in IPM synchronous motor drives", European Conference on Power Electronics and Applications, pp. 1-10, September 2007;
- [10] S. Kim, Y.-D. Yoon, S-K Sul, K. Ide, and K. Tomita, "Parameter Independent Maximum Torque per Ampere (MTPA) Control of IPM Machine Based on Signal Injection", 2010;
- [11] T. M. Jahns, G. B. Kliman, and T. W. Neumann, "Interior permanent magnet synchronous motors for adjustable speed drives," IEEE Transactions on Industry Applications, vol. IA-22, no. 4, pp. 738-747, Jul./Aug. 1986;
- [12] J.M. Kim, and S.K. Sul, "Speed control of interior permanent magnet synchronous motor drive for the flux weakening operation," IEEE Transactions on Industry Applications, vol. 33, no. 1, pp. 43-48, Jan./Feb. 1997;
- [13] H.B. Kim, J. Hartwig, and R.D. Lorenz, "Using on-line parameter estimation to improve efficiency of IPM machine drives", IEEE Power Electronics Specialists Conference, 2002, pp. 815-820;
- [14] Y.I. Mohamed, and T.K. Lee, "Adaptive self-tuning MTPA vector controller for IPMSM drive system," IEEE Transactions on Energy Conversion, vol. 21, no. 3, pp. 636-644, Sep. 2006;
- [15] P. Niazi, H.A. Toliyat, and A. Goodarzi "Robust maximum torque per ampere (MTPA) control of PM-assisted SynRM for traction application," IEEE Trans on Vehicular Technology, vol. 56, no. 4, pp. 1538-1545, Jul. 2007;
- [16] S. Morimoto, M. Sanada, and Y. Takeda "Effects and compensation of magnetic saturation in flux-weakening controlled permanent magnet synchronous motor drives," IEEE Transactions on Industry Applications, vol. 30, no. 6, pp. 1632-1637, Dec. 1994;
- [17] G. Kang, J. Lim, K. Nam, H.B Ihm, and H.G. Kim "A MTPA control scheme for an IPM synchronous motor considering magnet flux variation caused by temperature," in IEEE 2004 Applied Power Electronics Conference and Exposition, 2004, pp. 1617-1621;
- [18] H.B. Kim, J. Hartwig, R.D. Lorenz, "Using on-line parameter estimation to improve efficiency of IPM machine drives", IEEE 33rd Power Electronics Specialists Conference, vol. 2, pp. 815-820, June 2002;

- [19] Z.Q. Zhu, Y.S. Chen, and D. Howe "Online optimal flux-weakening control of permanent-magnet brushless AC drives," IEEE Transactions on Industry Applications, vol. 36, no. 6, pp. 1661-1668, Nov./Dec. 2000;
- [20] S. Bolognani, R. Petrella, A. Prearo, and L. Sgarbossa "Automatic tracking of MTPA trajectory in IPM motor drives based on AC current injection," in IEEE 2009 Energy Conversion Congress and Exposition, 2009, pp. 2340-2346;
- [21] D. Anton, Y.K Kim, S.J Lee, S.T Lee "Robust self-tuning MTPA algorithm for IPMSM, Industrial Electronics, IECON 2008, 34th Annual Conference of IEEE
- [22] I. Boldea "Reluctance Synchronous Machines and drives" book, chapter 7, OUP, Oxford, U.K., 1996.

Chapter 4

V/f with Stabilizing Loops Control of Distributed Windings IPMSM: Principles and Digital Simulation Results

During this chapter a rather novel fast dynamics V/f with two correction loops control is introduced [18]. Theoretical background and digital simulation results are presented and the results are discussed.

The active flux concept (previously described in Chapter 3) is introduced in reference [6] and it is used to develop the two novel stabilizing loops for V/f control. The use of the proposed control strategy avoids the usual switching from signal injection based to model-based position estimation in FOC [1] and DTFC [2-5] during starting and it was implemented in order to improve standard V/f control [7], [8].

All on-line calculations are based on the active flux concept in order to simplify mathematical expressions with securing both maximum torque per ampere condition [9], [10] up to base speed and (or) close to maximum efficiency operation in the process.

4.1. Standard V/f Control

Standard V/f control (Fig. 4.1.) can be successfully implemented for permanent magnet synchronous machines equipped with squirrel cage (damper winding), as it is able to resynchronize the PM machine, if needed. This open loop control approach, used for PMSMs with damper winding is similar to the one used for induction machines and it is suitable for applications which do not require fast speed and torque response, like pumps and fans. More than that, the open loop scalar drives are vulnerable to fast ramp accelerations and large torque perturbation. This type of drive has as main convenience the fact that slip compensation is not required, as it is required for IM Drives [11].

Things are different for the PMSM without damper winding, for which neither the rotor synchronization with the excitation frequency, nor the stable operation is assured. In this case, the control has to be designed to function in closed loop fashion [12], [13]. One of the main advantages of using this control method is that the machine can start from any rotor position, thus we no longer need to use a separate starting strategy [14-17].

The voltage amplitude is determined from (4.1), where V_0 is the voltage boost and it is necessary for the drive functioning in the low speeds region.

$$V = V_0 + k \cdot f^* \tag{4.1}$$

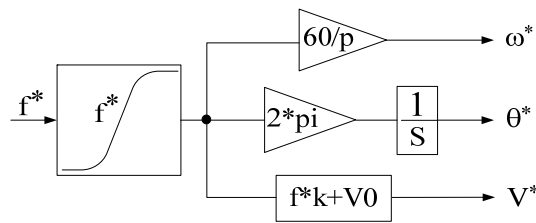


Fig. 4.1. Standard V/f scheme, with reference speed, position and voltage calculation.

Firstly, **digital simulations** have been conducted to prove the theoretical approach for open loop V/f control, so speed and torque response results for motor acceleration from zero speed up to 1500 rpm, at no load are shown in Fig. 4.2.

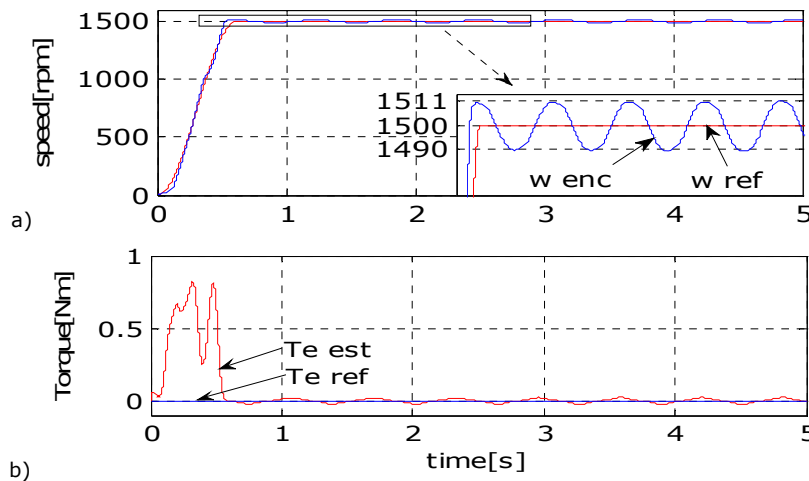


Fig. 4.2. Standard V/f control–Simulation results for motor acceleration from zero speed up to 1500 rpm at no load: a) speed response, b) torque response;

Machine acceleration from zero speed up to 1500 rpm, at no load is represented in Fig. 4.2a, while torque response is shown in Fig. 4.2b. The machine accelerates in about 500 ms, so it does not fulfill the fast dynamic response requirement.

During Fig. 4.3, the machine speed and torque response for a 5 Nm ramp load torque is illustrated. The ramp reference torque was applied at 0,65 s, after the machine speed stabilization (Fig. 4.3b), but the collapse of the drive under 800 ms ramp of 5 Nm torque perturbation is evident, which indicates the open loop V/f control poor performances.

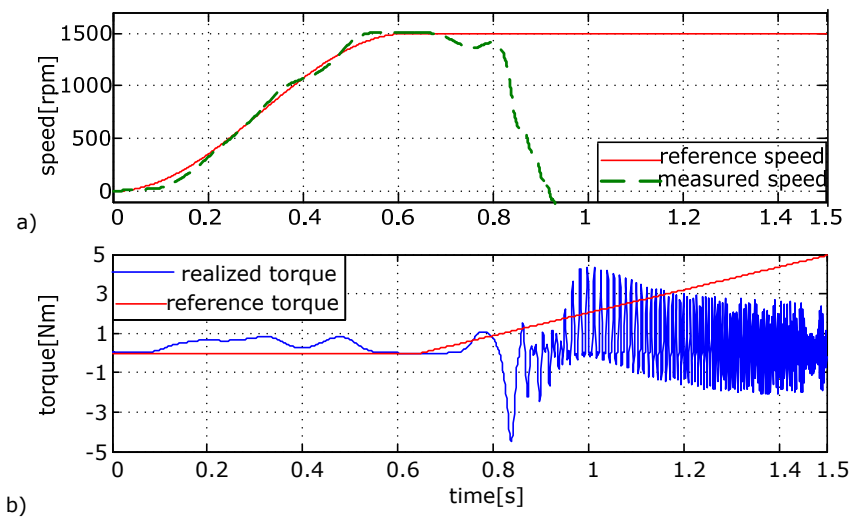


Fig. 4.3. Standard V/f control–Simulation results for motor acceleration from zero speed up to 1500 rpm at 5 Nm ramp load: a) speed response; b) torque response.

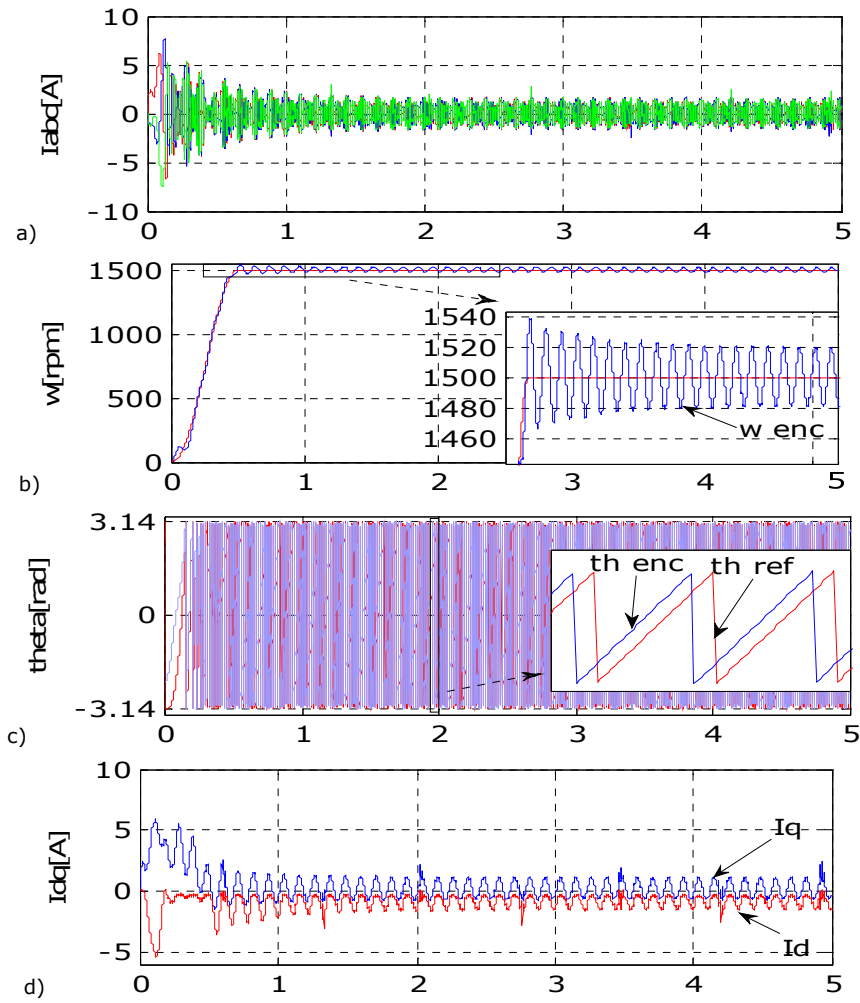
Considering the fact that there was a delay in time between simulations and experiments, we have to mention that the latter were realized for a different IPM synchronous machine, with different parameters than the ones used for simulations. The specifications for the IPMSM used in simulations can be found in Table 4.1, while the IPMSM parameters used for experiments are shown in Table 7.1.

Therefore, **experiments** have been performed in similar conditions as during simulations and the results for both no load and load operation are shown in Fig. 4.4 and Fig. 4.5., respectively.

Initially, the results for motor acceleration from zero up to 1500 rpm at **no load** will be discussed.

As shown in Fig. 4.4b, the motor accelerates in 500 ms and the speed oscillates continuously with ± 10 rpm around the target. Maintained oscillations are also present in currents (Fig. 4.4a,d,e) and voltages (Fig. 4.4f) waveforms.

The difference between the reference and the actual rotor position can be seen in Fig. 4.4c.



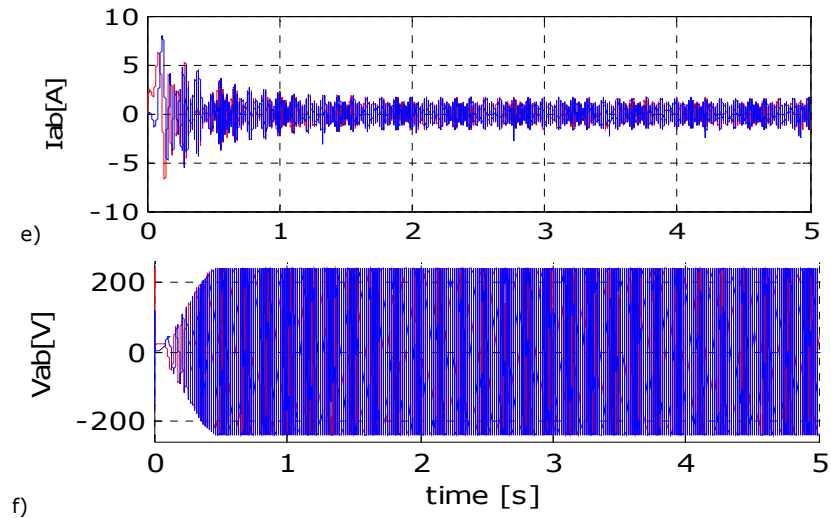


Fig. 4.4. Experimental results for standard V/f control from zero up to 1500 rpm at no load: a) I_{abc} currents; b) speed; c) rotor position; d) dq currents; e) $\alpha\beta$ currents; f) $\alpha\beta$ voltages.

Further on, experimental results and the machine response **at load** are presented in Fig. 4.5.

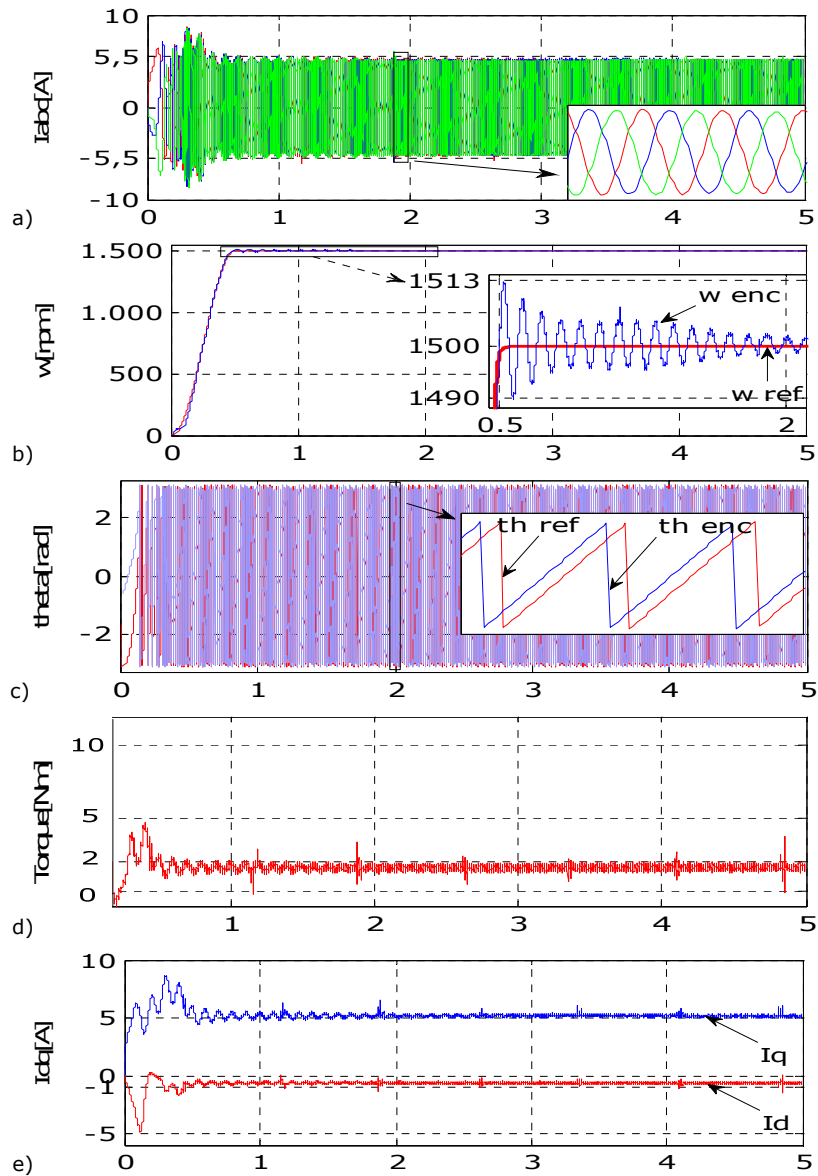
Simultaneously with the motor acceleration up to 1500 rpm (Fig. 4.5b), a proportional with speed up to 2 Nm load torque was applied (Fig. 4.5d). The maintained oscillations are present in both speed and torque responses, but are also visible in currents and voltages waveforms (Fig. 4.5 a,e,f,g).

These oscillations are slowly decreasing under 10 rpm and their influence can be traced more than 2s, as highlighted in the figure zoomed region.

In Fig. 4.5c, the reference and actual rotor position are shown.

As we could observe from simulation results in Fig. 4.3, the motor speed collapse was imminent, even though a smooth ramp load torque was prescribed. During experiments, as Fig. 4.5b shows, the motor speed did not fall when the load was applied, but we have to say that the applied load torque represents only 15% of its nominal value; furthermore, the motor managed to realize it with the price of high current values, almost equal with the motor maximum values.

Thus, both simulation and experimental results have shown, as it is well known, that open loop V/f control is characterized by instability, low dynamics and maintained oscillations. Similar speed and torque response were achieved in both experiments and simulations.



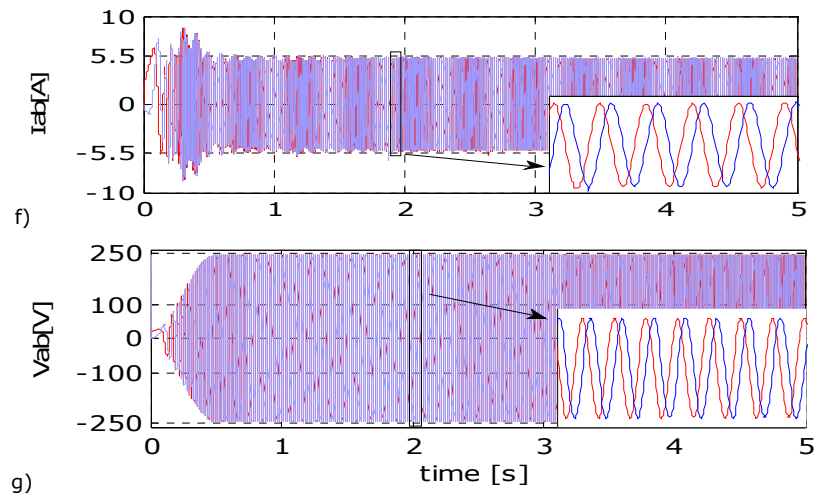


Fig. 4.5. Experimental results for V/f open loop control for fastest frequency acceleration available up to 1500rpm and 500 ms, proportional with speed, 2 Nm load torque response: a) I_{abc} currents; b) speed; c) rotor position; d) torque response; e) dq currents; f) $\alpha\beta$ currents; g) $\alpha\beta$ voltages.

During experiments, a proportional with speed, 2 Nm load torque was applied, so if we compare the no-load with the load results, we can easily see that in the latter case, the voltages have higher values, the currents are three times higher and the oscillations are slowly decreasing. We also have to mention that the no load V/f control is characterized by maintained oscillations, whereas at load the oscillations slowly decrease and after a while it become barely visible.

During both no load and load operations, there is a visible difference of about 1 rad between the reference and the encoder position.

All these results have shown that open loop V/f control is characterized by reduced performances and it can be easily applied for applications which do not require fast response or high efficiency. Therefore, to obtain drive high dynamic response, some corrections for the standard V/f control have to be implemented and analyzed.

Further on, two correction loops will be added to the standard V/f control scheme, both of them based on the *active flux concept* and having included the *maximum torque per ampere condition*.

4.2. V/f with Stabilizing Loops Control

4.2.1. The Proposed Active Flux Error-Based Voltage Amplitude Stabilizing Loop

In order to eliminate or at least reduce the open loop V/f control drawbacks, with the main purpose to obtain comparable results with the ones achieved with sensorless field oriented control, but with less computation effort, a novel V/f with two correction loops has been proposed. The afore mentioned corrections are calculated through PI controllers. So, it is important to specify that the controllers do not influence directly the measures, they only correct them.

The core of the proposal consists in driving to zero, through a closed loop, the active flux error, between its reference Ψ_d^{a*} and its estimated value $\hat{\Psi}_d^a$. The active flux $\hat{\Psi}_d^a$ of any AC machine has been previously defined in Chapter 3, as the flux which multiplies the I_q current to produce the machine estimated torque.

In order to obtain the estimated active flux, the stator flux correct estimation is mandatory, thus the stator flux components along $\hat{\Psi}_\alpha$ and $\hat{\Psi}_\beta$ have to be initially determined (4.2). Above 2-3 Hz, only the voltage model may be used:

$$\hat{\Psi}_\alpha = \frac{T}{1+sT} (V_\alpha^* - R_s \cdot i_\alpha); \quad \hat{\Psi}_\beta = \frac{T}{1+sT} (V_\beta^* - R_s \cdot i_\beta); \quad (4.2)$$

Where T is in the order of one second.

Knowing the stator flux components along α and β axes, we can easily obtain the active flux components in stator coordinates from (4.3) and afterwards, the active flux amplitude (4.4).

$$\hat{\Psi}_{d\alpha}^a = \hat{\Psi}_\alpha - L_q \cdot i_\alpha; \quad \hat{\Psi}_{d\beta}^a = \hat{\Psi}_\beta - L_q \cdot i_\beta \quad (4.3)$$

$$\hat{\Psi}_d^a = \sqrt{\hat{\Psi}_{d\alpha}^a{}^2 + \hat{\Psi}_{d\beta}^a{}^2} \quad (4.4)$$

To determine the active flux reference value (4.6), the reference current along d axis (4.5) has to be achieved from MTPA condition (explained in detail in Chapter 3).

$$i_d^* = -\frac{1}{4} \cdot \frac{\Psi_{PM}}{L_d - L_q} - \frac{1}{2} \cdot \sqrt{\frac{1}{4} \cdot \left(\frac{\Psi_{PM}}{L_d - L_q} \right)^2 + 2 \cdot I_s^2}; \quad (4.5)$$

$$\Psi_d^{a*} = \Psi_{PM} + (L_d - L_q) \cdot i_d^* \quad (4.6)$$

Knowing the active flux reference and its estimated value, we can write the active flux error:

$$\Delta\Psi_d^a = \Psi_d^{a*} - \hat{\Psi}_d^a \quad (4.7)$$

Next, equation (4.8) reflects a hybrid PI plus a simplified sliding mode (SM) closed loop that will correct the voltage amplitude of the V/f system.

$$\Delta V^* = -\Delta\Psi_d^a \left(\frac{k_{pv}}{1 + T_{iv} \cdot s} \right) - k_{SM} \cdot \text{sign}(\Delta\Psi_d^a) \quad (4.8)$$

4.2.2. The Proposed Speed Error-Based Voltage Phase Angle Stabilizing Loop

A novel stabilizing loop for voltage phase angle correction $\Delta\gamma$ in the V/f control is proposed here. It is based on the speed error, $\Delta\omega_r^*$, where $\hat{\omega}_r$ is the rotor estimated speed, also known as the active flux speed:

$$\hat{\omega}_r = \omega \left(\hat{\Psi}_d^a \right) = \frac{\hat{\Psi}_{d\alpha}^a[k-1] \cdot \hat{\Psi}_{d\beta}^a[k-1] - \hat{\Psi}_{d\beta}^a[k-1] \cdot \hat{\Psi}_{d\alpha}^a[k-1]}{T_s \cdot \left(\hat{\Psi}_{d[k]}^a \right)^2} \quad (4.9)$$

Where, T_s is the sampling time. Some filtering is required, so a low pass filter will be implemented, although it introduces signal delay.

Alternatively, a PLL observer may be used for the speed or angle estimation.

Correction for dc offset of the integral, of inverter nonlinearities and of stator resistance for low speed estimation of Ψ_α , Ψ_α are feasible but they complicate the drive.

The angle correction loop equation is based on speed error and its equation is written below:

$$\Delta\gamma^* = -\Delta\omega_r \left(\frac{k_{pv}}{1 + T_{\gamma i} \cdot s} \right) - k_{SM} \cdot \text{sign}(\Delta\omega_r) \quad (4.10)$$

4.2.3. The Proposed Control System

The generic control system with the two above mentioned stabilizing loops is illustrated in Fig. 4.6. and it is based on the active flux observer, previously described during Chapter 3.

Summarizing on the stabilizing loops we may infer that they may be equivalent to two model reference adaptive systems.

The proposed control (Fig. 4.6) characterization follows:

- It contains a V^*/f^* control to provide **self-starting** and satisfactory no load operation at all speeds of interest;
- It adds to it two stabilizing loops to correct voltage vector amplitude by ΔV^* and phase by $\Delta\gamma^*$, via two PI plus sliding mode regulators;
- It provides default **maximum torque/current** operation;

The two stabilizing loops embody PI plus SM regulators on the active flux amplitude error $\Delta\Psi_d^a = \Psi_d^{a*} - \bar{\Psi}_d^a$ and on the speed error, $\Delta\omega_r = \omega - \omega_{\Psi_d^a}$, respectively, to produce ΔV^* (amplitude) and $\Delta\gamma^*$ (angle) corrections to the V/f standard control tailored after no load.

The active flux $\bar{\Psi}_d^a$ observer is based here on the voltage model of stator flux $\bar{\Psi}_s$ (Fig. 3.1) after subtracting $L_q^* \bar{i}_s$, with \bar{i}_s measured; such an observer is to be used above a certain minimum frequency f_{\min} (reference speed) of a few Hz. Pure V/f control is used for $f^* < f_{\min}$.

The reference rather than measured voltages V_α^* , V_β^* are used, with adequate corrections for inverter nonlinearities [19], [20]. Inverter maximum voltage vector is estimated by measuring only the dc voltage.

The reference active flux amplitude $\Psi_d^{a*}(i_s)$ is not constant, but depends on the measured \bar{i}_s , such that to provide maximum torque/current conditions by using equations to settle $i_d^*(i_s)$ and then $\Psi_d^{a*}(i_s)$.

Magnetic cross-coupling saturation [21] is known to produce errors in stator flux or rotor position estimation [16]; in our case, the active flux observer is "touched" by cross-coupling saturation only by its influence on L_q . According to the unique d and q magnetic curves model for cross-coupling saturation, L_q is approximately a sole function of \bar{i}_s , which is measured.

The proposed control system avoids the speed and current regulators (and the coordinate transformations), but still uses two stabilizing loops (for voltage amplitude and angle).

However, it provides self-starting and wide speed control with implicit maximum torque/current operation and up to maximum torque/flux operation.

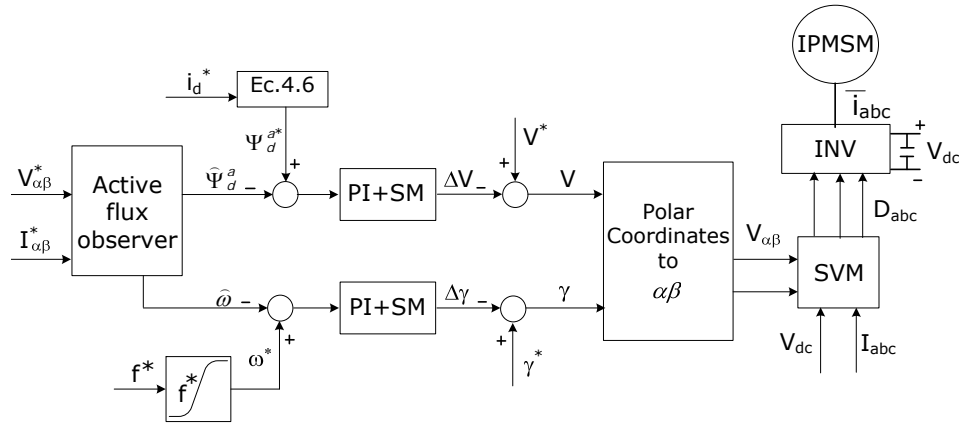


Fig. 4.6 V/f control with two active flux stabilizing loops: ΔV and $\Delta \gamma$ (for $\Delta V < 0$, max torque/current operation); for $\Delta V > 0$, towards max torque/flux operation is provided for max torque /speed envelope (flux weakening)

The above attributes and the fact that the proposed control can be applied for all ac motor drives, with small particularization changes for various motor types, should suggest its full potential.

The IPMSM under digital simulation investigation with the specifications given in Table 4.1 shows a rated saliency $L_q/L_d = 4/1$ so most torque is reluctance torque while the PM flux is rather small: wide torque-speed range is thus secured with reasonable max-speed emf (<150%).

The MATLAB implementation of the two correction loops described during Fig. 4.6. is shown in detail in Fig. 4.7a,b.

The control system parameters in Fig. 4.7 with PI plus sliding mode (SM) controller type, refer to the active flux error controller: $k_{p_d\psi}=51$, $k_{i_d\psi}=13.6$, $k_{sm_d\psi}=0.1$, while for the speed error controller, $k_{p_d\omega}=0.0007$, $k_{i_d\omega}=1.01$, $k_{sm_d\omega}=0.0001$. All these parameters have been introduced by the trial and error method. The V/f parameter, k , which represents the proportionality between the voltage and the frequency is $k=0.105$, while the initial (boost) voltage of about 0.1 V, characterize the standard V/f scheme.

First, a d-q current vector control system was programmed and run in Matlab to check the performance of the speed estimator (active flux speed $\hat{\omega}_r$) and the active flux estimated value ($\hat{\Psi}_d^a$).

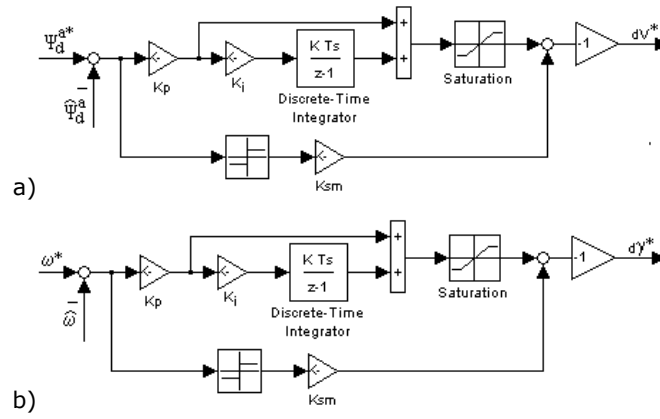
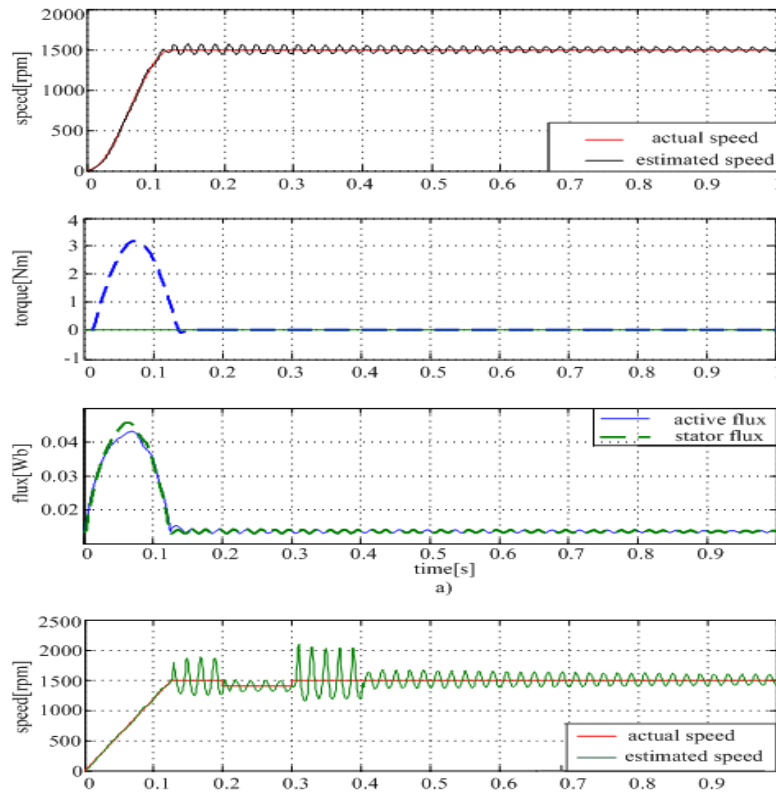


Fig. 4.7. Correction loops: a) Voltage amplitude correction loop; b) Voltage phase correction loop;



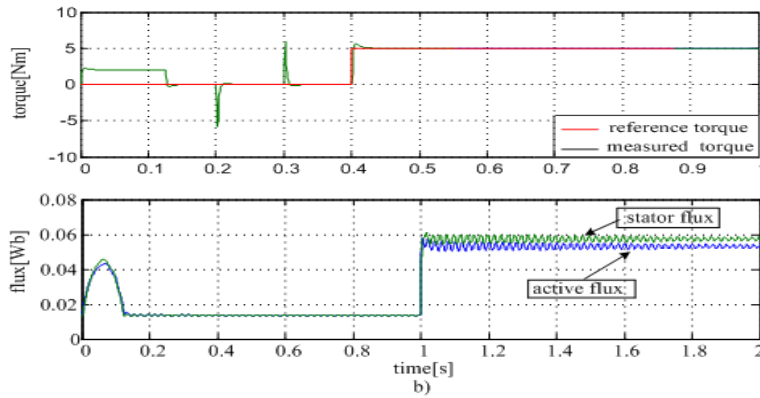


Fig. 4.8. Vector control results for motor fast acceleration up to 1500 rpm: a) Estimated speed, torque response and both stator flux and active flux variation during acceleration at no load; b) Estimated speed, torque response and both stator flux and active flux variation at 5Nm load, after a speed transient between 0,2 and 0,3 s

Figure 4.8 shows the results during rather fast speed transients. Quick acceleration by vector control to 1500 rpm at no load, is shown in Fig. 4.8a.

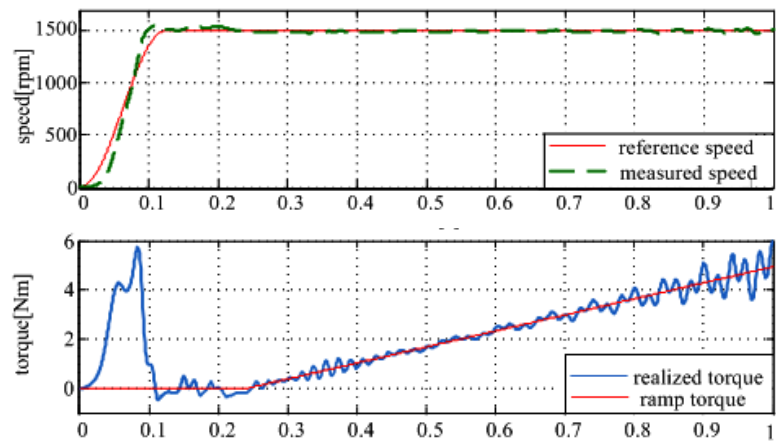
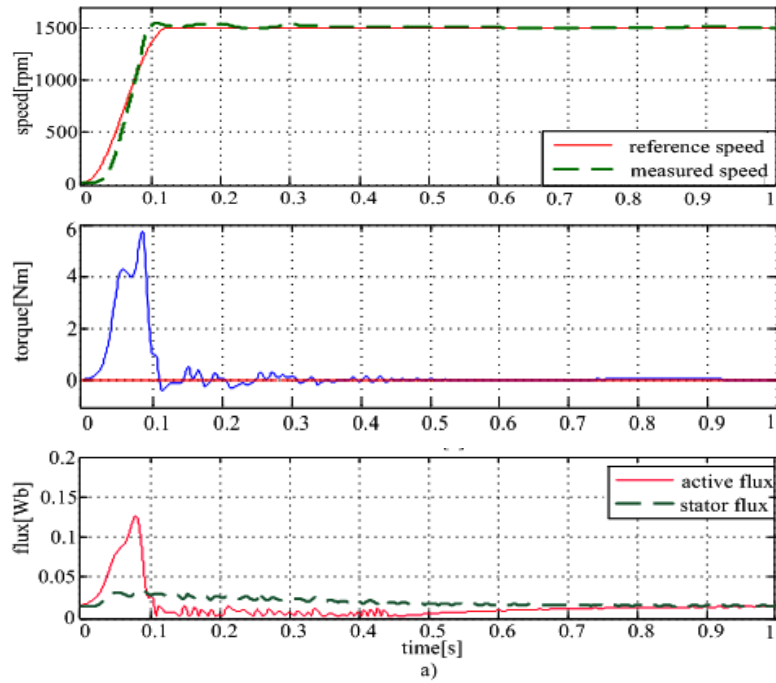
The persistent oscillations in the speed $\hat{\omega}_r$ and active flux $\hat{\Psi}_d^a$ estimators, mainly due to a compromise between response quickness and stability during fast speed and torque perturbations, need further treatment, but for the time being, they are considered acceptable to prove the concept.

Then, a step speed reduction from 1500 rpm to 1400 rpm at 0.2s, followed by a step speed recovery back to 1500 rpm at 0.3 s and then a step 5 Nm torque at 0.4s perturbation is presented in Fig. 4.8b.

The speed response is fast but some speed oscillations around the target persist. They are believed to be caused by the not so good quality of the active flux observer (Fig. 3.2).

A comparison between the stator and active flux is also shown, both at load and at no load (Fig. 4.8.). We can observe that the active flux increases and then it decreases, when the machine accelerates and then increases slightly when the 5Nm load occurs.

An 800 ms ramp 5Nm torque perturbation was applied at $t=0.2s$ (Fig.4.9b). The machine response is still stable but some small speed oscillations still persist as under no load. A step 5Nm load, as in vector control (Fig. 4.8b), was tried, but the proposed drive did not survive this severe transient test.



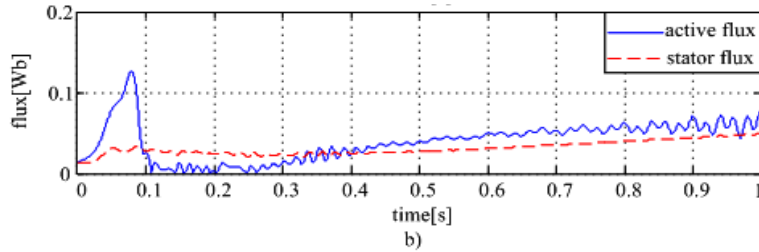


Fig. 4.9. Speed and torque response and flux variation at no load a) and at a ramp 5Nm load b) when the proposed V/f control with two stabilizing loops is considered

TABLE 4.1
IPMSM SPECIFICATIONS

Rated power	2.35 kW
Rated speed	1500 rpm
Rated frequency	50 Hz
Rated torque	5 Nm
Rated phase to phase voltage	22 V (rms)
Rated phase current	67 A (rms)
Rated battery voltage (V_{batt})	48 V
Number of pole pairs (p_1)	2
Stator resistance per phase (R_s)	0.05 Ω
d -axis inductance (L_d)	0.45 mH
q -axis inductance (L_q)	1.8 mH
Permanent magnet flux (Ψ_{PM})	0.0136 Wb
Total inertia (J)	1.6e-3 kg*m ²
Viscous friction coefficient (B)	1e-4 Nm s/rad

For active flux estimation (4.3), stator flux estimation is crucial. A combined voltage/current model observer is used here for the scope based on [24].

To avoid rotor position estimation we need to "fix" the desired longitudinal current i_d^* versus stator current i_s such that to consider both maximum torque/current below base speed for up to full torque and at low torque during flux weakening.

Maximum torque per flux for limited voltage (during full available torque requirement with flux weakening) at high speeds is obtained by adding a correction $-\Delta i_d^*$ to i_d^* when reference voltage $V_s^* > V_{smax}$ (V_{smax} - maximum PWM inverter voltage vector).

4.3. Conclusion

This chapter proposes two stabilizing loops in addition to the standard V/f control, which are based on the active flux concept, amenable to all ac machine drives.

The two stabilizing loops that „correct“ both the voltage vector amplitude ΔV^* and its angle $\Delta \gamma^*$, are based on active flux $\Delta \Psi_d^a$ and speed $\Delta \omega_r$ error, respectively.

The method also provides default max torque/current operation unless the voltage ceiling of the PWM is surpassed, when the d axis reference current i_d^* is corrected toward max torque/flux conditions. Consequently, wide torque-speed operation is implicit, with close to optimum efficiency. The speed and current control loops are eliminated, while current sensors are not.

As the built-in V/f control provides for light load starting (typical to pumps, blowers, centrifugal air compressors), the proposed method avoids a dedicated starting strategy (for synchronous machines).

First, simulation tests have been conducted to show the open loop V/f control capabilities, after that, the correction loops were added to prove their effectiveness. Secondly, experimental results have been achieved to strengthen the digital simulations results.

Due to the time delay between the simulations and the experiments, results have been achieved for two different IPM synchronous machines, with different specifications.

References

- [1] F. Blaschke, "The principle of field orientation as applied to the new transvector closed loop control system in a PWM inverter induction motor drive", Siemens Rev., vol. 39, no. 5, pp. 217–220, 1972;
- [2] I. Takahashi and T. Noguchi, "A new quick-response and high-efficiency control strategy of an induction motor", in Conf. Rec. IEEE IAS 1985 Annu. Meeting, pp. 496–502;
- [3] M. Depenbrock, "Direct self-control (DSC) of inverter-fed induction machine", IEEE Trans. Power Electron., vol.3, no.4, pp.420–429, 1988;

-
- [4] I. Boldea and S. A. Nasar, "Torque vector control (TVC)—A class of fast and robust torque-speed and position digital controllers for electric drives", *Electric Mach. Power Syst.*, vol. 15, no. 3, pp. 135–148, 1988;
 - [5] C. Lascu, I. Boldea, F. Blaabjerg, "Direct torque control of sensorless induction motor drives: A sliding-mode approach", *IEEE Trans.on Ind. Applicat.*, Vol. 40, No. 2, pp. 582–590, 2004;
 - [6] I.Boldea, M.C. Paicu, G.D. Andreescu, "Active flux concept for motion-sensorless unified ac. drives", *IEEE Transactions on Power Electronics*, vol. 23, no.5, pp. 2612–2618, Sept. 2008, ISSN: 0885-8993;
 - [7] C. Perera, "Sensorless Control of Permanent-Magnet Synchronous Motor Drives", Ph. D. Dissertation, December 2002, Institute of Energy Technology, Aalborg University, Denmark;
 - [8] P.D.C.Perera, F. Blaaiberg, J.K. Pedersen, P.T. Thogersen, "A sensorless stable V/f control method for PMSM drives", *Industry Application IEEE Trans. on Vol.39, no.3*, 2003, pp.783-791;
 - [9] S.M. Sue, T.W. Hung, J.H. Liaw, Y.F. Li, C.Y. Sun, "A new MTPA control strategy for sensorless V/f controlled PMSM drives", *Industrial Electronics and Applications (ICIEA)*, 2011 6th IEEE Conference on, 21-23 June 2011, pp. 1840–1844, ISBN: 978-1-4244-8754-7;
 - [10] Bolognani, S.; Petrella, R.; Prearo, A.; Sgarbossa, L.; "On-line tracking of the MTPA trajectory in IPM motors via active power measurement", *Electrical Machines (ICEM)*, XIX International Conference on, 6-8 Sept. 2010, pp. 1–7, ISBN: 978-1-4244-4174-7;
 - [11] M.H.V. Reddy, V. Jegathesan, "Open loop V/f control of induction motor based on hybrid PWM with reduced torque ripple", *Emerging Trends in Electrical and Computer Technology (ICETECT)*, 2011 International Conference on, 23-24 March 2011, pp. 331–336, ISBN: 978-1-4244-7923-8;
 - [12] R. Ancuti, I.Boldea, G.D. Andreescu, D. Iles, "Novel motion sensorless control of high-speed small-power surface mount PMSM drives with experiments", *Record of OPTIM-2008*, vol.3, pp.11-18; ISBN: 978-1-4244-1544-1;
 - [13] R. Ancuti, I.Boldea, G.D. Andreescu, "Sensorless V/f control of high-speed surface permanent magnet synchronous motor drives with two novel

- stabilising loops for fast dynamics and robustness”, *Electric Power Applications, IET*, Vol. 4, No. 3, pp. 149 – 157, ISSN: 1751-8660;
- [14] W.T. Joung; J.H. Lee; S.H. Moon; H.J. Wang; T.S. Hwang; C.H. Choi; Y.S. Kim, “Sensorless speed control and initial rotor position estimation of an IPMSM”, *Power Electronics, 2007, ICPE '07. 7th International Conference on*, 22-26 Oct. 2007, pp. 388 – 393, ISBN: 978-1-4244-1871-8;
- [15] M.E. Haque, L. Zhong, M.F. Rahman, “Initial rotor position estimation of interior permanent magnet synchronous motor without a mechanical sensor”, *School of Electrical Engineering and Telecommunications, The University of New South Wales, Sydney, Australia*;
- [16] Q. Jilong, T. Yantao, G. Yimin, Zhucheng, “A Sensorless Initial Position Estimation Scheme and Extended Kalman Filter Observer for the Discret Torque Controlled PMSM Drive”, *Proc. of Electrical Machines and Systems, 2008. ICEMS 2008. International Conference on*, pp. 3945-3950, 17-20 October, 2008, ISBN: 978-1-4244-3826-6;
- [17] H. Kim, K. K. Huh, M. Harke, J. Wai, R. D. Lorenz, and T. A. Jahns, “Initial rotor position estimation for an integrated starter alternator IPM synchronous machine”, in *Proc. 10th Eur. Conf. Power Electron. Applicat. (EPE-2003)*, Toulouse, France, 2003, pp. 1875–1881;
- [18] I. Boldea, A. Moldovan, V.C. Schramel, G.D. Andreescu, L. Tutelea, “A class of fast dynamics V/f sensorless AC general drives with PM-RSM as a case study”, *Optimization of Electrical and Electronic Equipment (OPTIM)*, 2010 12th Internat. Conf. on, 20-22 May 2010, pp. 453–459, ISBN: 978-1-4244-7019-8;
- [19] F. Blaabjerg, J.K. Pedersen, P. Thogersen, “Improved modulation techniques for PWM-VSI drives”, *IEEE Trans on Ind. Electronics*, Vol.44, No.1, pp. 87–95, Febr. 1997, ISSN: 0278-0046;
- [20] Y.K. Lin, Y.S. Lai, “Dead-time elimination of pwm-controlled inverter/converter without separate power sources for current polarity detection circuit”, *Sustainable Energy Technologies, ICSET 2008. IEEE International Conference on* pp. 130–135, 24-27 Nov. 2008, ISBN: 978-1-4244-1887-9;
- [21] P. Guglielmi, M. Pastorelli, A. Vagati, “Cross-Saturation Effects in IPM Motors and Related Impact on Sensorless Control”, *Industry Applications, IEEE Trans. on*, 2006, Vol. 42, No. 6, pp. 1516-1522, ISSN: 0093-9994.

Chapter 5

V/f with Stabilizing Loops and Sensorless Vector Control of IPMSM – Experimental Characterization

The PMSM utilization for electric drive applications requires the initial rotor position information [1-4], which is usually given by an encoder or a resolver, that is characterized by high cost of the drive, increased machine size, low reliability. Thus, fundamental control schemes [5-7] are used for motion sensorless control of the drive [9-13].

This chapter introduces both V/f [14] with stabilizing loops control and sensorless vector control results. The operating motor conditions were considered similar and their comparison is performed. A novel V/f control for surface PM synchronous motor with two stabilizing loops, both of them based on the reactive power, is described in reference [17].

5.1. V/f with Stabilizing Loops Control

The angle stabilizing loop, based on $\Delta\omega_r^* = \omega_r^* - \hat{\omega}_r$ is:

$$\Delta\gamma^* = -\Delta\omega_r \cdot \left(k_p + k_i \cdot \frac{1}{s} \right) \quad (5.1)$$

The reference speed, angle and voltage are calculated with the reference frequency ramp, where: $\theta = 2 \cdot \pi \int \hat{f}^* dt$ and $V^* = \hat{f}^* \cdot k + V_0$, with $V_0 \approx R_S \cdot I_N$; $k = const$.

The proposed V/f with the stabilizing loops control scheme is illustrated in Fig. 5.1. and it is characterized by a V^*/f^* -control [8] to provide self-starting and satisfactory no load operation at all speeds of interest and by two stabilizing loops to correct the voltage vector amplitude by ΔV^* and phase by $\Delta\gamma^*$.

The two stabilizing loops (See Fig. 5.2.) embody PI regulators on the active flux [15], [16] amplitude error $\Delta\Psi_d^a = \Psi_d^{a*} - \hat{\Psi}_d^a$ and, respectively, on the speed error $\Delta\omega_r = \omega^* - \hat{\omega}_{\Psi_d^a}$ to produce ΔV^* (amplitude) and $\Delta\gamma^*$ (angle) corrections to the V/f standard control, tailored after no load.

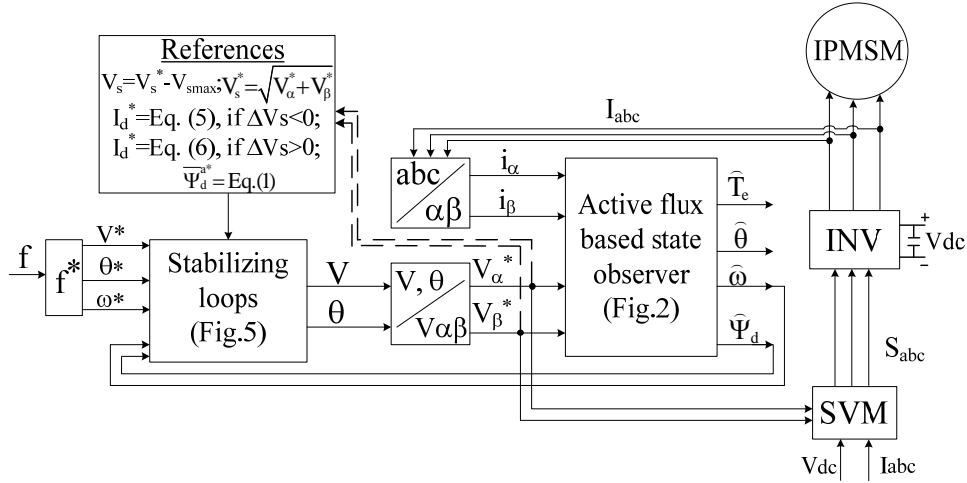


Fig. 5.1. V/f control with two active flux stabilizing loops: ΔV^* and $\Delta \gamma^*$.

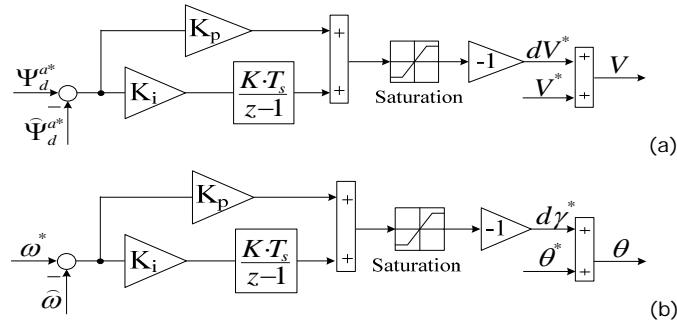


Fig. 5.2 Correction loops for stabilizing a) Voltage amplitude, ΔV^* ; b) Voltage phase, $\Delta \gamma^*$.

For fair comparisons, a sensorless vector control of the IPMSM used as case study was implemented and the block diagram is shown in Fig. 5.3. Experiments have been conducted both at no load and at load, for a speed range between 0.3 – 100 % of nominal speed. This control method uses the same active flux state observer, for speed and position calculation as in the proposed controllers.

The reference speed is calculated from the frequency ramp, and the speed and current regulators are used for the voltage calculation, which is then used in the space vector modulation block (SVM) to create the modulation method signals for the inverter. The active flux observer has the same structure as the one presented in Chapter 3.

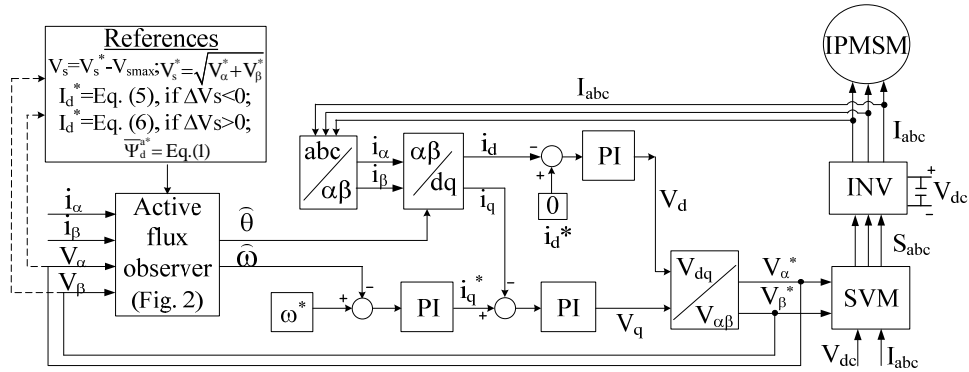


Fig. 5.3. Sensorless vector control used for bench-marking study.

5.2. Simulation Results

For sensorless vector control, simulations have been done and the controller parameters obtained are:

Table 5.1

Parameters of the controllers used in sensorless vector control simulations

PI speed controller	$K_p=0.4$	$K_i=2.5$
PI i_d controller	$K_p=30$	$K_i=2000$
PI i_q controller	$K_p=30$	$K_i=3000$

We have to mention that during both digital simulations and experiments, the MTPA conditions have been used in (5).

Comprehensive simulations have been performed for both the proposed V/f control and the sensorless vector control. For theoretical validation of the performance and response accuracy of the active flux observer, a sensorless vector control scheme for IPMSM has been implemented in the Matlab/Simulink package.

During the simulations some approximations have been made:

- the inverter was considered as ideal;
- for stator flux calculation, a pure integrator was used;

The simulation results are shown in Fig. 5.4., where fast speed response (100ms) and rather fast speed recovery (120ms) after load step of 50% rated torque has been applied and the results can be seen for the sensorless vector control. Fig. 5.5. shows the proposed V/f control corresponding to the simulation results. Table 5.2 specifies the data used.

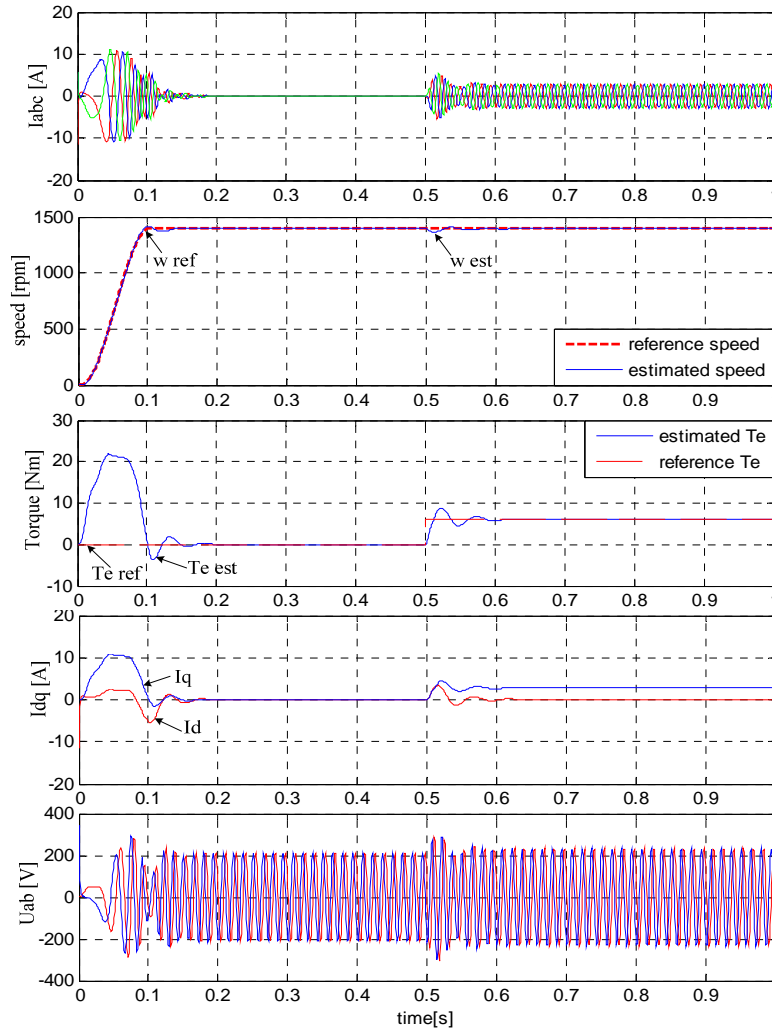


Fig. 5.4. Simulated IPMSM start-up response and sudden 50% rated torque for sensorless vector control at 0.5s.

The machine starts under the load of 50 % rated torque at target speed (load torque is proportional to speed), which explains the 50 ms delay during start-up. The 50 ms delay during the torque response can also be noticed.

As the simulation results show, the machine has almost the same behavior during the two control methods.

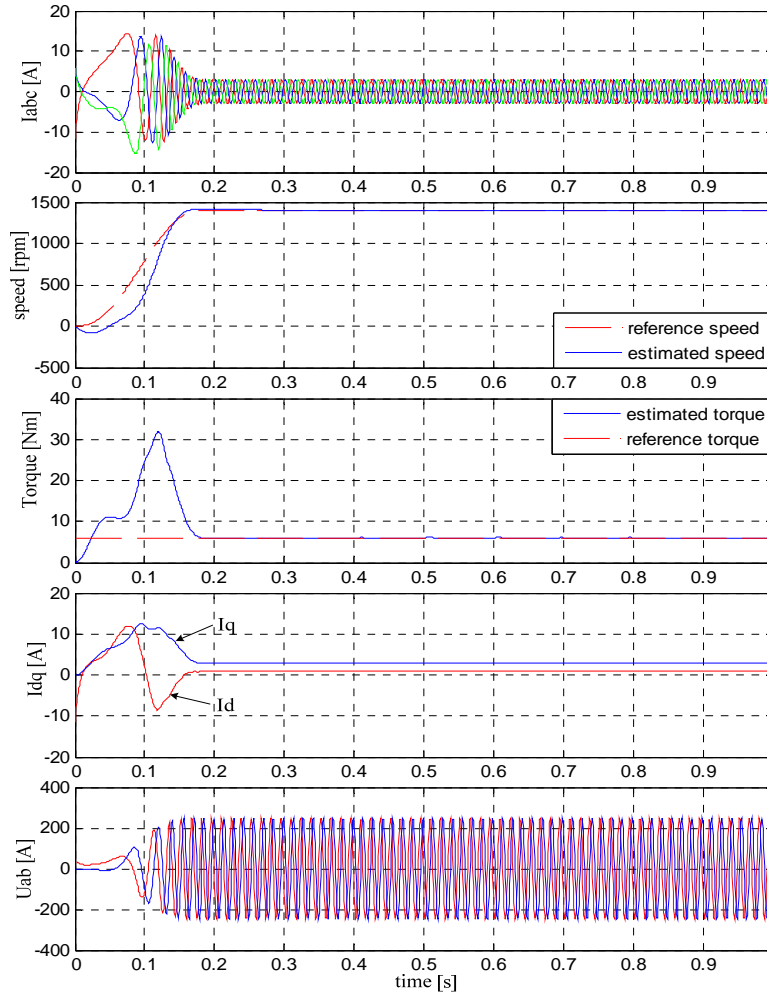


Fig. 5.5. Simulation of IPMSM start-up under 50% rated torque for V/f with stabilizing loops control.

Table 5.2

Parameters of the stabilization loops controllers in simulation

Active flux based PI controller	$K_p=150$	$K_i=10$
Speed error PI controller	$K_p=0.0068$	$K_i=0.1$

They have been obtained by trial and error.

To filter the estimated speed, a low pass filter with $k_{pF}=1$ and $T_{IF}=0.0033s$, has been implemented. The simulation constraints were investigated by the presented laboratory experiments.

5.3. Experimental Results

Using the active flux observer and the V/f with voltage magnitude and phase correction, experimental tests have been performed.

The experimental platform contains of a 2.2 kW IPMSM as the main component, a three-phase Danfoss Inverter-FC302 type, dSpace 1103 system and a 2.2 kW IPMSM, as load.

During experiments, the magnetic saturation was considered constant, as the IPMSM under investigation has the data given in Appendix A, that show a low rated saliency $L_q/L_d = 1.1$.

The experimental results for the proposed V/f with correction loops control, where the parameters are specified in Table 5.3, with self-starting from zero position angle and a PM generator using a resistive load (6 Nm at 1400 rpm) up to 1400 rpm are shown in Fig. 5.6. An acceptable 10 % speed overshoot can be observed in Fig. 5.6.b, followed by the position representation in Fig. 5.6.c, where a slight difference of less than 0.5 rad between the reference, estimated and the encoder values can be seen in the zoomed region. A 6 Nm load is also visible in Fig. 5.6.d.

Fig. 5.7. shows the experimental steady-state results at 5 rpm (after self-acceleration (not shown) by V/f control with stabilizing loops) at no load. Small oscillations of 3 rpm can be distinguished in Fig. 5.7.b. A less than 2 electrical degrees difference between the estimated and the encoder position can also be seen in Fig. 5.7.c. The last two graphs, Fig. 5.7.e and Fig. 5.7.f show the outputs of the two correction loops.

Table 5.3

Parameters of the stabilization loops controllers

Active flux based PI controller	$K_p=3$	$K_i=700$
Speed error PI controller	$K_p=0.001$	$K_i=0.15$
Voltage compensation	$K_p=15$	$K_i=15$

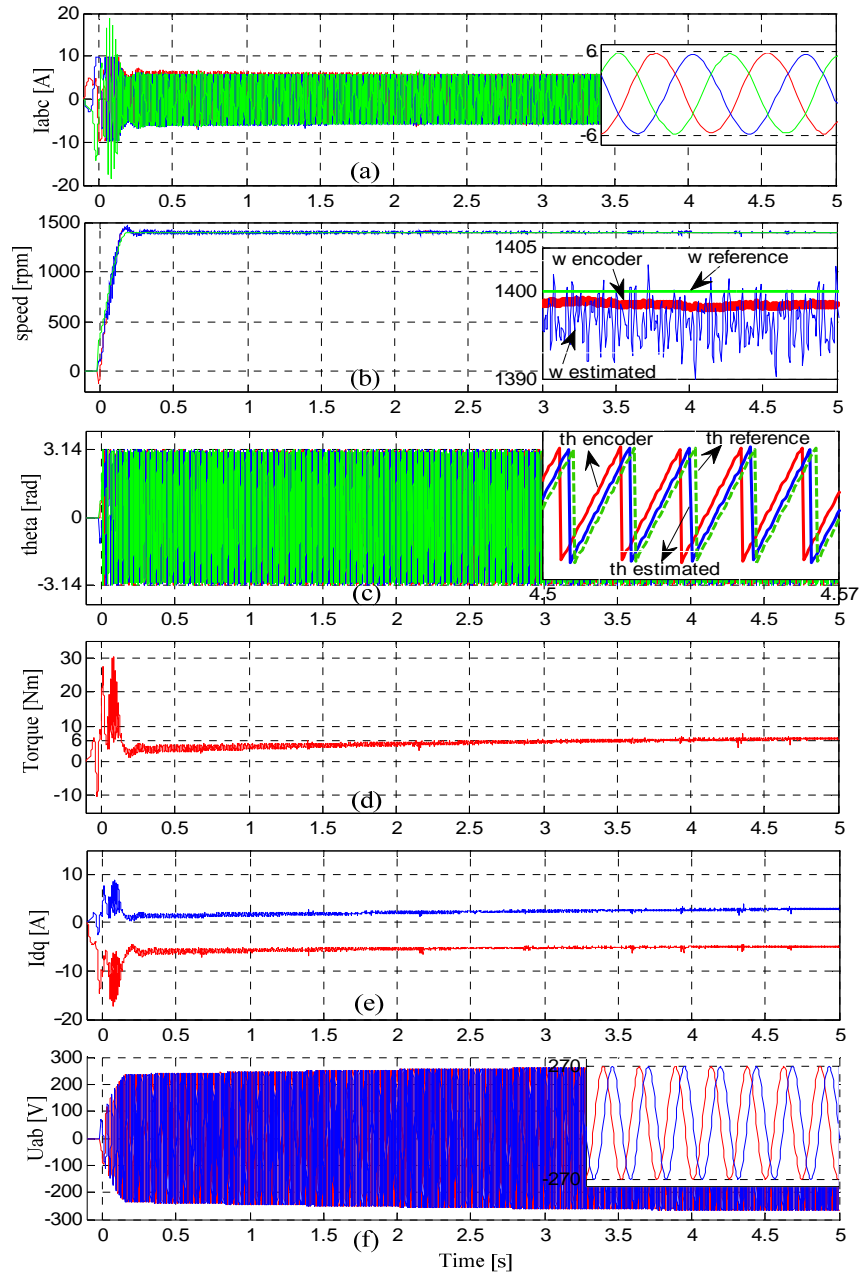


Fig. 5.6. V/f control with stabilizing loops—experimental results for 1400 rpm at 50 % of rated torque.

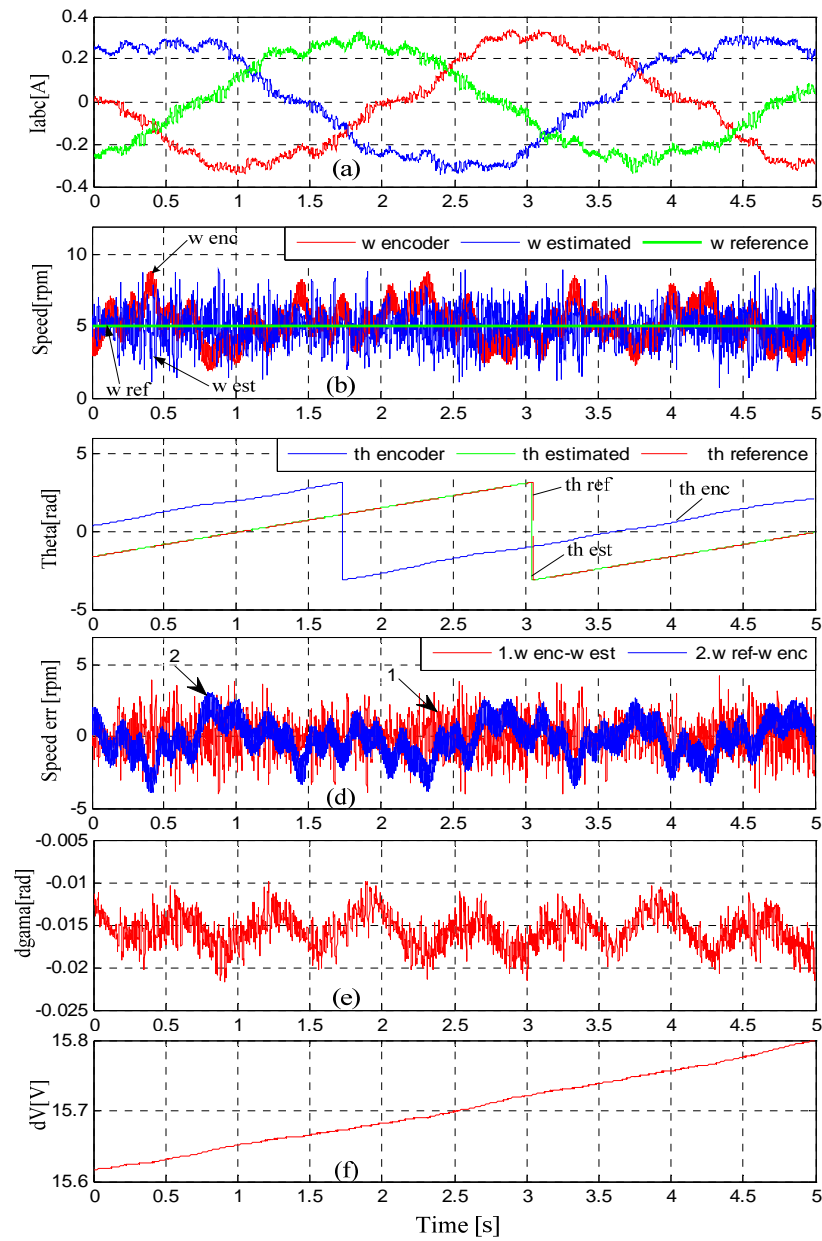


Fig. 5.7. V/f control with stabilizing loops – experimental results for 5 rpm at no load, during steady state.

A faster stabilization for angle correction loop can be noticed, in comparison with the voltage loop.

The controllers parameters were determined by trial and error.

Experimental results for sensorless vector control are further presented in Fig. 5.8. and in Fig. 5.9. As it can be noticed, some additional ripple is present in the vector control at high speed. The acceleration time of 150 ms, from zero to 1400 rpm (See Fig. 5.8.), is equal with the one for V/f control with stabilizing loops. This is believed to be a confirmation of the main goal: **fast torque (speed) response for a wide speed range**. Vector control with encoder feedback was used first for motor start-up, then, switched to sensorless control at 1.7 s and 50 % of rated torque is applied afterwards, at 3.6 s.

About ten times higher values for the currents can be seen at load, compared to no-load operation, shown in Fig. 5.8.a. When the load is applied, the speed decreases with about 50 rpm and in 35 ms it reaches the target again, see Fig. 5.8.b. The estimated position follows rather closely the encoder for the entire working period. The measured mechanical position has also been represented in Fig. 5.8.c. The value for the applied load can be seen in Fig. 5.8.d, while I_{dq} currents are shown in Fig. 5.8.e and Fig. 5.8.f shows the error between the estimated and real speed.

Fig. 5.9. shows the results for sensorless vector control at 5 rpm in steady-state at no load, where the parameters used are given in Table 5.4. The motor start-up has been done using encoder feedback, then, during steady state, the switching to sensorless operation has been applied. It can be noticed that the speed oscillates around the reference with about 5 rpm, though a few spikes around 8 rpm are also present. This makes the sensorless speed response for low speed values apparently worse than for the proposed V/f control.

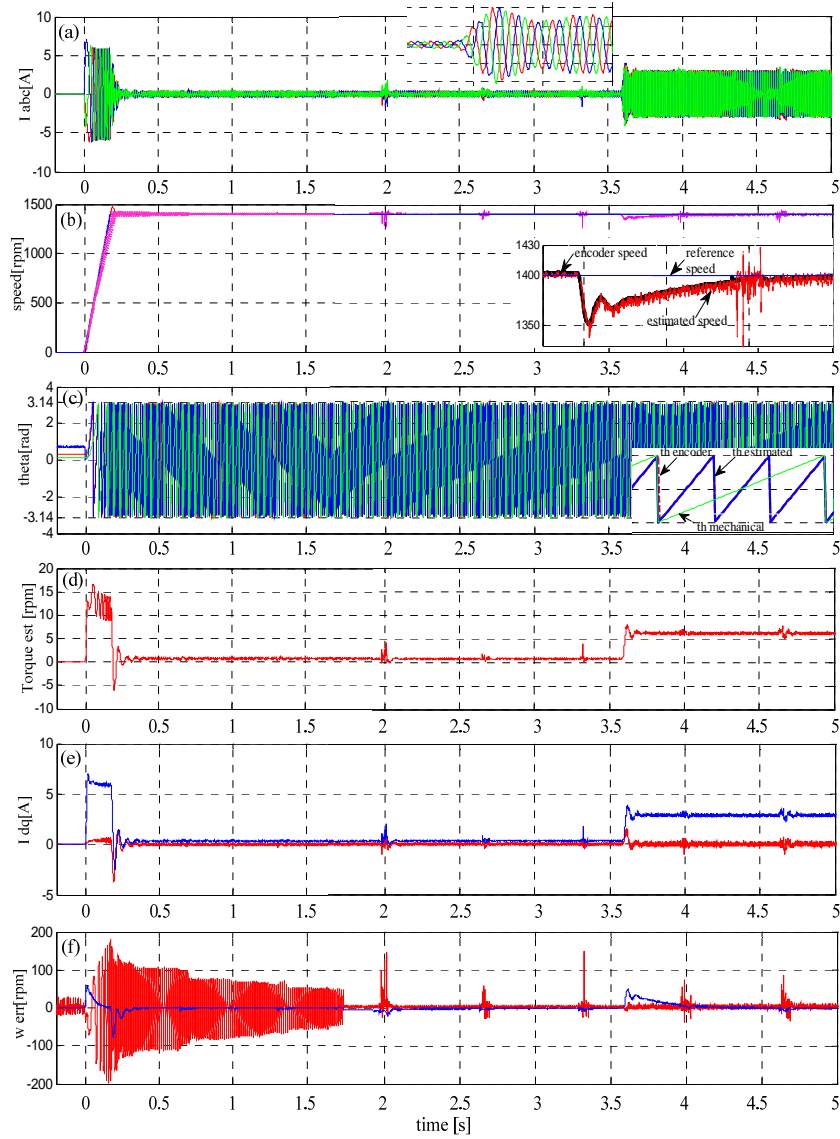


Fig. 5.8. Vector control no-load starting to 1400 rpm with position feedback, with switching on sensorless operation at 1.7 s and sudden 6 Nm load at 3.6 s

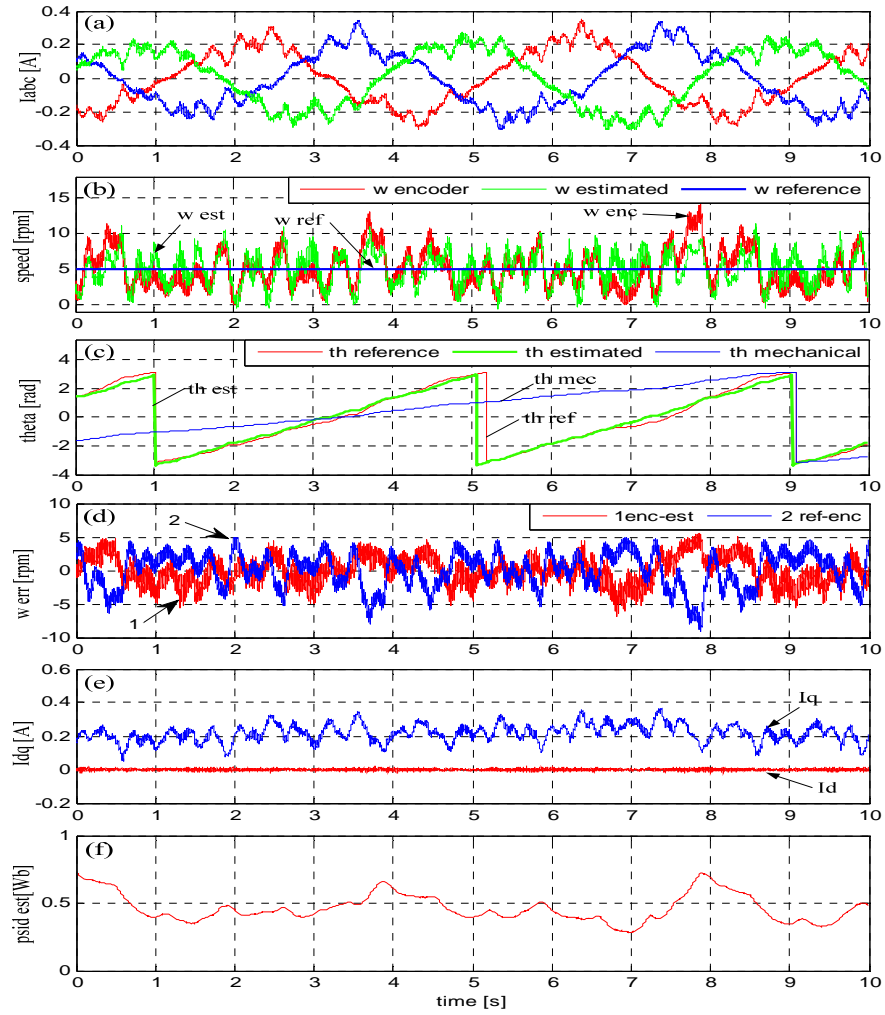


Fig. 5.9. Sensorless vector control at 5 rpm during steady-state.

Table 5.4

Parameters Values for the Sensorless Vector Control controllers

PI speed controller	$K_p=0.1$	$K_i=0.2$
PI i_d controller	$K_p=50$	$K_i=5000$
PI i_q controller	$K_p=30$	$K_i=3000$
Voltage compensation	$K_p=1$	$K_i=1$

The controllers parameters were determined by trial and error.

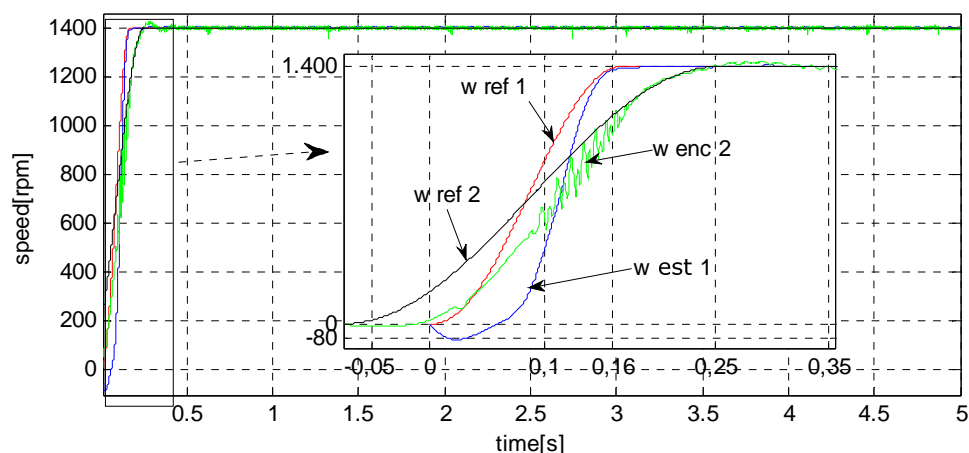


Fig. 5.10. Speed response comparison between the simulation and experimental results.

During Fig. 5.10, a comparison between the experimental and simulation results is illustrated and the results show that the machine accelerates faster during simulations (100ms) than in experiments (250 ms). In simulations the machine 50ms hesitation at start – up can be noticed. The speed waveforms marked by „1“, represent the reference and the estimated speed obtained from simulation results, whereas, the waveforms marked by „2“, show the experimental results.

5.4. Conclusion

The chapter presents a novel V/f control method with two stabilizing loops - one based on active flux balance for the voltage amplitude correction, the other one based on the speed error for the voltage phase correction. Both simulation and experimental results are shown during the same working conditions. The experimental results show that the machine starting response time to 1400 rpm (150 ms) is the same in both simulation and experiments.

To prove the main claim of the novel control – fast speed (torque) dynamic response – sensorless vector control [18] was also implemented and tested, again during both simulation and experiments. Even more, V/f control, with correction loops, for low speed (5 rpm) - steady state operation, seems to follow the target better than sensorless vector control, as indicated by the V/f control, where the speed oscillations are less than for sensorless vector control.

References

- [1] Q. Jilong, T. Yantao, G. Yimin, Zhucheng, "A Sensorless Initial Position Estimation Scheme and Extended Kalman Filter Observer for the Discret Torque Controlled PMSM Drive", Proc. of Electrical Machines and Systems, 2008. ICEMS 2008. International Conference on, pp. 3945-3950, 17-20 October, 2008, ISBN: 978-1-4244-3826-6;
- [2] G. Wang; R. Yang; Y. Wang; Y. Yu; D. Xu; "Initial rotor position estimation for sensorless interior PMSM with signal injection", Proc. of Power Electronics Conference (IPEC), 2010 Internat, pp. 2748-2752;
- [3] C. Xiang, G. Shan Mao, Y. Sheng Wen, W. Lei, "Study on initial rotor position identification of permanent magnet synchronous motor based on high frequency signal injection", Proc. of Informatics in Control, Automation and Robotics (CAR), 2010 2nd International Asia Conference on, Vol.2, ISSN 1948-3414;
- [4] H. Kim, K. K. Huh, M. Harke, J. Wai, R. D. Lorenz, and T. A. Jahns, "Initial rotor position estimation for an integrated starter alternator IPM synchronous machine", in Proc. 10th Eur. Conf. Power Electron. Applicat. (EPE-2003), Toulouse, France, 2003, pp. 1875–1881;
- [5] C. Lasca, I. Boldea, F. Blaabjerg, "Direct torque control of sensorless induction motor drives: A sliding-mode approach", IEEE Trans.on Ind. Applicat., Vol. 40, No. 2, pp. 582–590, 2004;
- [6] P. Guglielmi, M. Pastorelli, G. Pellegrino, A. Vagati, "Position sensorless control of permanent-magnet-assisted synchronous reluctance motor", IEEE Trans. on Ind. Applicat., Vol. 40, No. 2, pp. 615–622, 2004;
- [7] S. Morimoto, M. Sanada, Y. Takeda, "Mechanical sensorless drives of IPMSM with online parameter identification", IEEE Trans.on Ind. Applicat., Vol. 42, No. 5, pp. 1241–1248, 2006;
- [8] T. Halkosaari, "Optimal U/f-control of high speed permanent magnet motors", Industrial Electronics, 2006 IEEE International Symposium on, 9-13 July 2006, vol. 3, pp. 2303 – 2308, ISBN: 1-4244-0496-7;
- [9] M.Hasegawa, S. Yoshioka, and K. Matsui, "Position Sensorless Control of IPMSM Using Unknown Input Observer for High-Speed Drives", IEEE Trans on Ind Applicat, Vol. 45, No.3, pp. 1059-1064, 2009;

- [10] S. Koonlaboon, S.Sangwongwa M.Hasegawa, S. Yoshioka, K. Matsui, "Position Sensorless Control of IPMSM Using Unknown Input Observer for High-Speed Drives", IEEE Trans on Ind Applicat, Vol. 45, No.3, 2009;
- [11] R.Ancuti, G.D. Andreescu and I.Boldea, "Four rotor position and speed simplified estimators for vector control of high-speed SPMSM with test comparisons", Journal of Electrical Engineering, JEE, Vol.7, No.4, Politehnica Publishing House, Timisoara, 2007, pp. 1-8;
- [12] R. Ancuti, I.Boldea, G.D. Andreescu, D. Iles, "Novel motion sensorless control of high-speed small-power surface mount PMSM drives with experiments", Proc of OPTIM -2008, Vol.3, pp.11-18, 2008;
- [13] M. Linke, R. Kennel, and J. Holtz, "Sensorless speed and position control of synchronous machines using alternating carrier injection", in Proc. of IEEE Int. Electric Mach. Drives Conf. (IEMDC'03), Madison,WI, 2003, Vol. 2, pp. 1211–1217;
- [14] P.D.C.Perera, F. Blaabjerg, J.K. Pedersen, P.T. Thogersen, "A sensorless stable V/f control method for PMSM drives", IEEE Trans. on Ind Applicat, Vol.39, No.3, 2003, pp.783-791;
- [15] M.C. Paicu, "Active Flux"Based Wide Speed Range Motion Sensorless Control of Permanent Magnet Synchronous Machines, Phd Thesis, 2009, UPT, Timisoara, ISBN: 978-973-625-911-1;
- [16] I.Boldea, M.C. Paicu, G.D. Andreescu, "Active flux concept for motion-sensorless unified ac. drives", IEEE Transactions on Power Electronics, Vol. 23, No.5, 2008, pp. 2612-2618;
- [17] R. Ancuti, I. Boldea, G.D. Andreescu, "Sensorless V/f control of high-speed surface permanent magnet synchronous motor drives with two novel stabilizing loops for fast dynamics and robustness",Electric Power Applications, IET, Vol. 4, No. 3, 2010, pp. 40-57;
- [18] J.-I. Itoh, N. Nomura, H. Ohsawa, "A comparison between V/f control and position-sensorless vector control for the permanent magnet synchronous motor", Power Conversion Conference, 2002. PCC Osaka, Proceedings of the, pp. 1310–1315, vol. 3, ISBN: 0-7803-7156-9.

Chapter 6

Alternative, New, Stabilizing Loops Control of Tooth Wound IPMSM: Principles and Digital Simulations

Due to its simplicity, AC permanent magnet machine is considered the most attractive from all the PMs machines [1], thus during the last two decades, it has been increasingly used in many industrial drives [2], as high performance variable speed motor. Because of the low torque pulsations, the PM machine are also characterized by low vibration and noise [3].

This chapter presents three different V/f with stabilizing loops control methods for IPMSM. Just two of the proposed control methods use the “active flux” concept [4], while all of them are based on maximum torque per current (MTPA) condition [5-7]. The proposed V/f control methods are studied in order to obtain an optimal sensorless control for IPMSM [8-10], with the elimination of the initial position information [11]. The most important target of the corrected V/f control methods is to obtain fast dynamic speed and torque response, without using the standard speed and current regulators, which can be mostly found in vector control schemes. Other objectives of these control methods are the computation effort decrease and the elimination of coordinate transformation.

The first control method uses two correction loops: one based on magnetic energy balance for voltage amplitude correction, the other one based on torque error for voltage phase correction. The second control strategy uses the reactive power error through a PI controller, to correct the voltage amplitude, while the voltage phase correction is again obtained using the torque error. These two methods use the “active flux” concept. The third control method main aim is to cancel the speed and torque oscillations by using the active power and a high pass filter [12], [13], and to correct the voltage amplitude based on the power factor angle error.

6.1. V/f with Magnetic Energy & Torque Based Correction Loops

The core of this first proposal consists in “driving to zero” to a close loop the ΔW_m magnetic energy difference (6.5) between its expressions in α, β (stator coordinates–(6.1)) and in d, q (rotor coordinates–(6.4)), without any rotor position (or speed) estimation, to obtain the voltage amplitude correction, ΔV^* (6.6). Equation (6.6) includes the PI plus sliding mode formulae.

The magnetic energy in dq coordinates is based on the prescribed “ d ” current, i_d^* , determined from MTPA condition. The ac machine magnetic energy in $\alpha\beta$ coordinates $W_{m\alpha\beta}$ is written in (6.1).

$$W_{m\alpha\beta} = \frac{3}{2} \int (V_\beta^* i_\alpha - V_\alpha^* i_\beta) dt \quad (6.1)$$

With V_α^*, V_β^* as the reference voltages and i_α, i_β calculated from the measured currents i_a, i_b .

In steady state, dq coordinates, the same magnetic energy may be expressed in quite a unique form by using the active flux ($\bar{\Psi}_d^a$) concept by which all ac machine models “loose” their magnetic saliency [1].

$$\bar{\Psi}_d^a = \bar{\Psi}_s - L_q \cdot \bar{I}_s \quad (6.2)$$

Where $I_s = \sqrt{i_d^{*2} + i_q^{*2}}$ is the stator current and $\bar{\Psi}_s$ is the stator flux vector.

The active flux expression for IPMSM in rotor flux coordinates is expressed in (6.3).

$$\bar{\Psi}_d^a = \Psi_{PM} + (L_d - L_q) \cdot i_d^* \quad (6.3)$$

Where, L_d, L_q are the d, q synchronous inductances, and Ψ_{PM} is the permanent magnets flux linkage, all were considered constant.

The dq formula for the steady state stored magnetic energy is written in (6.4).

$$W_{mdq} = \frac{3}{2} * (\Psi_d^a i_d^* + L_q i_s^2); \quad (6.4)$$

$$\Delta W_m = W_{m\alpha\beta} - W_{mdq} \quad (6.5)$$

$$\Delta V^* = -\Delta W_m * \left(\frac{k_{pi}}{1 + T_{ii} * s} + k_{SMi} * \text{sign}(\Delta W_m) \right) \quad (6.6)$$

To avoid the rotor position estimation we need to “fix” the desired longitudinal current i_d^* , (6.8), such that to consider the maximum torque per current, condition (6.7), below base speed for up to full torque.

$$2 \cdot i_d^{*2} + (i_d^* \cdot \lambda_{PM}) / (L_d - L_q) = i_s^2 ; \quad (6.7)$$

$$i_d^* = -\frac{1}{4} \cdot \frac{\lambda_{PM}}{L_d - L_q} - \frac{1}{2} \cdot \sqrt{\frac{1}{4} \cdot \left(\frac{\lambda_{PM}}{L_d - L_q} \right)^2 + 2 \cdot i_s^2} \quad (6.8)$$

A similar stabilizing loop for voltage phase angle correction, $\Delta\gamma$, in the V/f control is proposed around the $\alpha\beta$ and dq torque formula, which are basically the same in active flux coordinates, for all ac machines:

$$T_{e\alpha\beta} = \frac{3}{2} * p_1 (\widehat{\Psi}_\alpha * i_\beta - \widehat{\Psi}_\beta * i_\alpha); \quad (6.9)$$

The torque expression in dq coordinates is also depending on the active flux:

$$T_{edq} = \frac{3}{2} * p_1 * \Psi_d^{*a} * i_q; \quad i_q^* = \sqrt{i_s^2 - i_d^{*2}} \quad (6.10)$$

To estimate the α, β flux components, $\widehat{\Psi}_\alpha$ and $\widehat{\Psi}_\beta$, the voltage model will be used:

$$\widehat{\Psi}_\alpha = \frac{T}{1+sT} * (V_\alpha^* - R_s * i_\alpha); \quad \widehat{\Psi}_\beta = \frac{T}{1+sT} * (V_\beta^* - R_s * i_\beta); \quad (6.11)$$

With i_d^* and $\overline{\Psi}_d^a$ reference values, as described above, the torque stabilizing loop is simply described by (6.12) and (6.13):

$$\Delta T_e = T_{e\alpha\beta} - T_{edq} \quad (6.12)$$

$$\Delta\gamma^* = -\Delta T_e * \left(\frac{k_{pi}}{1 + T_{ii} * s} + k_{SMI} * \text{sign}(\Delta T_e) \right) \quad (6.13)$$

The general control scheme is drawn below (Fig. 6.1.) and digital simulation results for the imposed requirements will be presented afterwards. The PI regulators structure is shown in Fig. 6.2. and their corresponding coefficients are displayed during Table 6.1.

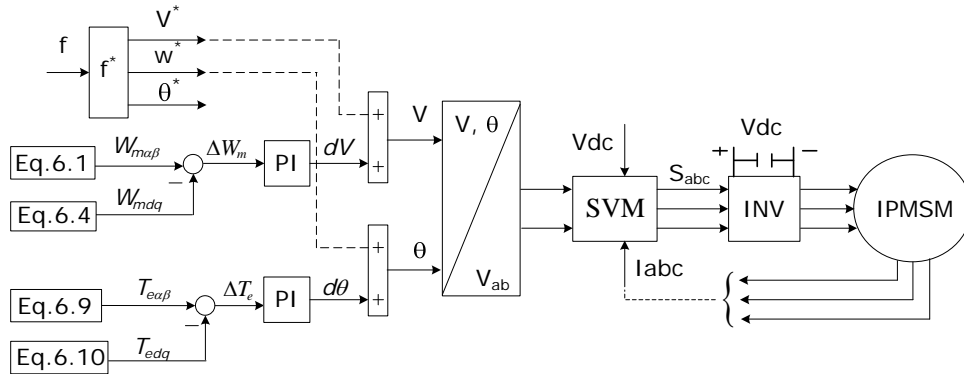


Fig. 6.1. V/f with stabilizing loops control – general scheme

Depending on the ramp prescribed frequency, the reference values for voltage amplitude (6.14), speed (6.15) and angle (6.16) were previously calculated:

$$V = V_0 + k \cdot f^* ; V_0 = R_s \cdot I_n \quad (6.14)$$

$$w^* = 2 \cdot \pi \cdot f^* \quad (6.15)$$

$$\theta^* = \int \omega^* dt \quad (6.16)$$

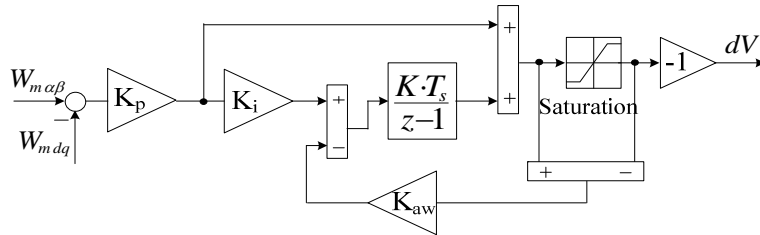
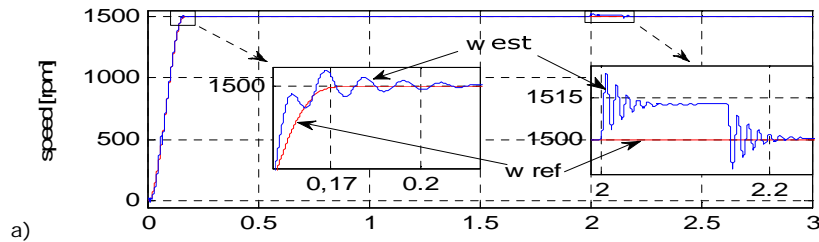
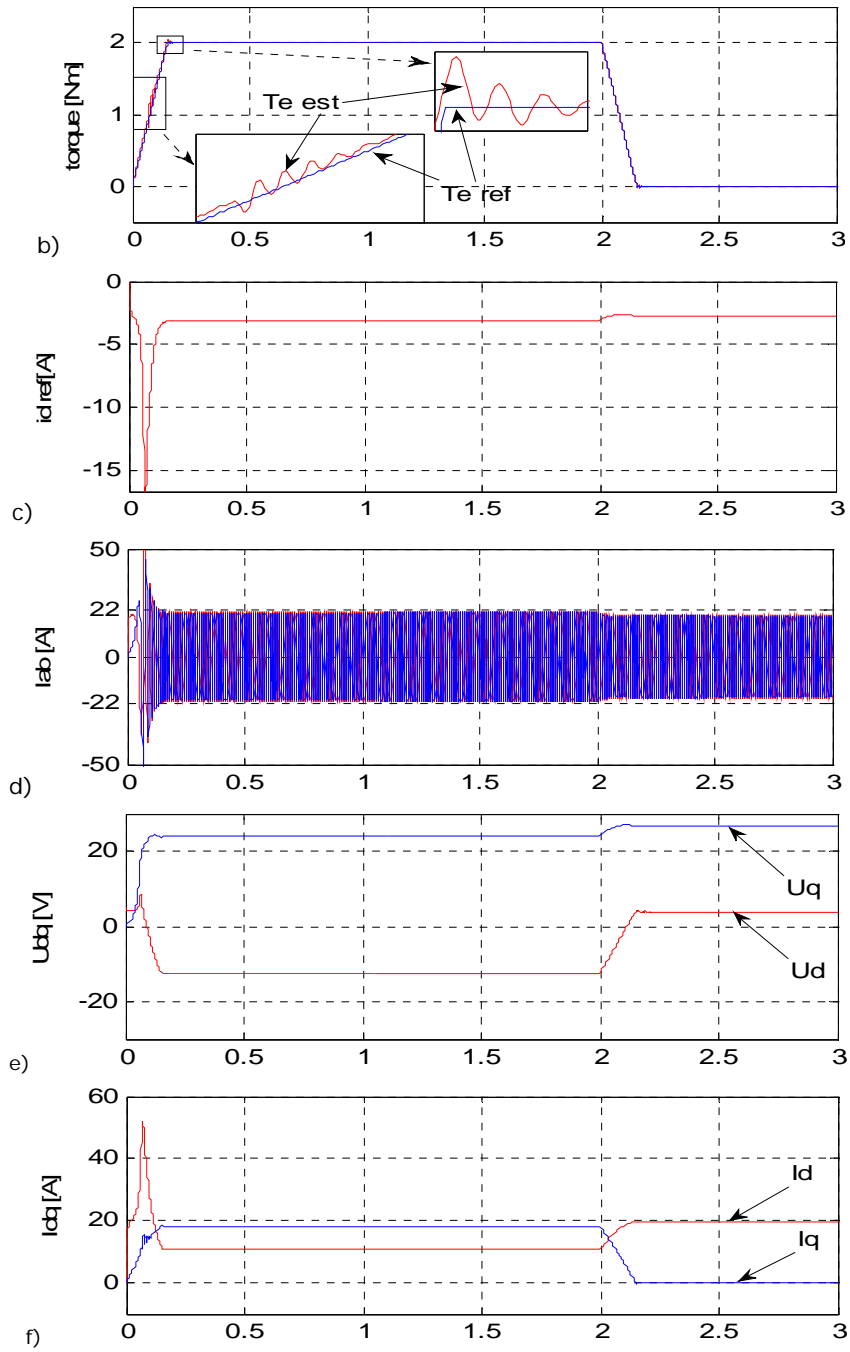


Fig. 6.2. PI regulator structure

Simulations have been conducted when the machine accelerates from 0 up to 1500 rpm and a proportional with speed, 2Nm load torque is applied. The machine unloading is applied at 2s, when a slight speed increase occurs. The results are presented further on in Fig. 6.3.





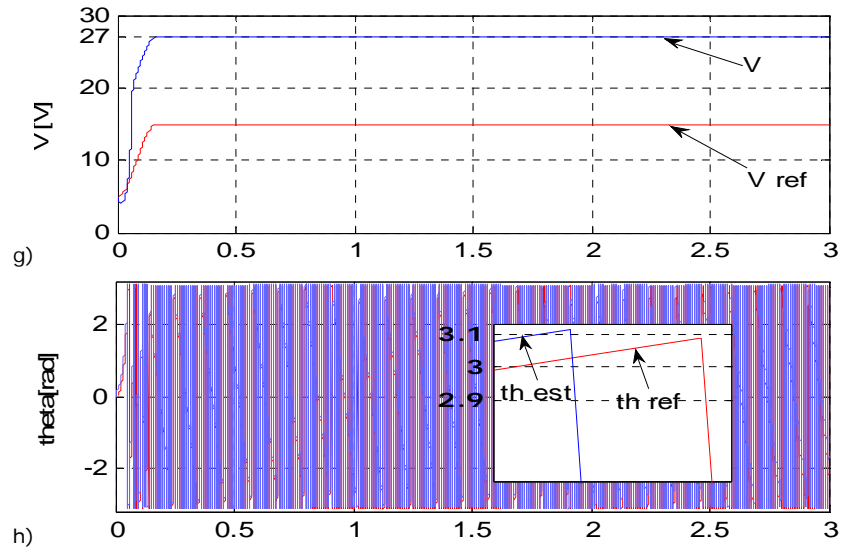


Fig. 6.3. Digital simulation results for V/f with magnetic energy and torque stabilizing loops: a) speed; b) torque; c) i_d^* reference current; d) α, β current; e) d, q voltage; f) d, q current; g) voltage vector amplitude; h) voltage vector phase angle

A rather fast acceleration of the machine from zero speed up to 1500 rpm, in 170 ms and a slight difference between the reference and the actual motor speed is visible in Fig. 6.3a. The real speed oscillates around the target with about ± 5 rpm, during transients; when the unloading 150 ms slope occurs, the speed increases with 15 rpm and afterwards it stabilizes in about 220 ms.

The realized torque oscillates with less than ± 0.1 Nm around the reference (Fig. 6.3b.) and the current decrease from 21 A to 19 A when the unloading is applied (Fig. 6.3d.). It should be noted that the machine does not realize (Fig. 6.3f.) the negative imposed i_d^* (Fig. 6.3c.), yet. The corrected voltage vector amplitude and its reference value is shown in Fig. 6.3g., while the 0.1 rad (5.73 electrical degrees) difference between the reference and estimated phase angle is drawn in Fig. 3h.

6.2. V/f with Reactive Power and Torque Based Correction Loops

The basis of the second proposal consists in driving to zero through a close loop the reactive power difference between its expressions in α, β and d, q coordinates, without using any rotor position (or speed) estimation, to obtain the voltage amplitude correction, ΔV^* . The MTPA condition, is again considered to impose i_d^* current (6.8) for d, q reactive power calculation. The ac machine reactive power in α, β coordinates, $Q_{\alpha\beta}$, is given in (6.17).

$$Q_{\alpha\beta} = \frac{3}{2} (V_\beta^* i_\alpha - V_\alpha^* i_\beta) \tag{6.17}$$

With V_α^*, V_β^* as the reference voltages and i_α, i_β calculated from the measured currents. In steady state, d, q coordinates, the same reactive power may be expressed in quite a unique form by using the active flux concept $\bar{\Psi}_d^a$ (6.3) [1].

For active flux estimation, stator flux estimation is crucial, thus a combined voltage/current model observer is used [1]. The dq formula for the steady state reactive power, Q_{dq} , is written in (6.18).

$$Q_{dq} = \frac{3}{2} * \omega_r^* * (\Psi_d^{*a} i_d^* + L_q i_s^2); \tag{6.18}$$

The torque stabilizing loop has the same structure as exposed during the previous section, thus the torque error (6.12) and the voltage phase correction (6.13) are easily calculated. The corresponding control scheme has the same structure with the one in Fig. 6.1., though the magnetic energy is replaced by the reactive power correction loop (Fig. 6.4).

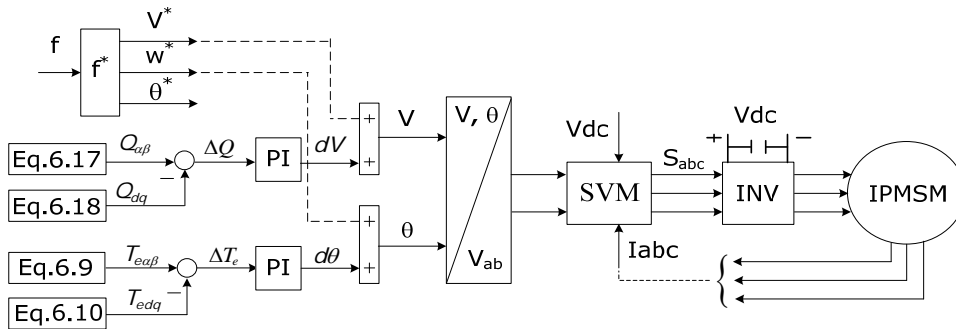


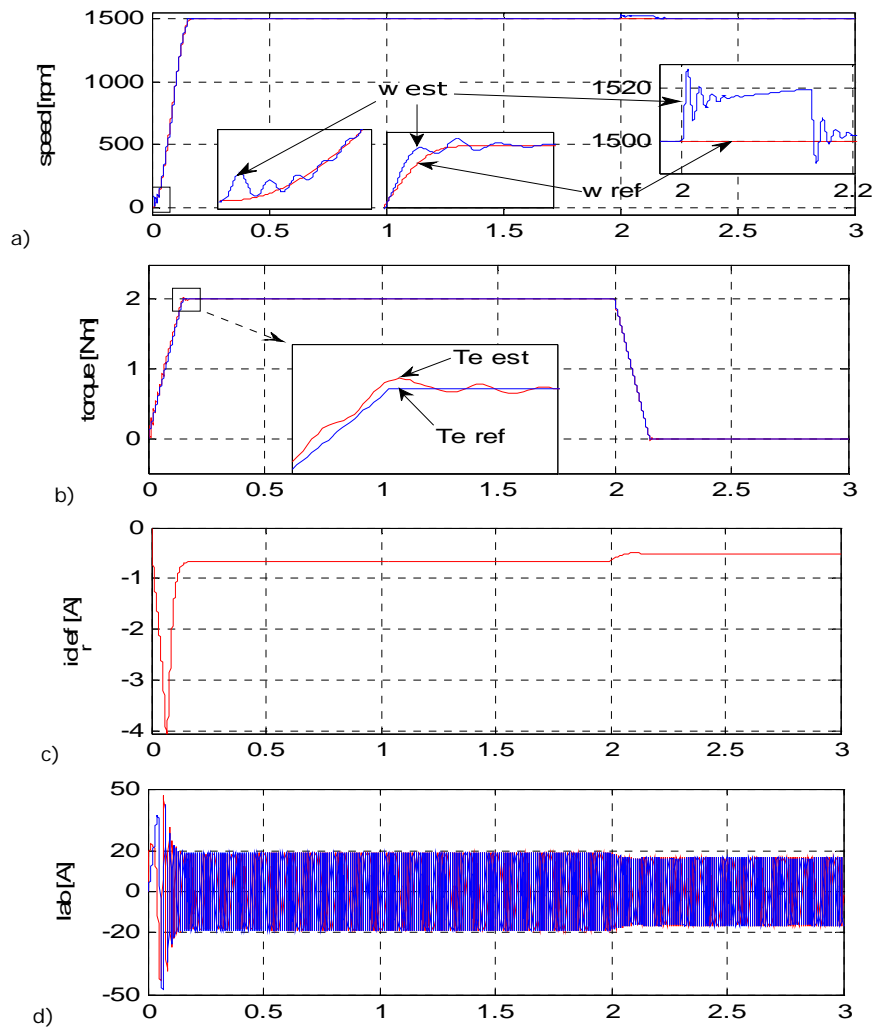
Fig. 6.4. V/f with stabilizing loops control – general scheme

Table 6.1. Reactive power and torque formulas in steady state

Machine type	Induction machine (IM) Synchronous coordinates in rotor flux orientation $\omega_b = \omega_1$	Surface PMSM (SPMSM) Rotor coordinates $\omega_b = \omega_r$	Interior PMSM (IPMSM) Rotor coordinates $\omega_b = \omega_r$	Reluctance Synchronous motor (RSM) Rotor coordinates $\omega_b = \omega_r$
d, q magnetic energy W_{mdq}	$Q_{dq} = \frac{3}{2} (L_s \cdot i_d^2 + L_{sc} \cdot i_q^2) \cdot \omega_1^*$ $= \frac{3}{2} \cdot [(L_s - L_{sc}) i_d^{*2} + L_{sc} \cdot i_q^{*2}] \cdot \omega_1^*$ $= \frac{3}{2} \cdot (\Psi_d^{*a} \cdot i_d^{*2} + L_{sc} \cdot i_s^{*2}) \cdot \omega_1^*$ $i_s = \sqrt{i_d^{*2} + i_q^{*2}}$ $T_{edq} = \frac{3}{2} \cdot p_1 \cdot (L_s - L_{sc}) \cdot i_d^* \cdot i_q^*$ $= \frac{3}{2} \cdot p_1 \cdot \Psi_d^{*a} \cdot i_q^*$ $S \cdot \omega_1 = \frac{i_d^* R_r}{i_d} \cdot L_r$ $\omega_{11}^* \rightarrow \omega_1^* + S \omega_1; \omega_{11}^* \rightarrow \omega_r$	$Q_{dq} = \frac{3}{2} (\Psi_{PM} \cdot i_d^* + L_s \cdot i_s^{*2}) \cdot \omega_r^*$ $= \frac{3}{2} (\Psi_d^{*a} \cdot i_d^{*2} + L_s \cdot i_s^{*2}) \cdot \omega_r^*$ for $i_d^* = 0$ $Q_{dq} = \frac{3}{2} \cdot L_s \cdot i_s^{*2} \cdot \omega_r^*$ $T_{edq} = \frac{3}{2} \cdot p_1 \cdot \Psi_{PM} \cdot i_q$ $\omega_1^* \rightarrow \omega_r$ $(L_d = L_q = L_s)$	$Q_{dq} = \frac{3}{2} \left[\omega_r^* \cdot (\Psi_{PM} + (L_d - L_q) i_d^*) \cdot i_d^* \right. \\ \left. + \frac{3}{2} \cdot L_q \cdot i_s^{*2} = \frac{3}{2} (\Psi_d^{*a} \cdot i_d^{*2} + L_q \cdot i_s^{*2}) \cdot \omega_r^* \right]$ for $i_d^* < 0$ $T_{edq} = \frac{3}{2} \cdot p_1 \cdot \Psi_d^{*a} \cdot i_q$ $(L_d < L_q)$ $\omega_1^* \rightarrow \omega_r$	$Q_{dq} = \frac{3}{2} (L_d \cdot i_d^{*2} + L_q \cdot i_q^{*2}) \cdot \omega_r^*$ $= \frac{3}{2} [(L_d - L_q) i_d^{*2} + L_q \cdot i_s^{*2}] \cdot \omega_r^*$ $= \frac{3}{2} (\Psi_d^{*a} \cdot i_d^{*2} + L_q \cdot i_s^{*2}) \cdot \omega_r^*$ $T_{edq} = \frac{3}{2} \cdot p_1 \cdot \Psi_d^{*a} \cdot i_q$ $(L_d > L_q);$ $i_d^* > 0;$ $\omega_1^* \rightarrow \omega_r$

The PI controllers used in Fig. 6.4, for voltage amplitude and phase correction have the same structure as previously shown in Fig. 6.2 and the voltage, speed and angle reference values have the formulae written in (6.14) – (6.16).

As in previous section, tests have been conducted when the machine accelerates from zero speed up to 1500 rpm and a proportional with speed, 2Nm load torque was applied; the machine unloading is also applied at 2s and the simulation results are shown in Fig. 6.5.



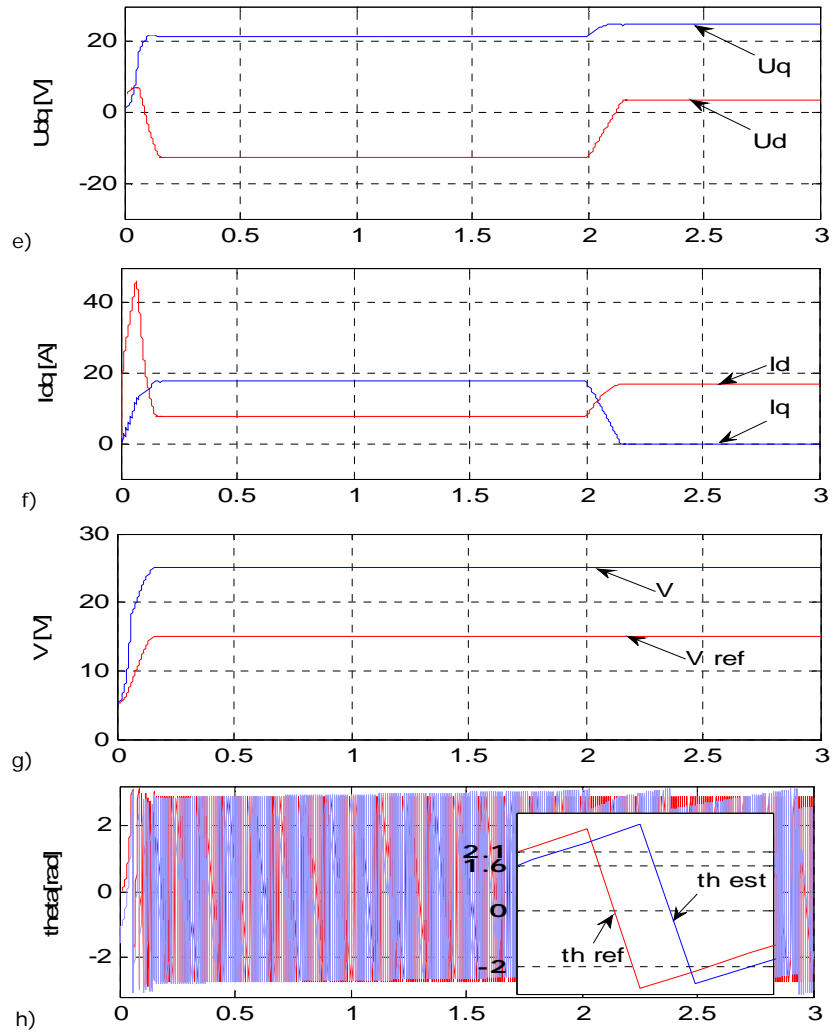


Fig. 6.5. Digital simulation results for V/f with reactive power and torque stabilizing loops: a) speed; b) torque; c) I_a^* reference current; d) α , β current; e) d, q voltage; f) d, q current; g) voltage vector amplitude; h) voltage vector phase angle

As it can be seen from Fig. 6.5a, the machine accelerates from zero speed up to the prescribed value in about 170ms; the actual speed oscillates around the reference one with ± 5 rpm and when the machine unloading occurs, the speed increases with 20 rpm.

A 2Nm ramp torque, proportional to speed is prescribed for the motor loading; an 150 ms slope was applied for the machine unloading, at 2s (Fig. 6.5b).

The realized torque oscillates during transients with less than ± 0.1 Nm around the prescribed waveform. The currents value decrease from 19A to 17A when the load is cancelled, which can be easily seen in (Fig. 6.5d). Again, the prescribed negative i_d^* (Fig. 6.5c) is not realized, yet (Fig. 6.5f).

The corrected voltage vector amplitude and its reference value is shown in Fig. 6.5g, while the 0.5 rad (28.66 electrical degrees) difference between the reference and estimated angle waveforms is drawn in Fig. 6.5h.

Both V/f with correction loops control methods described and analyzed above were tested during the same operating conditions (0 up to 1500 rpm machine acceleration, with a proportional with speed 2 Nm load torque), thus similarities and differences can be discussed further on. As mentioned before, the machine speed and torque response is the same for both cases. One major difference between the two control methods can be noticed between Fig. 6.3h and Fig. 6.5h; the difference between the reference and the actual rotor position is five times bigger in the second control strategy (0.5 rad) than during the first one (0.1 rad). A slight difference between the current and voltage values, which are higher for the first control method can also be observed.

6.3. V/f control with voltage phase angle correction and active power calculation

The V/f control strategy proposed during this section is slightly different from the above described control methods, especially because it does not use the active flux concept.

First of all, we will use the MTPA condition to prescribe the stator voltage and the current vector angles (6.19), (6.20). The difference between the two angles is φ^* (6.22) and it will be used, further on, for voltage amplitude correction. To obtain the estimated value of the angle, $\hat{\varphi}$, we need to know the active and the reactive power (6.25), (6.26). The error between the calculated angle using MTPA (6.22) and the estimated one will represent the input of a PI controller which will be used further on to correct the voltage vector amplitude (6.24). The general scheme used for voltage vector amplitude correction is drawn below, in Fig. 6.6.

$$\psi = \psi_{MTPA}(I_s) = \text{asin} \left(\frac{-\lambda_{PM} + \sqrt{\lambda_{PM}^2 + 8 \cdot (L_q - L_d)^2 \cdot I_s^2}}{4 \cdot (L_q - L_d) \cdot I_s} \right) \quad (6.19)$$

$$\delta = \text{asin}\left(\frac{x_q^* I_s^* \cos(\Psi) + R_s^* I_s^* \sin(\Psi)}{V_s(\Psi)}\right) \quad (6.20)$$

$$\text{Where, } V_s(\Psi) = \sqrt{[E_0 - x_d^* I_s^* \sin(\Psi) + R_s^* I_s^* \cos(\Psi)]^2 + [\omega^* L_q^* I_s^* \cos(\Psi) + R_s^* I_s^* \sin(\Psi)]^2} \quad (6.21)$$

$$\varphi^* = \varphi_{MTPA} = \delta - \Psi \quad (6.22)$$

$$\hat{\varphi} = \text{atan}\left(\frac{P_r}{P_a}\right) \quad (6.23)$$

$$\Delta V = \Delta \varphi^* (K_p \cdot (1 + K_i \cdot s)) \quad (6.24)$$

$$P_a = \frac{3}{2} \cdot (U_\alpha \cdot I_\alpha + U_\beta \cdot I_\beta) \quad (6.25)$$

$$P_r = \frac{3}{2} \cdot (U_\beta \cdot I_\alpha - U_\alpha \cdot I_\beta) \quad (6.26)$$

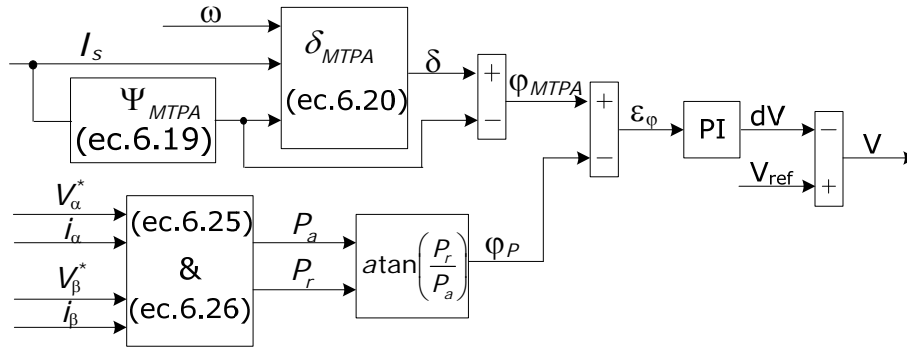


Fig. 6.6 Voltage vector amplitude correction scheme

The second correction purpose is to cancel the speed and torque oscillations and it consists of the active power (6.25) as the input of a high pass filter (HPF) [2-3]. The HPF (6.27) main role is to cut out the continuous component of the input signal. Afterwards, the output of the HPF is added to the reference speed and the result is then integrated to obtain the estimated voltage vector position used for voltage coordinate transformations (Fig. 6.7).

$$H_{HPF} = \frac{s}{s+\alpha}; \quad H_{HPF} = 1 - H_{LPF} \quad (6.27)$$

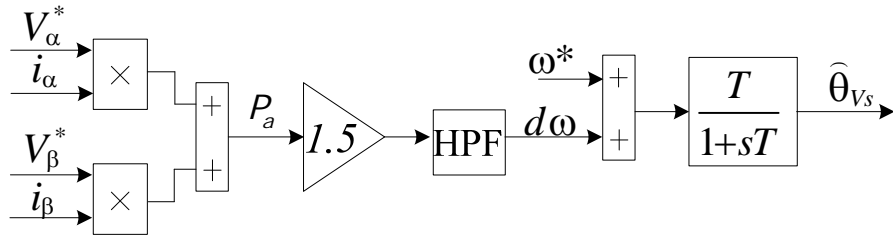
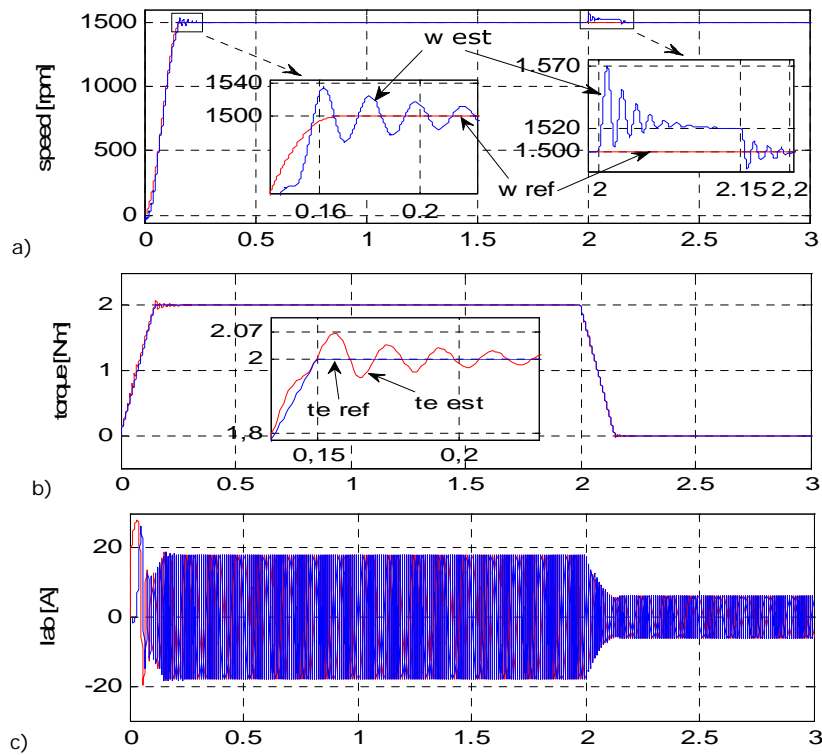


Fig. 6.7. The voltage phase correction, where $\omega^* = 2 \cdot \pi \cdot f_0$

Digital simulation tests, again at 1500 rpm speed and a proportional with speed, 2 Nm load torque were implemented and their results are shown in Fig. 6.8.



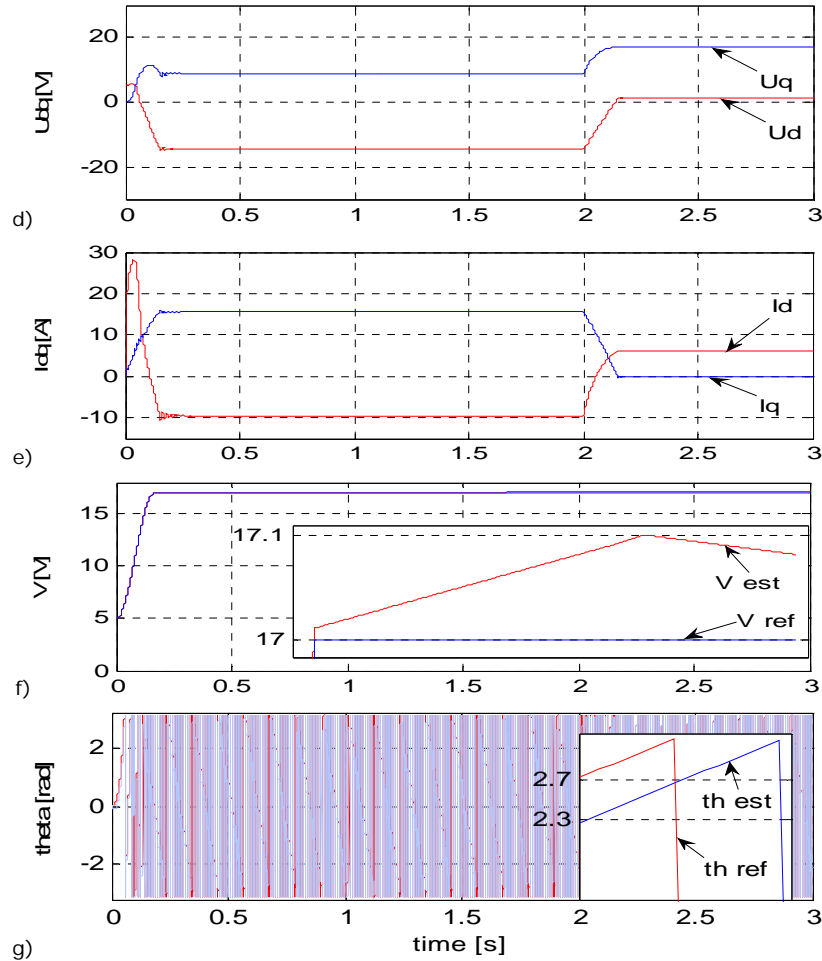


Fig. 6.8 Digital simulation results for V/f with magnetic energy and torque stabilizing loops: a) speed; b) torque; c) α , β current; d) d, q voltage; e) d, q current; f) voltage vector amplitude g) estimated voltage vector angle

The machine accelerates from zero speed up to 1500 rpm in about 160 ms (Fig. 6.8a), though some oscillations of ± 36 rpm around the reference speed, are present during transients. A proportional with speed, 2 Nm load torque was applied (Fig. 6.8b) and an 150 ms slope was also used for the machine unloading, at 2 s.

The real torque oscillates with less than ± 0.1 Nm around the reference waveform. This time the negative I_d was realized (Fig. 6.8e), though it was not prescribed for this control method. Even if the control main goal was to eliminate the speed and torque oscillations, some pulsations still persist during transients. As

Fig. 6.8c) shows, after the machine unloading, the currents become three times smaller, as they decrease from 18A to 6A. During Fig. 6.8f), the reference and the corrected voltage vector amplitude is represented. The reference and the corrected phase angle are both plotted in Fig. 6.8g), and a 0.4 rad (almost 23 degrees) difference between them is shown during the graph zoomed part.

For a better comparison of the obtained results, the speed and torque waveforms corresponding to all three above described control methods are plotted in Fig. 6.9. and Fig. 6.10. respectively.

All three control methods are characterized by both advantages and drawbacks. The most important similarity between all three of them is our main claim: fast speed and torque response (150–170 ms). The first two control methods use the active flux concept current, the MTPA condition and need a negative prescribed „d” current, which neither of them manage to realize. The third V/f control method uses only the MTPA condition and the negative „d” current is realized, though it is not imposed. Some fairly small speed and torque oscillations around the target signals are visible for the first two control strategies, but the third control method shows three times higher pulsations in speed response and two times higher pulsations in torque response, as it can be traced below, in Fig. 6.9. and in Fig. 6.10., respectively.

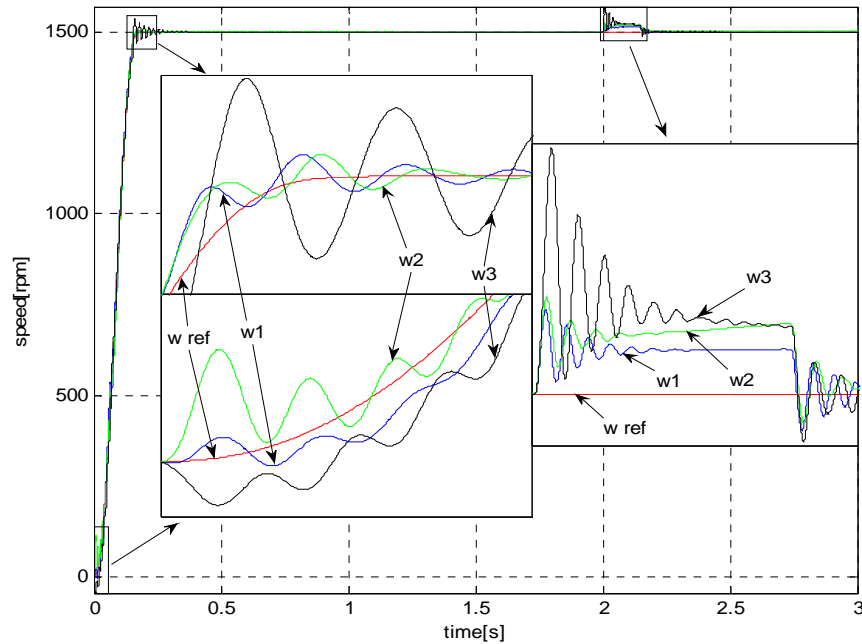


Fig. 6.9. Speed waveforms corresponding to all three proposed control methods

First, the reference value can be seen (with red), then the results for the proposed methods are shown, considering the order in which the three control methods were described.

Thus, w1 represents the estimated speed obtained for the V/f control with magnetic energy and torque error based stabilizing loops, w2 represents the estimated speed obtained for the V/f control with reactive power and torque error based stabilizing loops, while w3 represents the estimated speed obtained for the V/f control with voltage phase angle correction and active power calculation.

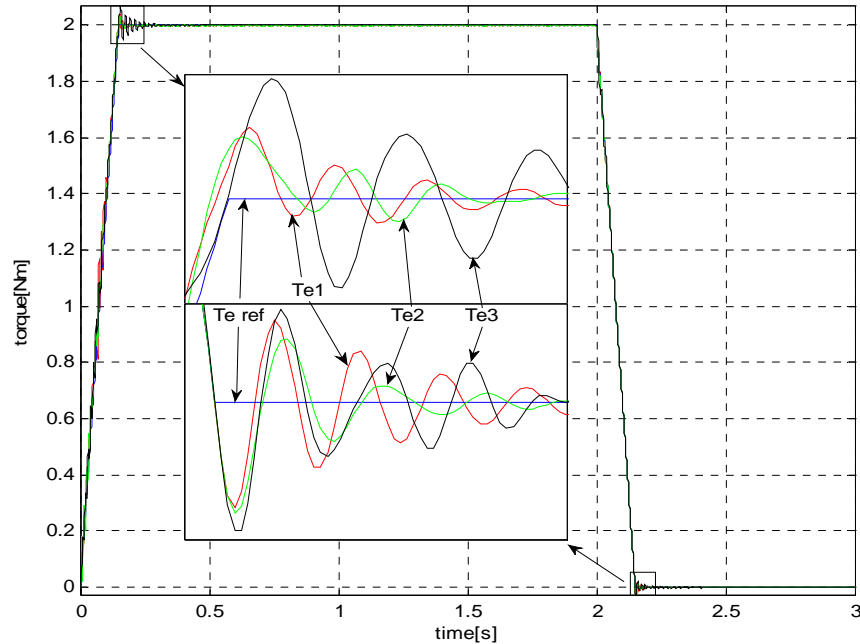


Fig. 6.10. Torque waveforms corresponding to all three proposed control methods

Figure 6.10 shows the torque response for the three proposed V/f with stabilizing loops control method, considering the reference with blue. We can easily see that the oscillations are higher in the beginning, when the machine loading occurs and are smaller when the machine unloading is applied.

After the unloading occurs, the currents value becomes lower with a few amperes for the first two control methods, but they decrease three times for the last proposed V/f with stabilizing loops control method. While the first V/f with stabilizing loops control strategy shows a slight difference of less than six electrical degrees between the reference and real rotor position, the next two methods show approximately four or five times bigger values.

6.4. Conclusion

This chapter aims to find a sensorless control method for an IPMSM, which can provide the imposed requirements: fast speed and torque response, without the utilization of the standard current and speed regulators, without coordinate transformations and with less computation effort. Therefore, three different control strategies were investigated and their results were analyzed and discussed.

We have to admit that the analyzed V/f control methods still use PI controllers, with the statement that their presence affects only the variables correction, so their output is not the variable itself.

The speed (1500 rpm) and torque (2 Nm) requirements were the same for each control strategy. During each of the proposed V/f control strategies, the machine accelerates rather fast, in about 160 – 170 ms, though some oscillations are visible along the transients. Both actual speed and torque waveforms follow closely the reference ones. When the machine unloading occurs, lower current values are registered.

References

- [1] R. Ancuti, „Fast Dynamics Response of Sensorless Control of High Speed Surface Permanent Magnet Synchronous Motor Drives”, Ph. D. Thesis, „Politehnica” Publishing House, 2008.
- [2] R. Dutta, M. F. Rahman “A Comparative Analysis of Two Test Methods of Measuring d- and q- Axes Inductances of Interior Permanent – Magnet Machine”, IEEE Transactions on Magnetics, vol.42, No.11, ISSN: 0018-9464, November 2006.
- [3] R. Krishnan, “Permanent Magnet Synchronous and Brushless DC Motor Drives”, CRC Press, Taylor and Francis, IEEE Press, ISBN-13: 978-0824753849, 25 September 2009;
- [4] I. Boldea, M.C. Paicu, G.D. Andreescu, “Active flux concept for motion-sensorless unified ac. drives”, IEEE Trans on Power Electronics, Vol. 23, No. 5, Sept. 2008, pp. 2612-2618, ISSN: 0885-8993;
- [5] G. Foo, M.F. Rahman, „Sensorless Sliding-Mode MTPA Control of an IPM Synchronous Motor Drive Using a Sliding-Mode Observer and HF Signal Injection”, Industrial Electronics, IEEE Trans on, Vol.57, No.4, pp. 1270–1278, ISSN: 0278-0046;
- [6] S. Bolognani, R. Petrella, A. Prearo, L. Sgarbossa, “Automatic tracking of MTPA trajectory in IPM motor drives based on AC current injection”, Energy Conversion Congress and Exposition, 2009, ECCE IEEE, pp. 2340–2346, ISBN: 978-1-4244-2893-9;
- [7] S. Bolognani, R. Petrella, A. Prearo, L. Sgarbossa, “On-Line Tracking of the MTPA Trajectory in IPM Motors Via Active Power Measurement”, XIX International Conference on Electrical Machines-ICEM 2010, pp. 1-7, ISBN 978-1-4244-4174-7, Rome, Italy, 6-8 Sept. 2010;
- [8] L. Zhao, C. H. Ham, Q. Han, T.X. Wu, L. Zheng, K.B. Sundaram, J. Kapat, L. Chow, „Design of an optimal V/f control for a super high speed permanent magnet synchronous motor”, Industrial Electronics Society, IECON, 30th Annual Conference of IEEE, 2-6 Nov. 2004, pp. 2260–2263, Vol. 3, ISBN: 0-7803-8730-9;
- [9] J. Itoh, N. Nomura, H. Ohsawa, “A Comparison between V/f Control and Position-Sensorless Vector Control for the Permanent Magnet Synchronous

- Motor", Power Conversion Conference, 2002. PCC Osaka Proc. of the, Vol. 3, pp. 1310-1315, ISBN: 0-7803-7156-9, Osaka, 02-05 Apr. 2002;
- [10] T. Halkosaari, "Optimal U/f-control of high speed permanent magnet motors", Industrial Electronics, IEEE International Symposium on, Vol.3, pp.2303–2308, ISBN: 1-4244-0496-7, 9-13 July 2006, Montreal, Quebec, Canada;
- [11] H. Kim, K. K. Huh, M. Harke, J. Wai, R. D. Lorenz, and T. A. Jahns, "Initial rotor position estimation for an integrated starter alternator IPM synchronous machine", in Proc. 10th Eur. Conf. Power Electron. Applicat. (EPE-2003), Toulouse, France, 2003, pp. 1875–1881;
- [12] A. Borisavljevic, H. Polinder, J. A. Ferreira, „Realization of the I/f Control Method for a High-Speed Permanent Magnet Motor", Electrical Machines (ICEM), 2010 XIX International Conference on, p. 1-6, ISBN: 978-1-4244-4174-7, Rome, Italy, 6-8 Sept.;
- [13] P.D.C. Perera, F. Blaabjerg, J.K. Pedersen, P.T. Thogersen, "A sensorless stable V/f control method for PMSM drives", IEEE Trans. on Ind Applicat, Vol.39, No.3, 2003, pp.783-791.

Chapter 7

Experimental Platforms

This chapter presents an extended description of the laboratory setups used for experiments shown in previous chapters.

One of the two platforms was realized in the Dspace Lab, Institute of Energy Technology, Aalborg, Denmark. The other one was realized in the PEMC Lab, Faculty of Electrical Engineering, Timisoara, Romania.

Their intended purpose was to prove and gain novel information about the sensorless vector control and of the proposed V/f with correction loops control of the interior permanent magnet synchronous machine.

During this chapter both platforms will be presented.

Each experimental setup mainly consists of the test machine and the load drive. Besides them, there are also the measuring circuits (of the phase currents, of the dc voltage link and of the machine speed and rotor position) and the control system software.

This chapter discusses the experimental setups as well as the implementation of various experimental tests, which were performed in order to validate the proposed sensorless control schemes under various conditions.

7.1. The First Experimental Setup

First of all the experimental setup realized in the Dspace Lab, Institute of Energy Technology, Aalborg, Denmark will be presented. Making use of it, the results for sensorless vector control – active flux based have been achieved in the first place, followed by the validation of the proposed V/f with correction loops control.

A short presentation of this experimental setup (Fig. 7.1.) follows. As it can be seen a three-phase 2.2 kW IPMSM is directly coupled to the load machine, the latter being also an interior PM synchronous motor, with similar specifications, as those of the motor.

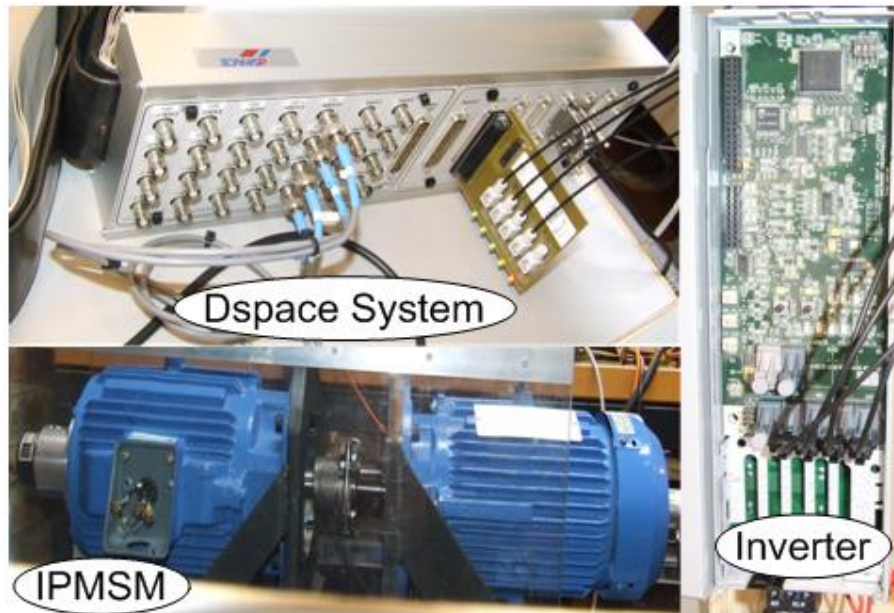


Fig. 7.1. Aalborg laboratory experimental setup.

A three-phase IGBT inverter, supplied at a dc-link voltage of 540V was used to feed the IPMSM. The sampling frequency and PWM frequency were set to 5 kHz. Phase currents were measured using magnetic current transducers. The actual rotor position and speed were provided by an incremental encoder with 2048 pulses per revolution, only for comparison.

It can be said that the whole experimental setup is divided in few subsystems:

- * The test machine
- * A three phase inverter
- * The load control system
- * Current sensors
- * dc voltage link measurement
- * rotor speed measurements
- * encoder for rotor position measurement
- * The dSpace 1103 platform

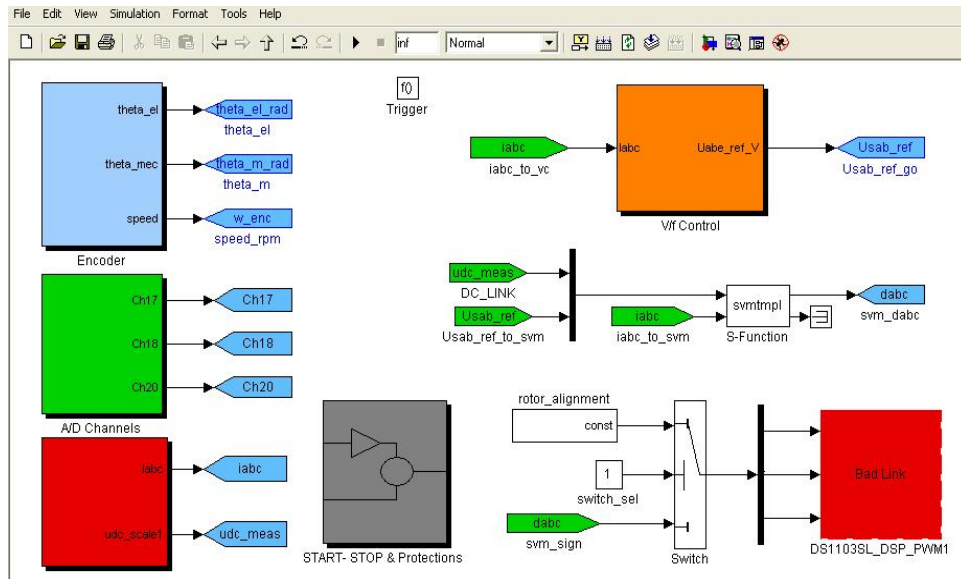


Fig. 7.2. Control software in Matlab/Simulink: encoder, current acquisitions, current protection, V/f control block,

The measure and protection are the main parts of the developed software (Figure 7.2.) and can be divided into three main parts: signal acquisition and digital filtering of the acquired signals; encoder interface; system protections.

The A/D channels are set to acquire two phase currents (the third current is calculated from the measured ones as seen from Fig. 7.3) and the dc – link voltage.

The acquisition process is triggered with the help of the slave – DSP timer interrupt with the same frequency as the switching (10 kHz).

As it is shown in Fig. 7.3, the measured values are scaled, considering the scaling factors of the sensors.

In order to prove the sensorless position estimation techniques, the IPMSM motor has been equipped with an incremental encoder, as witness.

in the encoder interface, displayed in Fig. 7.4., the electrical rotor position of the rotor and its speed are computed knowing the encoder resolution (number of pulses per one revolution) and the system sampling time.

The protections block, Fig. 7.5 contains the protection for over – current and over – speed, which must be well implemented in order to allow a proper command of the inverter.

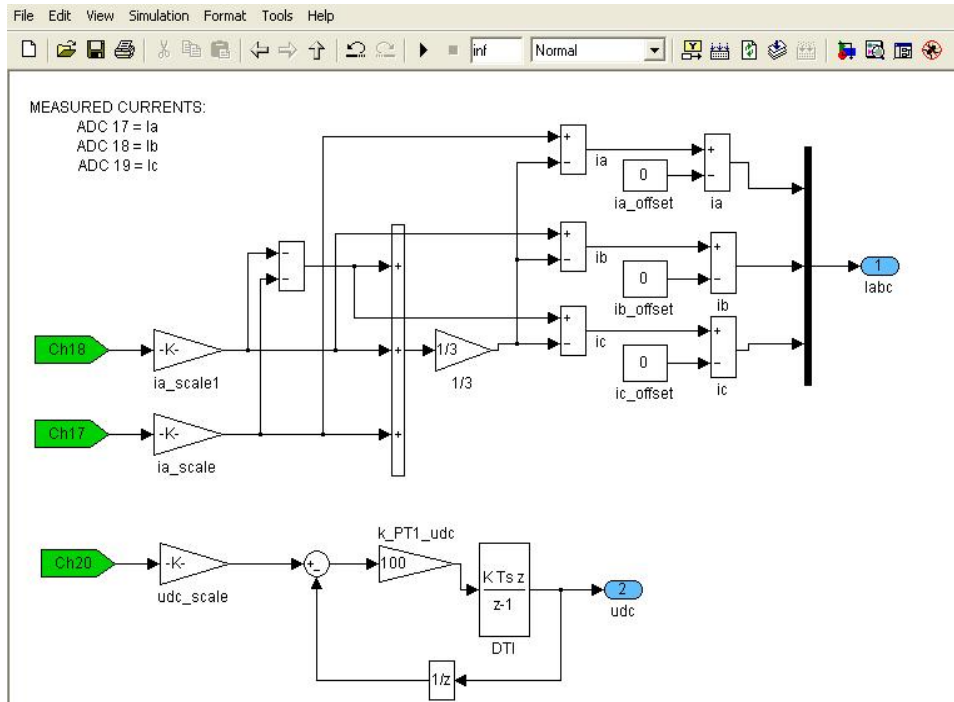


Fig. 7.3. Currents acquisition block

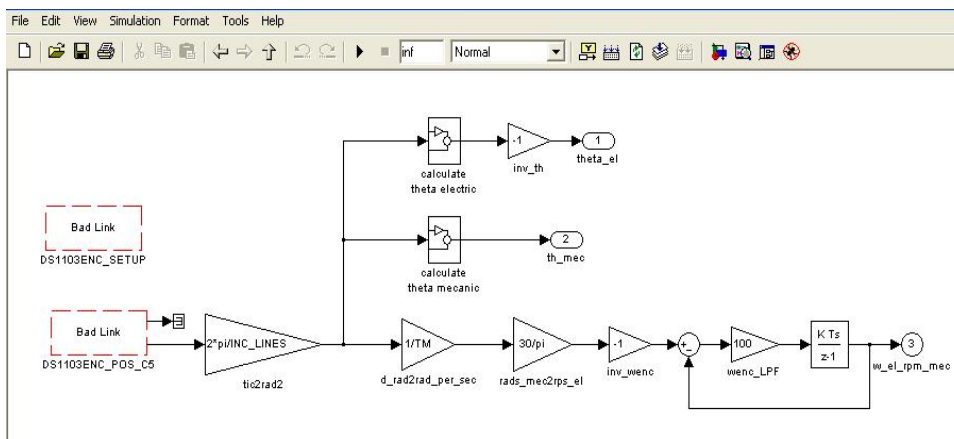


Fig. 7.4. Incremental encoder interface

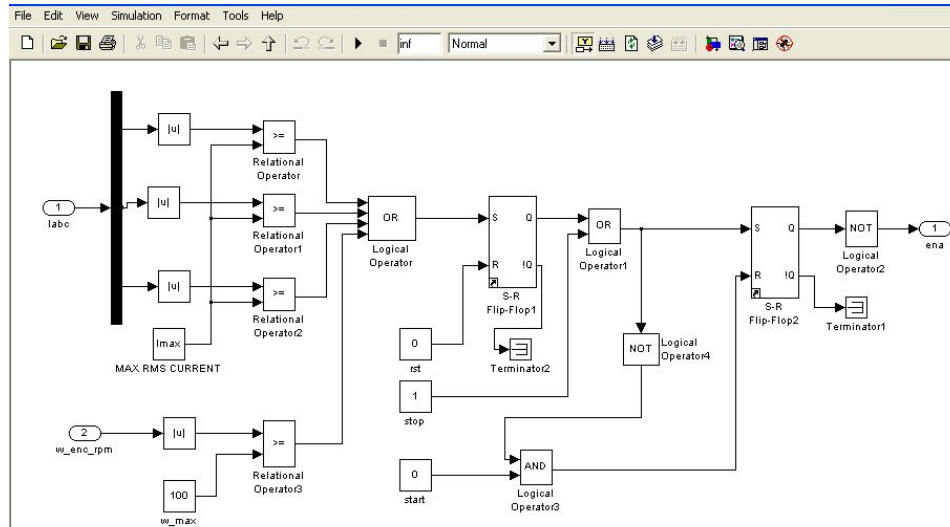


Fig. 7.5. Protection block – the over-current and over-speed protection implementation

7.1.1. Test machine (IPMSM)

The main component in the setup is the interior permanent magnet synchronous motor (IPMSM), manufactured by Yaskawa (see Fig. 7.1.).

TABLE 7.1.

IPMSM SPECIFICATIONS

Rated power	2.2 kW
Rated speed	1750 rpm
Rated frequency	87.5 Hz
Rated torque	12 Nm
Rated phase to phase voltage	380 V (rms)
Rated phase current	4.1 A (rms)
Number of pole pairs (p_1)	3
Stator resistance per phase (R_s)	3.3 Ω
d-axis inductance (L_d)	41.6 mH
q-axis inductance (L_{qn})	57.1 mH
Permanent magnet flux (λ_{PM})	0.483 Wb
Total inertia (J)	10.1x10 ⁻³ kgm ²
Viscous friction coefficient (B)	20x10 ⁻⁴ Nm s/rad
Windings connection	star connection

7.1.2. Three phase inverter

The three phase inverter used for this experimental setup is a Danfoss FC 302 type (displayed in Fig. 7.1.).

A frequency converter rectifies AC voltage from mains into DC voltage, after which this DC voltage is converted into an AC current with a variable amplitude and frequency.

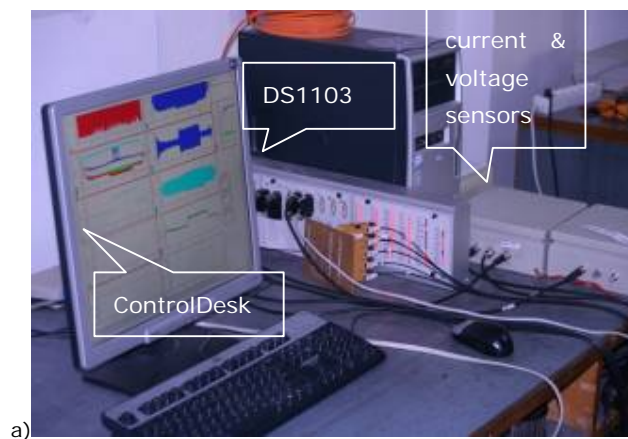
The motor is thus supplied with variable voltage and frequency, which enables variable speed control.

7.2. The Second Experimental Setup

This experimental setup was realized in the PEMC Lab, in Faculty of Electrical Engineering, "Politehnica" University of Timisoara and it is presented in Fig. 7.6. a,b.

As it can be seen in Fig. 7.6.b, the three phase 2 kW IPMSM is coupled via a transmission belt with a three phase 5.5kW induction machine (IM), which is DTC sensorless driven by an ABB ACS600 bidirectional converter. The IPMSM is feed from a three – phase MOSFET inverter, which is supplied at a 48 V dc - link voltage.

The setup main component is the interior PM synchronous motor prototype, manufactured at Electromotor SA Timisoara, which has the specifications given in Table 7.2.



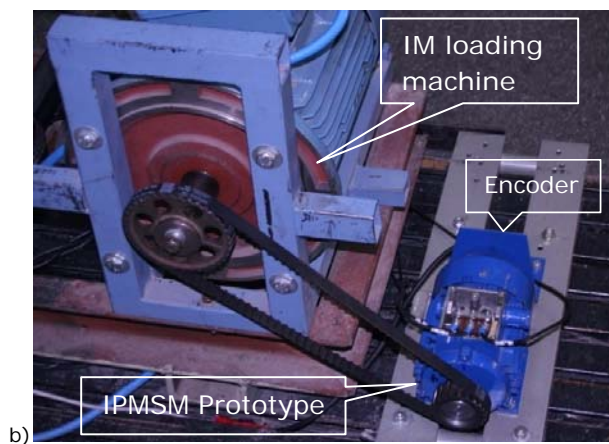


Fig. 7.6. Experimental setup: a) the acquisition platform; b) IPMSM-laboratory prototype and the loading IM Drive

TABLE 7.2.
IPMSM SPECIFICATIONS

Rated power	2 kW
Rated speed	6000 rpm
Rated frequency	400 Hz
Rated torque	2 Nm
Rated phase to phase voltage	31 V (rms)
Rated phase current	40 A (rms)
Number of pole pairs (p_1)	4
Stator resistance per phase (R_s)	0.138 Ω
d-axis inductance (L_d)	1.14 mH
q-axis inductance (L_{qn})	1.286 mH
Permanent magnet flux (λ_{PM})	0.02 Wb
Total inertia (J)	40x10 ⁻⁶ kg*m ²
Viscous friction coefficient (B)	1x10 ⁻⁶ Nm s/rad
Windings connection	Star connection

During both experimental platforms, we used dSpace DS1103 platform, especially designed for the control of electric drives. It features high computational capability and I/O periphery, built for real-time control system. It is fully programmable from Simulink block diagram environment, so it represent a quick and easy way to implement control functions and reduces the implementation time to minimum.

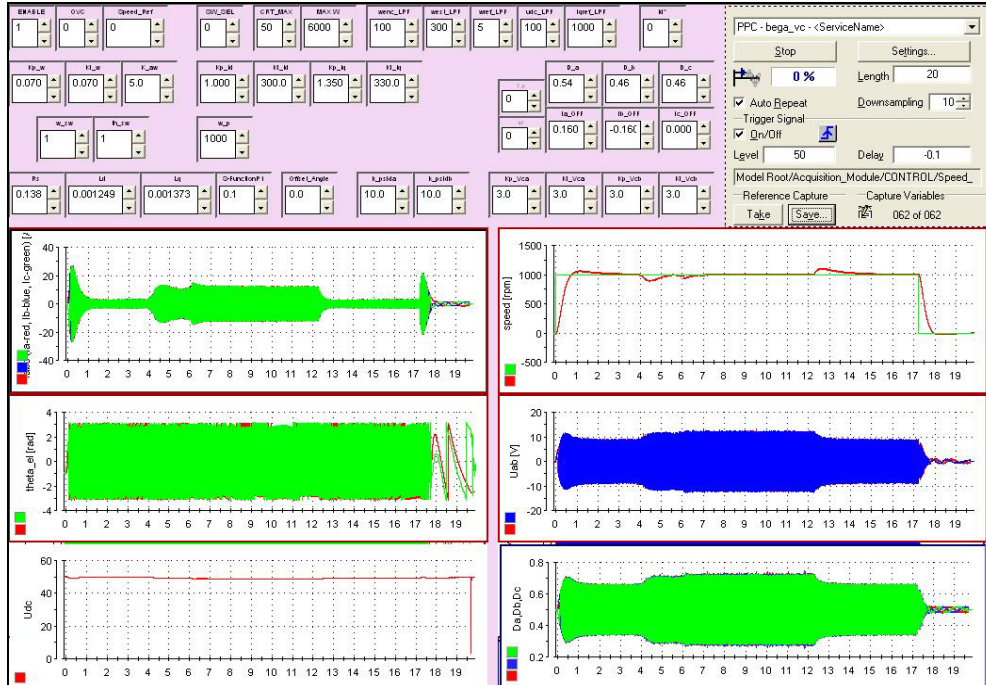


Fig. 7.7. DSpace Control Desk environment

The Control Desk experimenting software allows real-time management of the running process by providing a virtual control panel with instruments and scopes.

After the soft is ready and it has no errors, it can be compiled using the command „build” and afterwards the soft is loaded in the Dspace Control Desk interface (Fig. 7.7.). After this step, the interface contains all system parameters and allows their visualization, acquisition and changing.

7.3. Conclusion

The experimental test platform used during the tests of state observers and sensorless controls of an interior permanent magnet synchronous machine system was presented in this chapter.

All the hardware components of the system were presented, discussed and analyzed. The software used for acquisition, inverter protection were also explained.

The way the software developed in Matlab Simulink and the interface Control Desk Developer from the dSpace platform interact was presented.

Chapter 8

Conclusion and Contributions

8.1. Conclusion

Nowadays, one main concern in electric drives is to reduce the drive cost as much as possible, thus, there is a constant need for position sensor elimination, which means that a sensorless control is needed.

Motion-sensorless FOC and DTFC have spread in a spectacular way to all servo-drives, but **high dynamics response** in general AC drives is still a problem we have to deal with.

Consequently, the present thesis proposes a novel sensorless control strategy for general ac drives that can be successfully implemented for all ac motors, but interior permanent magnet motor was used as a case study, considering its well known advantages.

Further on, the sensorless control method is described and the main conclusions are summarized.

The proposed sensorless control method uses the open loop V/f control, to which correction loops were added. The added stabilizing loops were used to correct the voltage vector amplitude and phase.

This control method is based on the *active flux concept* and it also uses the maximum torque per ampere condition.

The **main claims** for this control method are:

- ❖ **fast speed and torque response** without using the well known speed or current PI controllers,
- ❖ no coordinate transformation,
- ❖ reduced computation time,
- ❖ the capability of **self – starting**
- ❖ **maximum efficiency** for a wide speed range.

Note: We have to admit that the proposed control method uses PI regulators to correct the voltage amplitude and phase, but they influence only the variable corrections, not the variable itself.

The active flux concept was previously described in Chapter 3, as the *torque-producing flux*, which renders all salient-pole traveling-field (induction and synchronous) machines into nonsalient-pole machines. The estimation of rotor position and speed based on the active-flux observer proved to be simpler than the existing solutions.

First of all, for a better comparison, sensorless vector control, based on the active flux observer and considering the MTPA condition, has been developed and both simulation and experimental tests have been performed. In order to know the control capabilities, tests were conducted in a speed range down to 5 rpm and up to 1500 rpm both low and high speeds and for different load torque values.

8.2. Original contributions

The main contributions in the thesis, from the author point of view, are summarized below:

- ❖ Four **novel V/f control** methods **with stabilizing loops** have been designed, implemented and tested;
- ❖ One of the four methods has been tested through both simulations and experiments. The first of its stabilizing loops was used to correct the voltage amplitude and it is based on the active flux error, while the other one was used to correct the voltage phase and it is based on speed error. The control method was tested in a large speed range, from 5 rpm (0,25 Hz), up to 1400 rpm (70 Hz), at 50% rated torque.
 - * The related **results proved to be similar** to the ones obtained with sensorless vector control;
 - * Fast speed and torque response was achieved;
 - * Even more, **V/f control** with correction loops, for **low speed** (5 rpm) - steady state operation, at no load – seems to follow the target with **less oscillations** than with sensorless vector control.
- ❖ **The second proposed control method** uses the magnetic energy balance to correct the voltage amplitude and the torque error to correct the voltage phase, while **the third method** uses the reactive power error to correct the voltage amplitude and again the torque error is used to correct the voltage phase. These two V/f control methods use both the active flux concept and the maximum torque per ampere condition to prescribe the *d* axis current. The last V/f control method uses only the maximum torque per ampere

condition to prescribe the stator current phase. The angle between the stator current vector and stator voltage vector is prescribed and estimated and its error is used to correct the voltage amplitude. To eliminate the speed oscillations a high pass filter is applied on the active power.

- * All the last three V/f control methods were implemented and tested through Matlab / Simulink digital simulations and all of them proved **fast dynamic speed and torque response**, though only the last method manages to make the d current negative.
- ❖ To prove once more the effectiveness of the correction loops, both simulations and experiments were conducted under **standard V/f control**, which proved to be characterized by **slow dynamics, higher currents**, the speed and torque oscillate around their target, while the encoder position is completely different to the reference one.

8.3. Future work

- Improvements are still needed for V/f with stabilizing loops control, e.g. full load step, has yet to be tested.
- The motor capability of functioning above base speed has yet to be verified.
- The system stability has to be analyzed.
- The operation above base speed has to be investigated.
- Experimental tests have to be achieved for the three proposed V/f solutions.

Summary in Romanian

Sumar

Teza de fata are ca principal scop analiza performantelor controlului V/f cu bucle de corectii pentru actionari cu masini sincrone cu magneti permanenti interiori. Lucrarea prezinta si investigheaza atat prin simulari digitale cat si experimental cateva solutii noi de control V/f cu corectii pentru amplitudinea si respectiv faza vectorului tensiunii.

Acest control se doreste a fi o alternativa buna, cu performante comparative cu cele ale controlului vectorial fara senzor de pozitie, cu raspuns rapid in cuplu si viteza, dar fara utilizarea reguletoarelor de viteza si curent, fara transformari de coordonate si cu efort de calcul mai redus. Mai mult, aceasta strategie de control, rezolva pornirea masinii sincrone cu magneti permanenti, nefiind astfel necesara dezvoltarea unei strategii distincte pentru determinarea pozitiei initiale a rotorului.

Metoda de control propusa initial utilizeaza conceptul de flux activ pentru estimarea vitezei si pozitiei rotorului. In plus, schema cuprinde conditia de cuplu maxim pe curent in regiunea de cuplu constant. Utilizarea strategiei de control propusa a dus la obtinerea unui raspuns dinamic, rapid in viteza si cuplu, fara eroare de regim stationar, metoda ce poate fi aplicata cu succes pentru toate masinile de curent alternativ.

Simularile corespunzatoare controlului propus au fost realizate cu ajutorul pachetului soft Matlab/Simulink, in timp ce sistemul dSpace a fost utilizat pentru achizitia rezultatelor experimentale.

Au fost investigate in prima instanta raspunsul si performantele masinii, controlata vectorial, cu si fara senzor de pozitie. Testele au fost realizate atat cu masina la functionarea in gol cat si la incarcare, in unele cazuri pana la cuplu nominal. Comparatiile intre controlul vectorial fara senzor de pozitie si controlul V/f corectat au fost realizate in vederea validarii performantelor acestuia din urma, atat la functionarea in gol, cat si in sarcina.

Pentru a demonstra eficienta corectiilor pentru amplitudinea si faza tensiunii, adaugate controlului V/f standard, acesta din urma a fost de asemenea implementat si testat in bucla deschisa. Rezultatele au dovedit necesitatea si performantele corectiilor utilizate. Daca in cazul controlului V/f in bucla deschisa, masina este caracterizata de instabilitate in functionare, iar viteza oscileaza in jurul tintei, in

cazul controlului V/f cu corectii, oscilatiile sunt eliminate, iar masina poate fi incarcata pana la cuplu nominal.

Au fost dezvoltate patru strategii diferite de control V/f cu corectii, dintre care doua au dovedit rezultate bune, comparative cu cele obtinute cu control vectorial.

Organizarea tezei

Lucrarea se intinde de-a lungul a opt capitole dupa cum urmeaza:

Primul capitol trateaza masinile de curent alternativ in general, in special pe cele sincrone cu magneti permanenti si metodele de control aferente acestora.

Capitolul al doilea propune controlul vectorial cu utilizarea encoderului pentru feedback-ul pozitiei rotorului. Raspunsul masinii in viteza si cuplu este analizat atat la mersul in gol cat si la incarcare.

In capitolul al treilea se prezinta conceptul de flux activ si este descrisa conditia de cuplu maxim pe curent. De asemenea este evidentiata aplicarea acestor conditii pentru diminuarea pierderilor si eficientizarea raspunsului in viteza si cuplu, atat in rezultate de simulare, cat si experimental, pentru diferite conditii de functionare ale masinii sincrone cu magneti permanenti interiori.

Capitolul al patrulea descrie in prima parte controlul V/f standard, cu prezentarea si interpretarea rezultatelor obtinute atat in simulari cat si experimental. In cea de-a doua parte a capitolului se descriu bucele de corectie care se adauga controlului V/f standard.

Prima corectie se refera la amplitudinea vectorului de tensiune, corectie obtinuta prin intermediul unui regulator de tip proportional-integrator, care are ca intrare eroarea amplitudinii fluxului activ. Se prescrie curentul i_d din conditia de cuplu maxim pe curent, cu ajutorul caruia se calculeaza apoi fluxul activ. Pornind de la integrala tensiunii, se estimeaza fluxul statoric din care se extrage termenul $L_a \cdot i_s$ obtinand astfel componentele estimate, dupa axele α si β , ale fluxului activ. Din componentele fluxului se obtine amplitudinea acestuia, ca valoare estimata. Diferenta dintre marimea prescrisa si cea estimata reprezinta intrarea regulatorului de corectie a amplitudinii vectorului tensiunii.

Cea de-a doua corectie, a fazei unghiului vectorului de tensiune, se bazeaza pe eroarea dintre viteza de referinta si viteza estimata (viteza fluxului activ), eroare considerata ca fiind intrarea celui de-al doilea regulator de tip proportional-integrator.

In acest capitol sunt prezentate rezultate de simulare corespunzatoare, in timp ce rezultate experimentale sunt discutate in al cincilea capitol. Tot in cadrul celui de-al cincilea capitol este realizata compararea rezultatelor obtinute pe de-o parte cu metoda vectoriala fara senzor de pozitie, cu rezultatele obtinute cu metoda de control propusa. Discutiile comparative intre rezultatele obtinute prin cele doua metode de control fara senzor de pozitie sunt realizate atat la viteze mari, apropiate de viteza nominala a masinii, cat si la viteze mici (0.25 Hz) ale masinii.

Capitolul al saselea descrie trei metode diferite de control V/f cu bucle de corectii. Rezultatul simularilor efectuate arata faptul ca dintre cele trei metode, doar una singura realizeaza curentul i_d negativ, motiv pentru care este propusa implementarea experimentală a acesteia. Toate cele trei metode de control V/f cu corectii utilizeaza conditia de cuplu maxim pe curent, in timp ce doar doua dintre acestea se bazeaza pe conceptul de flux activ.

In capitolul al saptelea se descriu platformele experimentale utilizate. Una dintre cele doua platforme a fost realizata la Univ. din Aalborg, Danemarca, standul al doilea apartinand Laboratorului PEMC, din cadrul Departamentului de Inginerie Electrica, Timisoara.

Capitolului opt este rezervat pentru concluziile finale si contributiile tezei.

Contributiile tezei

Utilizarea senzorului de pozitie in actionari electrice inseamna un avantaj in ceea ce priveste pornirea si raspunsul in cuplu si viteza, deoarece encoderul furnizeaza exact viteza si pozitia rotorului, inasa dezavantajele introduse de acesta se refera la fiabilitatea scazuta, cost ridicat al actionarii, precum si volumul mai mare al intregului ansamblu.

Pentru a cunoaste performantele actionarii studiate a fost implementat initial, controlul vectorial cu si fara senzor de pozitie.

In continuare, a fost dezvoltat controlul de tip V/f cu bucle de corectii pentru amplitudinea si respectiv faza tensiunii.

Principalele obiective ale metodei de control propuse sunt in primul rand raspunsul rapid in cuplu si viteza, fara utilizarea reguletoarelor conventionale de viteza si curent, fara transformari de coordonate si cu efort de calcul redus; se remarca de asemenea capabilitatea actionarii de a porni fara utilizarea unei strategii suplimentare, precum si eficienta ridicata pentru un domeniu larg de viteze.

Rezultatele obtinute cu ajutorul metodei de control propuse sunt similare celor obtinute cu control vectorial. In plus, se remarca rezultatele la viteze mici (0,25 Hz), unde raspunsul in viteza si cuplu realizat cu metoda de control propusa pare sa urmareasca referinta cu oscilatii mai mici decat cele obtinute cu control vectorial fara senzor de pozitie.

Atat rezultatele de simulare cat si cele experimentale arata, asa cum este bine cunoscut, faptul ca actionarea cu reglaj de tip V/f standard este caracterizata de o dinamica lenta, cu valori mari ale curentilor. De asemenea, raspunsul in viteza si cuplu este oscilant, intregul sistem fiind astfel caracterizat de instabilitate in functionare. Se evidentiaza astfel necesitatea si eficienta utilizarii buclelor de corectii.

Au fost astfel implementate si testate prin intermediul simularilor digitale alte trei metode distincte de control V/f cu corectii pentru amplitudinea si faza unghiului vectorului de tensiune, doar una dintre acestea dovedind performante dinamice ridicate, cu rezultate experimentale promitatoare.

Author's papers related to the Ph. D. thesis

- [1] I. Boldea, A. Moldovan, V. Coroban, Gh. D. Andreescu, L. Tutelea, "A Class of Fast Dynamics V/f Sensorless AC General Drives with PM-RSM as a Case Study", OPTIM 2010;
- [2] A. Moldovan, F. Blaabjerg, I. Boldea, "Active-Flux-Based, V/f-with-Stabilizing-Loops Versus Sensorless Vector Control of IPMSM Drives", ISIE 2011;
- [3] A. Moldovan, Ion Boldea, Gh. D. Andreescu, "V/f Control with Active Flux and Power Stabilizing Corrections for IPMSM Drives", ASTR 2011;
- [4] A. Moldovan, S. Agarlita, I. Boldea, Gh. D. Andreescu, C. Lascu, "Wide Speed Range V/f with Stabilizing Loops Control of Tooth-Wound IPMSM Drives", *pending for* OPTIM 2012;
- [5] Gh.D. Andreescu, C. Coman, A. Moldovan, I. Boldea, "Stable V/f Control System with Unity Power Factor for PMSM Drives", *pending for* OPTIM 2012;

Author's CV

Ana Adela MOLDOVAN

Home Address Str. Ing. Anghel Saligny, bl.12A, et.3, ap.11
 Timisoara
 Romania
 Mobile +40 741 088 676

E-Mail: anamoldovan2003@yahoo.com

EDUCATION

2008-2012 PhD student at "Politehnica" University of Timișoara,
 Romania, Department of Electrical Engineering;
2003-2008 University " Politehnica " of Timișoara, Romania
1999-2003 Industrial School Group "Mihai Viteazul", Ineu, Arad,
 Romania

PROFESSIONAL EXPERIENCE

3 months in 2010 Guest Researcher at "Institute of Energy technology",
 Aalborg University, Denmark;

PERSONAL INFORMATION

Born: October 26th 1984

Family: Married

APPENDIX

The Space Vector Modulation (SVM) program (S-function implemented) used in experiments and which was created by Lect. Dr. Cristian LASCU

```
/******\
* Space Vector Modulation S-Function Template
* Proiect: PMSM Sensorless DTC drive
* Autor: Cristian Lascu, 2004
* Continut: Space Vector Modulation S-Function template for Simulink
* Input: Us.alfa, Us.beta, Vdc
* Output: Da, Db, Dc
\*****/

#define S_FUNCTION_NAME svmtmpl
#define S_FUNCTION_LEVEL 2

#include "simstruc.h"
#include "svm.c"

static void mdlInitializeSizes(SimStruct *S)
{
    ssSetNumSFcnParams(S, 1); /* Number of expected parameters */
    if (ssGetNumSFcnParams(S) != ssGetSFcnParamsCount(S)) {
        /* Return if number of expected != number of actual parameters */
        return;
    }

    ssSetNumContStates(S, 0);
    ssSetNumDiscStates(S, 0);

    if (!ssSetNumInputPorts(S, 2)) return;
    ssSetInputPortWidth(S, 0, 3);
    ssSetInputPortDirectFeedThrough(S, 0, 1);
    ssSetInputPortWidth(S, 1, 3);
    ssSetInputPortDirectFeedThrough(S, 1, 1);

    if (!ssSetNumOutputPorts(S, 2)) return;
    ssSetOutputPortWidth(S, 0, 3);
    ssSetOutputPortWidth(S, 1, 2);

    ssSetNumSampleTimes(S, 1);

    /* Take care when specifying exception free code - see sfuntmpl.doc */
    ssSetOptions(S, SS_OPTION_EXCEPTION_FREE_CODE);
    // ssSetOptions(S, 0);
}
```

```

static void mdlInitializeSampleTimes(SimStruct *S)
{
//  ssSetSampleTime(S, 0, CONTINUOUS_SAMPLE_TIME);
  ssSetSampleTime(S, 0, INHERITED_SAMPLE_TIME);
  ssSetOffsetTime(S, 0, 0.0);
}

static void mdlOutputs(SimStruct *S, int_T tid)
{
  InputRealPtrsType uPtr = ssGetInputPortRealSignalPtrs(S,0);
  InputRealPtrsType iPtr = ssGetInputPortRealSignalPtrs(S,1);
  real_T          *d = ssGetOutputPortRealSignal(S,0);
  real_T          *y = ssGetOutputPortRealSignal(S,1);
  real_T          *k = mxGetPr(ssGetSFcnParam(S,0));
  real_T u[3],i[3];
  u[0]=*uPtr[0];
  u[1]=*uPtr[1];
  u[2]=*uPtr[2];
  i[0]=*iPtr[0];
  i[1]=*iPtr[1];
  i[2]=*iPtr[2];
  SVM(u,i,d,y,k);
}

static void mdlTerminate(SimStruct *S)
{
}

#ifdef MATLAB_MEX_FILE /* Is this file being compiled as a MEX-file? */
#include "simulink.c" /* MEX-file interface mechanism */
#else
#include "cg_sfun.h" /* Code generation registration function */
#endif

" svm.c file"

* Space Vector Modulation *
* Proiect: PMSM Sensorless DTC drive * Autor: Cristian *
Lascu, 2004 *
* Continut: Space Vector Modulation * Input: Us.alfa, *
Us.beta, Vdc *
* Output: Da, Db, Dc

#include <math.h>
#include "vector.h"
#define R3 1.732051
#define Dmax 0.98
#define Dmin 0.02

```

```
// Space Vector Modulation

void SVM(real_T *u, real_T *i, real_T *d, real_T *y, real_T *k)
{
    struct Vector{float alfa,beta;} Us;
    float K=(*k)*tdead/h;
    float Umax=R3/u[0];
    float Da,Db,Dc;
    float T1,T2;
    int sector;

    Us.alfa = R3*Umax*u[1]; //normalizare - Holtz
    Us.beta = Umax*u[2];

    // Sectorul tensiunii si timpii de modulare
    if (Us.beta>0)
        if (Us.alfa>Us.beta)
            {
                sector=0;
                T1=0.5*(Us.alfa-Us.beta);
                T2=Us.beta;
            }
        else if (-Us.alfa<Us.beta)
            {
                sector=1;
                T1=0.5*(Us.alfa+Us.beta);
                T2=0.5*(Us.beta-Us.alfa);
            }
        else
            {
                sector=2;
                T1=Us.beta;
                T2=-0.5*(Us.alfa+Us.beta);
            }
    else if (Us.alfa<Us.beta)
        {
            sector=3;
            T1=0.5*(Us.beta-Us.alfa);
            T2=-Us.beta;
        }
    else if (-Us.alfa>Us.beta)
        {
            sector=4;
            T1=-0.5*(Us.alfa+Us.beta);
            T2=0.5*(Us.alfa-Us.beta);
        }
    else
        {
            sector=5;
        }
}
```

```

        T1=-Us.beta;
        T2=0.5*(Us.alfa+Us.beta);
    }

// Supramodularea Holtz
if (T1>1.0) T1=1.0,T2=0.0; //bang-bang
else if (T2>1.0) T2=1.0,T1=0.0; //bang-bang
else if (T1+T2>1.0) if (T1>T2) T2=1.0-T1; else T1=1.0-T2;//OVM

// Factorii de umplere - SVM
switch (sector) {
case 0: Da=0.5*(1.0+T1+T2);
        Db=0.5*(1.0-T1+T2);
        Dc=0.5*(1.0-T1-T2);
        break;
case 1: Da=0.5*(1.0+T1-T2);
        Db=0.5*(1.0+T1+T2);
        Dc=0.5*(1.0-T1-T2);
        break;
case 2: Da=0.5*(1.0-T1-T2);
        Db=0.5*(1.0+T1+T2);
        Dc=0.5*(1.0-T1+T2);
        break;
case 3: Da=0.5*(1.0-T1-T2);
        Db=0.5*(1.0+T1-T2);
        Dc=0.5*(1.0+T1+T2);
        break;
case 4: Da=0.5*(1.0-T1+T2);
        Db=0.5*(1.0-T1-T2);
        Dc=0.5*(1.0+T1+T2);
        break;
case 5: Da=0.5*(1.0+T1+T2);
        Db=0.5*(1.0-T1-T2);
        Dc=0.5*(1.0+T1-T2);
        break;
default:
        Da=0.0;Db=0.0;Dc=0.0;
}
// Stator voltage
y[0] = u[0]*(2.0*Da-Db-Dc)/3.0;
y[1] = u[0]*(Db-Dc)/R3;

// Dead-time compensation
Da = Da + K*sat(i[0],zone);
Db = Db + K*sat(i[1],zone);
Dc = Dc + K*sat(i[2],zone);

// Pulse drop
if (Da>Dmax) Da=1.0; else if (Da<Dmin) Da=0.0;
if (Db>Dmax) Db=1.0; else if (Db<Dmin) Db=0.0;

```

```
    if (Dc>Dmax) Dc=1.0; else if (Dc<Dmin) Dc=0.0;

    // Duty cycles
    d[0] = Da;
    d[1] = Db;
    d[2] = Dc;
}
```

"vector.h" file

```
* Project: PMSM Sensorless DTC drive
* Autor: Cristian Lascu, 2004
Variables and Constant Definitions

* Continut: Global

#ifndef VECTOR
#define VECTOR

// Sampling time
const float h=0.0001; // [s]

// SVM parameters
const float tdead = 2e-6; // dead time [s]
const float zone = 1.0; // linear zone [A]

// Constante matematice
const float pi=3.1415926;

// Saturation function
float sat(real_T x, real_T z)
{
    if (x>z) return 1.0;
    else if (x<-z) return -1.0;
    else return x/z;
}

#endif
```